

D.K.J. van der Wielen

Design optimization of a next-generation push divert sorter



Design optimization of a next-generation push divert sorter

By

D.K.J. van der Wielen

Master Thesis

in partial fulfilment of the requirements for the degree of

Master of Science

in Mechanical Engineering

at the Department Maritime and Transport Technology of Faculty Mechanical, Maritime and Materials Engineering of Delft University of Technology

to be defended publicly on March 16th, 2023 at 2:00 PM

Student number:	5182670	
MSc track:	Multi-Machine Engineering	
Report number:	2023.MME.8779	
Thesis committee:	Dr.ir. D.L. Schott, Ir. W. van den Bos Ir. J.J.M.J.P. Meens, Dr.ir. J.F.L. Goosen,	Chair, TU Delft Supervisor, TU Delft Company supervisor, Vanderlande Industries Committee member, TU Delft
Date:	March 16 th , 2023	

An electronic version of this thesis is available at <http://repository.tudelft.nl/>.

It may only be reproduced literally and as a whole. For commercial purposes only with written authorization of Delft University of Technology. Requests for consult are only taken into consideration under the condition that the applicant denies all legal rights on liabilities concerning the contents of the advice.

Preface

This thesis is the culmination of my graduate studies in Mechanical Engineering. It has been a challenging and rewarding experience, and I am grateful for the guidance and support I have received from my advisors, committee members, and colleagues.

The research presented in this thesis addresses the design optimization of a next-generation Push Divert Sorter (PDS). Through a combination of theoretical analysis and experiments, I have been able to find solutions for problems identified in the study.

I would like to extend my sincere thanks to my daily supervisor, Jasper Meens for his invaluable guidance throughout the course of my research. I would also like to thank Wouter van den Bos and Dingena Schott, for their valuable feedback and suggestions.

Additionally, I would like to acknowledge the support of my colleagues and friends, who have provided valuable insights and assistance during the course of my research.

Finally, I would like to thank my family for their unwavering support and encouragement throughout my academic pursuits.

Daan van der Wielen
Veghel, February 2023

Summary

Vanderlande Industries (VI) is a Dutch multinational specialized in the development of automated material handling equipment in the post and parcel, warehouse and airport market. One of the systems they offer to their customers is a Push Divert Sorter (PDS). This sorter is commonly used in Distribution Centers (DCs). It uses plastic components called sliders to push a single flow of parcels into specific outfeed destinations.

Increasing global parcel shipping volumes and just-in-time delivery force distribution centers to handle increasingly larger volumes of greatly varying parcel types. To stay competitive in these changing market conditions, VI is exploring the concept of a next-generation PDS. Yet, where the current generation sorters have different configurations for specific parcel types, the new generation sorter aims to handle all parcel types with a single configuration. However, it is unclear how these parcels, with differing characteristics, will behave when all sorted on the same sorter. Moreover, what the optimal design of this new sorter should be is also unclear.

The proposed sorter is first analyzed in greater detail. Equipment upstream and downstream (outfeeds) of the sorter are also analyzed. Key Performance Indicators (KPIs) for the design are derived based on important system properties. Moreover, parcel types, which could be processed on the system are analyzed by identifying and classifying their important characteristics.

This is followed by an analysis of unwanted parcel behaviour. First, all types of potential unwanted parcel behaviour are identified. Physical causes for each type of behaviour is analyzed. By a combination of experiments and theoretical analysis, a conclusion is drawn about which of the risks are significant and which can be discarded. This analysis concluded seven significant types of unwanted parcel behaviour.

Solutions are derived to reduce these seven problems. Finding solutions for these problems is split into two parts. Both improvements to the slider trajectory and the slider design are proposed. The slider design is derived based on design parameter objectives which are derived for each problem.

The effectiveness of the solutions is finally assessed on the basis of experimental test results. All solutions show a significant improvement (in terms of the KPIs). These improvements could yield a reduction of sorter dimensions with a potential length and width reduction of 14% and 16 % respectively. Numerous improvements to the parcel behaviour could also yield a significant capacity improvement.

Finally, to gain further performance improvement, VI could look at parcel behaviour

outfeeds. The current study is limited to the parcel behaviour on the sorter. Yet the behaviour of parcels when they have entered the outfeed also influences the overall system performance.

Contents

1	Introduction	2
1.1	Background	3
1.2	Problem definition	5
1.3	Research questions	5
2	Literature	7
2.1	Previous VI studies	7
2.2	Automatic Sortation Systems (ASS)	7
2.3	Physical phenomena dominant on a PDS	9
2.4	Slider and carrier design patents	11
3	System analysis and design requirements	13
3.1	Upstream equipment	13
3.2	Parcel input position and orientation	14
3.3	Sorter analysis	14
3.4	Downstream equipment (outfeed)	15
3.5	Material Handling Unit (MHU) analysis	16
3.6	Key Performance Indicators (KPIs)	21
3.7	Conclusion	22
4	Unwanted parcel behaviour analysis	24
4.1	Design parameters	25
4.2	Research methodology	26
4.3	Shift and rotation due to the impact	28
4.4	Drift due to airflow and vibrations	31
4.5	Slide onto or over the sliders	33
4.6	Backward toppling over the sliders	36
4.7	Shift and rotation due to secondary impact	37
4.8	Excessive rotation radius	39
4.9	Over-rotation due to angular momentum	42
4.10	Disadvantageous COR position	44
4.11	Length increase due to deformation	46
4.12	Unwanted rotation due to insufficient support	47
4.13	Slide along the sliders	50
4.14	Damage due to contact pressure	51
4.15	Deceleration during free sliding	54
4.16	Non-performance related constraints and objectives	56
4.17	Conclusion	58

5	Conceptual solutions	59
5.1	Morphological chart	59
5.2	Concept design (resulting from parameter objectives)	60
5.3	Carrier design	66
5.4	Conclusion	67
6	Results	68
6.1	Prototype	68
6.2	Reduce overrotation due to angular momentum	68
6.3	Increased rotation rate	69
6.4	Reduce unwanted rotation	70
6.5	Reduce space use during rotation	70
6.6	Reduce sliding along the sliders	71
6.7	Conclusion	72
7	Conclusion and recommendations	73
7.1	Conclusion	73
7.2	Recommendations	75
A	Figures and calculations	80
B	Conceptual design	90
C	Research paper	95

Chapter 1

Introduction

The volume of global parcel shipping amounted to over 131 billion parcels in 2020. In less than six years, this volume is expected to more than double and reach 266 billion parcels [33]. This would mean the volume will have more than quadrupled in a decade. This incredible increase in parcel shipping volume is mainly driven by the growth of e-commerce [16]. Due to the COVID-19 pandemic, many governments were forcing shops to close, resulting in further growth of e-commerce, which is projected to continue for the next few years [16]. Technology is transforming the entire supply chain and revolutionizing the parcel industry, and it is quickly becoming a critical facilitator in enhancing efficiency and meeting customer expectations for the coming years.

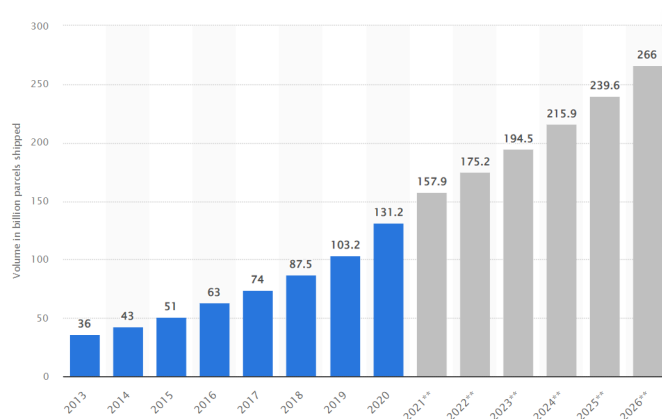


Figure 1.1: Global parcel shipping volume between 2013 and 2026 (in billion parcels) [33]

To understand the challenges e-commerce distribution centres face today, it helps to reflect on how quickly the fulfilment market has changed. The just-in-time philosophy promoted a change in the market conditions going from large orders of the same product to small orders of a variety of products. Furthermore, productivity, agility, and customization are the main necessities driven by market conditions [5]. These changes in market scenario turned product life cycles shorter and changed the paradigms for automation, moving from high volumes to small volumes with variety [19]. The variety of packaging types forces postal operations to find sortation solutions with the capability to keep up. An important feature of sortation systems is becoming gentle handling of a range of products such as letters, soft packs, polybags, corrugated cases, cartons, totes and other odd or oversized items [8].

Additionally, add in the need for distribution centres to store a broader assortment of

products than ever before to satisfy the expectations of customers, and it becomes evident that available distribution centre floor space is at a premium [17]. Also, shifts in population dynamics and urbanization, push post and parcel carriers to serve greater volumes in areas with limited, more expensive real estate. Distribution centre operators, therefore, need to maximize floor space utilization [8].

1.1 Background

1.1.1 Old system

One of the systems Vanderlande Industries (VI) currently offers to its customers is a PDS. This system is commonly used in DCs to sort a single flow of items into specific outfeed destinations.

The machine (shown in Figure 1.2) is comprised of a series of aluminium extrusion profiles which are referred to as carriers. Each carrier is equipped with a movable plastic component called a slider, which can slide back and forth along the length of the carrier. The carriers are connected to each other by a chain and are driven by an electric motor moving the carriers in a conveyor-like loop (in the "direction of movement" indicated in the figure). A flow of parcels is scanned and their desired outfeed location is determined before they enter the sorter. When a parcel nears its designated outfeed, a switch is activated forcing a pin on the bottom of the slider into a guide track. This forces the slider to travel the path highlighted in green (Figure 1.2), pushing the parcel into the outfeed.

This sorter technology (using switch-frames) has proven successful over many years.

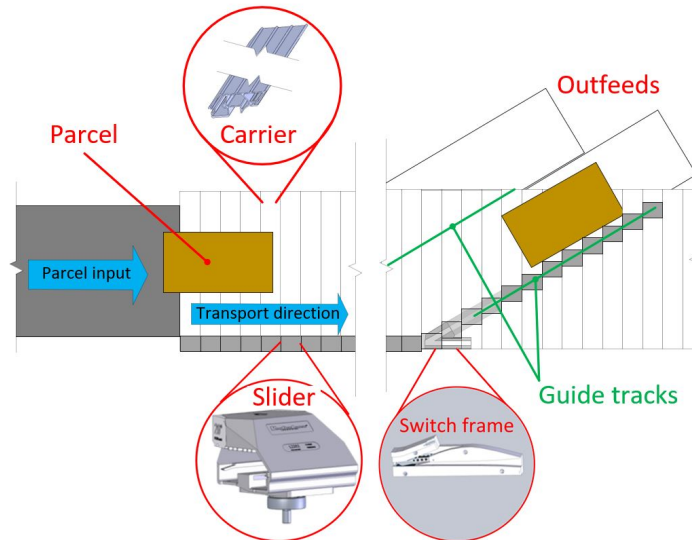


Figure 1.2: Positive slider sorting mechanism

However, the system faces some major downsides related to the rigid nature of the guide frame principle. These downsides are mainly related to the limited control over the motion of the sliders (which can only travel in one fixed line). This limits the sorter performance

in terms of capacity, accuracy and parcel types it can handle.

The old sorter has different configurations (see Figure 1.3), each applicable for a limited parcel range with a dedicated slider and carrier for that specific parcel range.



Figure 1.3: Current sorter designs (1: parcel type that can be handled on the system, 2: slider and carrier design, 3: an overview of sorter) [14]

1.1.2 Sort strategy

PDSs generally use one of two sorting strategies; parallel or sequential sorting. With sequential sorting, the parcel is rotated to align it with the outfeed before sorting (Figure 1.4a). The downside of this strategy is that the parcel requires more space due to the rotation, which reduces the sorter capacity. The rotation motion is also challenging for some parcel types and introduces additional uncertainty in the parcel position and orientation.

With parallel sorting the parcel is diverted without rotating it (Figure 1.4b). Since the parcel is not rotated it is possible to reduce the gaps between parcels significantly, resulting in a higher capacity. However, parallel sorting requires a more complex switch frame. Also, parallel sorting is only possible if the outfeed is wide enough, since the parcel requires more space if it is not aligned with the outfeed.

1.1.3 Proposed new system

To overcome the downsides of the current sorters, M. de Jager [18] proposed a new actuation principle for the PDS. A sorter with this new actuation principle will be referred to as the new sorter. The system replaces the mechanical switch frame structure with individual drive systems on each carrier. This enables actuating each slider individually (Figure 1.5a). The system will be analysed in greater detail in Section 3.3.

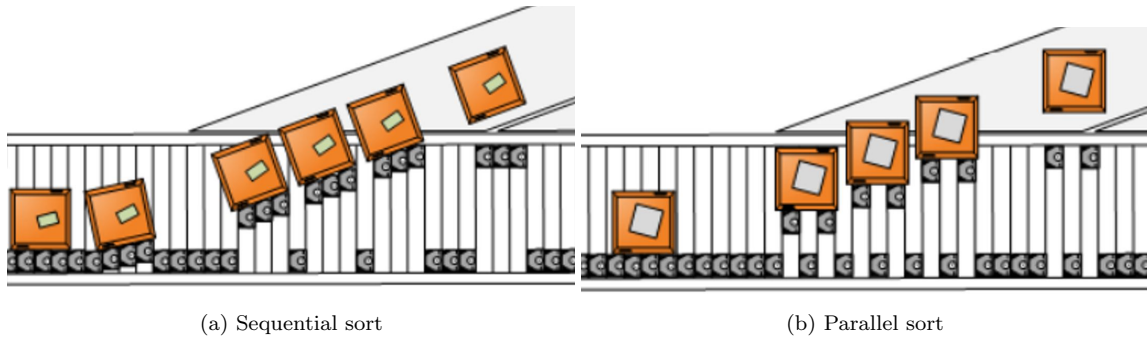


Figure 1.4: Sort strategies [18]

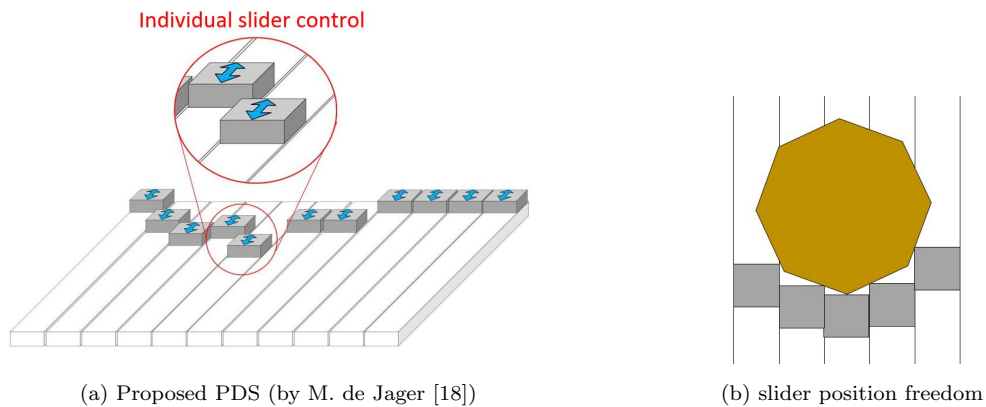


Figure 1.5: New sorter

1.2 Problem definition

Current generation VI sorters have different configurations (shown in Figure 1.3), each with a dedicated design (of slider and carrier) and sort strategy for a specific parcel type. Each configuration is specially designed to cope with the unique challenges of the parcel type it handles. The proposed new sorter should be able to handle all parcel types and sort strategies with only a single slider and carrier design. Yet, it is unknown how all these parcels, with hugely varying characteristics, will behave on the same sorter. It is also unclear how the design (of slider and carrier) and slider trajectory influence their behaviour and what design and slider trajectory would be optimal.

1.3 Research questions

Research questions are defined to guide the research process and to provide a framework for analysis. Two main research questions are defined, these are answered based on seven sub-questions.

How do the design (of slider and carrier) and slider trajectory influence the sorter performance?

What design (of slider and carrier) and slider trajectory yield the highest sorter performance?

1. What Key Performance Indicators (KPIs) should be used for the current study?
2. What system requirements and parcel characteristics influence the behaviour of parcels on the sorter?
3. What type of unwanted parcel behaviour could negatively impact the sorter performance?
4. What are the physical causes for this behaviour and what parameters of the slider and carrier design influence it?
5. What unwanted parcel behaviour is most significant?
6. What slider and carrier design reduce this unwanted behaviour?
7. How effective is the new slider and carrier design in improving the performance of the sorter?

Chapter 2

Literature

This chapter will describe the most important findings from the literature study. A literature study is done to provide an understanding of what has been published on topics related to the current study and what gaps exist in current knowledge. Both academic papers, patents and internal VI documents have been reviewed for the literature study.

2.1 Previous VI studies

A series of studies into the new sorter concept have already been done. An initial analysis [18] of the proposed concept was conducted to gain insight into the added value of such a system. Moreover, a conceptual design of the system was proposed and the main challenges of such a system were identified. A follow-up study explored controlling the slider position [40].

Another study [1] defined seven key drivers for developing the new sorter based on interviews with stakeholders. These seven key drivers are; accuracy, flexibility, availability, capacity, gentle handling, cost and productivity.

2.2 Automatic Sortation Systems (ASS)

The sorter proposed by M. de Jager is a type of Automated Sortation System (ASS). To understand what sets it apart from other systems, a literature review is conducted of different ASSs which are currently offered by competitors.

The sorter is classified as a conveyor-based sorting systems. Within this category, there are line and loop sorters. These systems have very different capabilities and footprints (Figure A.1) and therefore don't compete directly. What further sets the sorter apart is the method of diverting products (moving the product sideways into outfeeds), which is done by pushing (see Figure 2.1). The two other methods are friction driven (using a belt for example) or gravity-driven (using a tilting tray for example) mechanisms. The method using pushing is considered the most accurate.

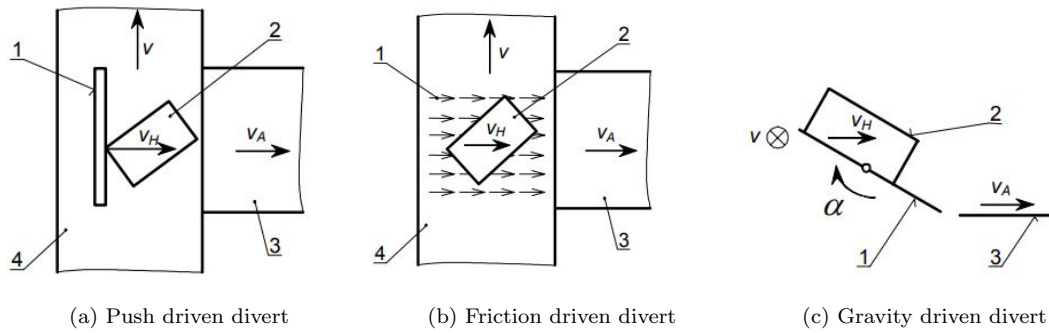


Figure 2.1: Divert methods used in automated sortation systems [28]

2.2.1 Product variety

One of the most important aspects of a sortation system is the packaging type it can handle [17]. Packaging is used for five main reasons; 1) to make transport easier, 2) protection of goods, 3) provide information, 4) make storage more convenient and 5) improve appearance of goods [4].

Their extent of use varies by operation, but modern fulfilment centers should consider the degree to which they currently (or will increasingly) handle a mix of malleable poly-bags, rigid corrugated cases and flexible bubble mailers. This means deploying a sortation system capable of reliably handling the unique challenges of all packaging types. Figure A.2 illustrates the ability of different sorters to sort a variety of product types (ranging from easy to hard to handle). These are a rule of thumb and actual systems could differ from what is depicted. Manual processing is capable of handling the highest range of products as could be expected.

2.2.2 Throughput

With continuous growth in the volume of packages shipped globally, [33] it is apparent that throughput capacity (often expressed in terms of cartons per hour or pieces per hour) is among the most important aspects of a sortation system.

However, a common misunderstanding about throughput rates is that the speed of a sorter is the same as throughput [17]. Another essential aspect influencing the throughput is the gap between items. The gapping is dependent on item divert stability and accuracy. Many modern sorter systems have reached higher throughput rates by minimizing gapping instead of increasing speed. This reduces wear, energy usage and noise while extending equipment life. However, it also makes the machine control system much more critical. The theoretical throughput can be calculated using the conveyor speed, product gap and product length, as can be seen in Figure 2.2.

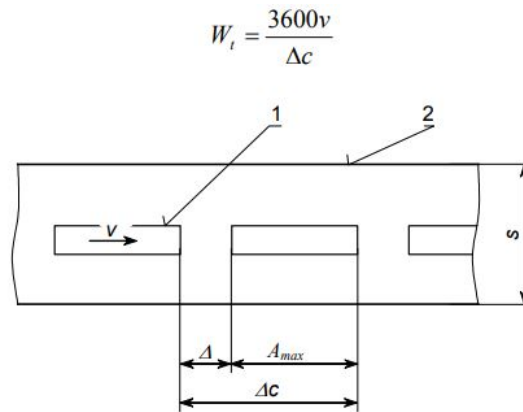


Figure 2.2: Theoretical sorter throughput [28]

2.3 Physical phenomena dominant on a PDS

To understand understanding package behaviour on a PDS it is important to analyse the two dominant physical phenomenon in the sortation process; dry sliding friction and impact. Due to the complexity of these phenomena, there are numerous models to make predictions of real-life situations. Models are applicable to a limited range of situations. The most applicable models and theories found in the literature are discussed below.

2.3.1 Planar dry friction

The behaviour of parcels on sortation systems is influenced by friction. Friction forces can be found in all mechanical systems that have two contact surfaces with relative motion. The literature discusses numerous types of friction, however dry sliding friction is dominant within the current study. Other types of friction such as fluid friction, internal friction, skin friction and lubricated friction [13] are of less importance in this context. Dry friction models used nowadays can be divided into two groups: static or kinematic (also referred to as dynamic or sliding friction). The best-known friction theory is that of Coulomb. It can be said that the Coulomb friction law was the predecessor for all of the other friction models [23].

Coulombs model states that when a body is moving along a plane, a friction force acts in the opposite direction of movement and is fixed to the center of friction. The friction force is proportional to the normal force pressing the surfaces together and is also proportional to a constant, which is called the Coefficient of Friction (CoF), which is often referred to with the symbol " μ ". In this case, there is no moment of friction with respect to the center of gravity preventing the body from rotating. However, in reality a friction moment prevents the objects from rotating, which is proportional to the force normal between the surfaces and the CoF between the two materials. Methods for calculating pure friction moments are presented by [6],[7]. Yet, pure rotation or translation is rarely

the case. [10] and [11] derived an effective method for calculating the frictional force and moment in case of a combination of a rotational and translational sliding movement.

2.3.1.1 friction cone

The friction cone concept is a way to model the forces that act on an object in contact with a surface. It states that the forces can be represented as a cone shape, with the base touching the surface and the apex pointing away from it. The size and shape of the friction cone depend on the properties of the object and surface, such as the CoF and the normal force. The total contact force must lie on or inside the cone. If the contact is sliding, the force felt by the object lies on the boundary of the friction cone maximally opposing the motion of the object relative to the contacting surface.

2.3.1.2 Center point definitions

Different definitions are used in the literature to indicate points in the slider plane. The most important definitions are described below. The Center Of Mass (COM) is the center of the mass distribution. The Center Of Pressure (COP) is the center of the pressure distribution between a sliding object and a support surface. When there are no external forces acting on an object, the COM is equal to the COP [10]. The Center Of Twist (COT) is the Center Of Rotation (COR) of an object when a pure moment is applied to it. Center Of Friction is the center of all friction forces during pure translation [10]. For uniform isotropic friction with only in-plane loads, all points (COM, COP, COT, COF) coincide.

2.3.2 Impact of bodies

During impact, energy is mainly dissipated in one of two ways: localized plastic deformation and energy transfer to elastic vibrations [34]. Energy dissipation through elastic vibrations is large for bodies with an elongated shape (bars, beams) while this effect is much smaller for bodies with dimensions in three mutually perpendicular directions of the same order. The kinetic energy loss is therefore characterized by the energy loss due to local deformations [28]. The most popular model for describing local deformations during impact is the linear Kelvin model [38], [39]. This model consists of a spring with stiffness k_p and a damper with a damping factor b_p connected in parallel (Figure 2.3a). The spring is used to account for the elastic deformation forces in the body and the damper for the absorption and dissipation of kinetic energy. The impact force F on the bodies can be calculated as:

$$F = b_p \dot{D} + k_p D \quad (2.1)$$

where:

D = deformation of colliding bodies ($D = y_b - y_p$)

\dot{D} = speed of deformation of colliding bodies ($\dot{D} = \dot{y}_b - \dot{y}_p$)

b_p = damping coefficient package

k_p = stiffness package

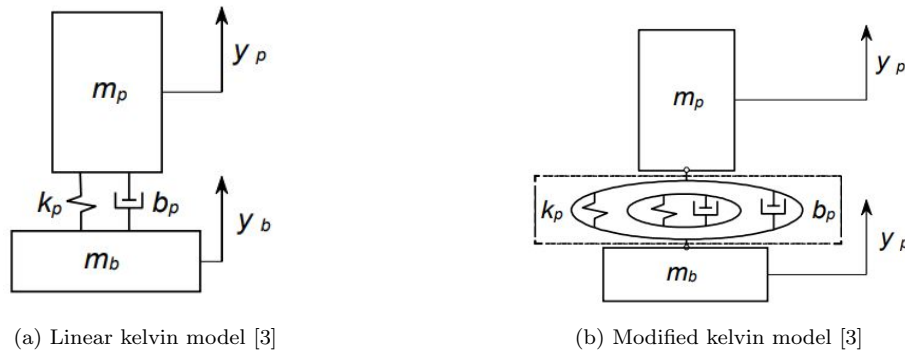


Figure 2.3: Impact models applicable for automated material handling equipment

2.4 Slider and carrier design patents

Minor features in slider and carrier design can have a large impact on sorter performance. Therefore, it is common in the industry to patent new slider designs when proven successful. 44 patents related to slider and carrier design have been reviewed. Many patents describe similar designs with minor differences, therefore the most important patents and features are described below.

All patents describe some kind of slider or pushing block, sliding along a carrier. Moreover, in all designs, the slider is actuated by a pin and wheel mechanisms. Nearly all slider designs have a pusher face (the face that comes in contact with parcels) angled to match the outfeed angle. The angles range between 0 and 45° relative to the travelling direction. The obvious reason for this is to maximize the contact area with parcels.

Most market-leading companies have a slider design featuring a rubber component positioned at the pusher face as illustrated in Figure 2.4, which is often referred to as "bumper". The bumper mostly consists of a material with a lower stiffness than the rest of the slider. The bumper is incorporated to increase gentle product handling (due to softness) and increase traction between the slider and product to reduce product slippage.

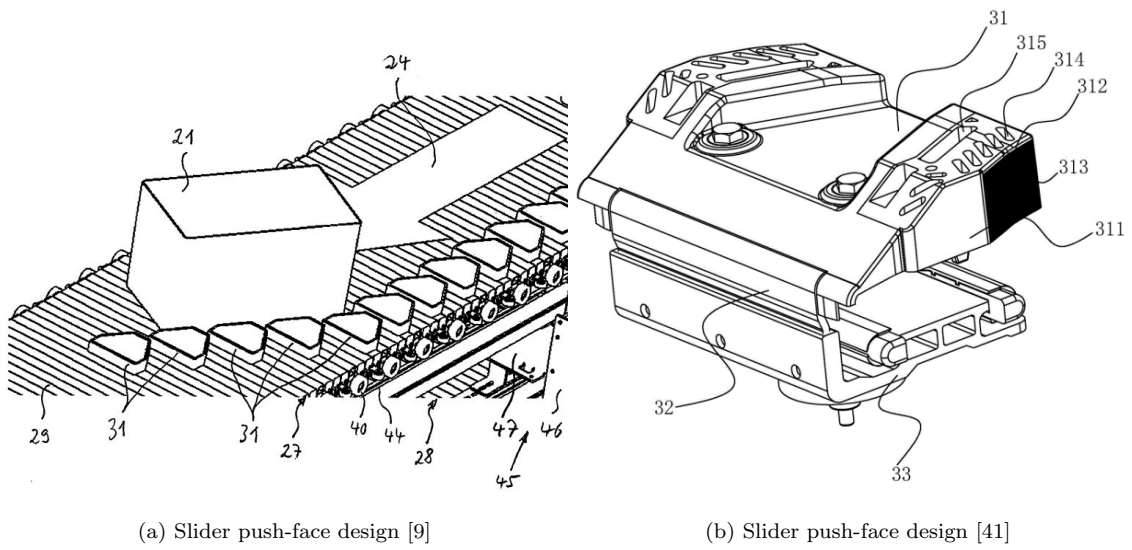


Figure 2.4: Slider design patents

Chapter 3

System analysis and design requirements

The sorter and its requirements are analysed in this chapter. Upstream and downstream equipment is analysed as well since these also influence the performance of the entire sortation system. Finally, parcel types, which could be processed on the system are analyzed by identifying and classifying their important characteristics.

A typical PDS sortation system comprises of a sorter, upstream equipment which are the Parcel Contour Scanner (PCS) and Parcel Gap Generator (PGG) and downstream equipment (outfeeds) and a recirculation loop (Figure 3.1).

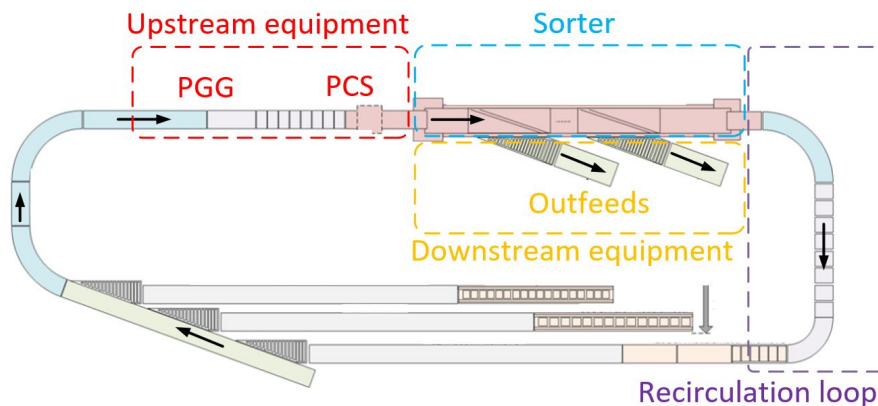


Figure 3.1: Standard lay-out PDS system [14]

3.1 Upstream equipment

Upstream equipment determines the state in which parcels enter the sorter (orientation, position and gap between parcels). Upstream equipment also determines what information is available about a parcel when it is fed to the system.

Two modules positioned upstream of the sorter, are important to consider in greater detail; the PGG and PCS (Figure 3.2). The PGG consists of multiple conveyor belts to which a stream of products with random gaps is fed. The machine creates customized gaps between products based on their transport length.

The PCS determines the required parcel properties, as described in Section D.2 (confidential Appendix).

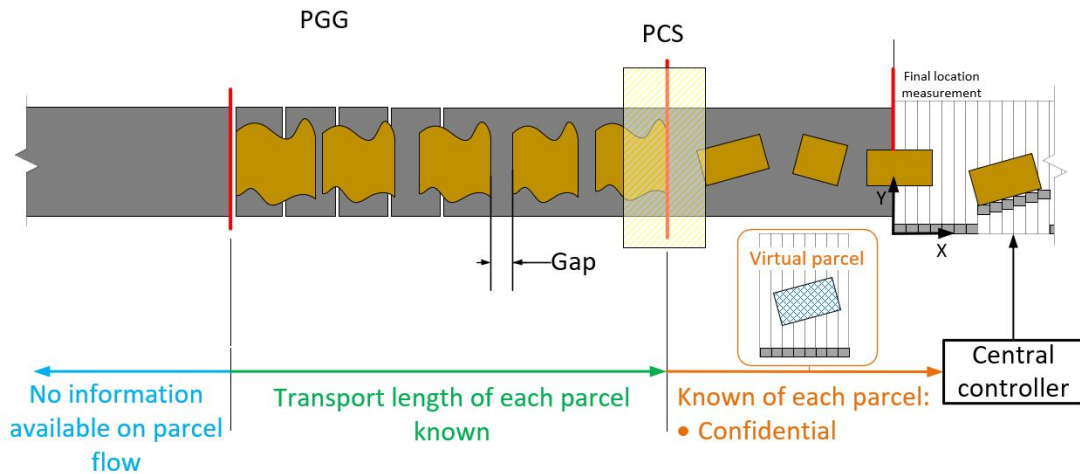


Figure 3.2: Explanation of the upstream equipment (PCS and PGG)

3.2 Parcel input position and orientation

Equipment upstream will ensure the parcel is always fed to the system in a specific orientation (the longest dimension aligned in the transport direction). Moreover, the parcel is always fed to the system in an orientation such that the height is equal to or lower than the width. Condition 3.1 thus holds for all parcels. Parcels are fed to the system in this orientation since it is the most advantageous orientation to ensure stable behaviour.

$$L_p \geq W_p \geq H_p \quad (3.1)$$

However, since this equipment has its limitations, the parcels are not always perfectly aligned (see $\theta_{mhu_initial}$ in Figure 3.3). The y-position of the parcel is random, however, there will always be a margin on both sides of the sorter which the parcel does not touch (highlighted in blue). The x-position with respect to the carriers is also random.

3.3 Sorter analysis

The new sorter principle proposed by M. de Jager has been analyzed briefly in Section 1.1.3, yet the overall sort operations have not yet been analyzed. A detailed description of the system is given in Section D.3 (confidential appendix). A simplified description is stated here. Item enters the PCS and the required parcel properties are gathered. Based on this information, the central controller defines sort trajectories (see Figure 12 in the confidential appendix). These sort trajectories are then executed by the individual drives attached to each carrier.

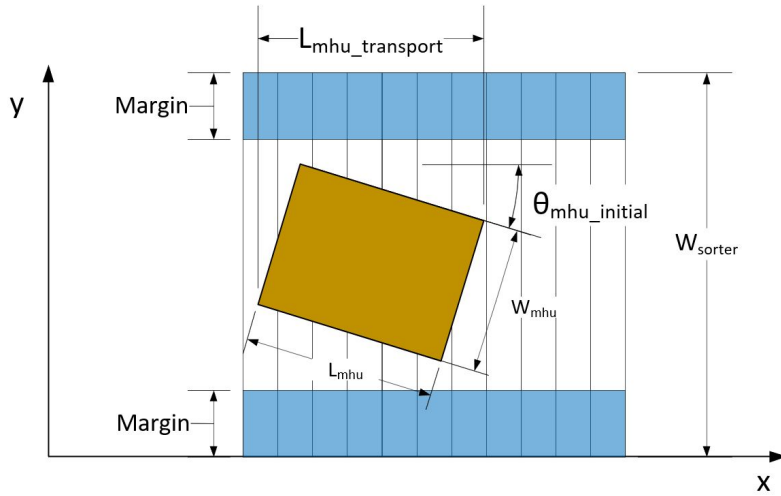


Figure 3.3: Parcel input state

3.4 Downstream equipment (outfeed)

The main parameters of the outfeed (Figure 3.4) are its angle ($\theta_{outfeed}$) and width ($W_{outfeed}$). These two parameters determine the length of the outfeed window ($L_{outfeed_window}$). The overall sorter length is determined by this outfeed window length and the number of outfeeds on the same side ($N_{outfeeds}$). The sorter length is determined by Equation 3.2.

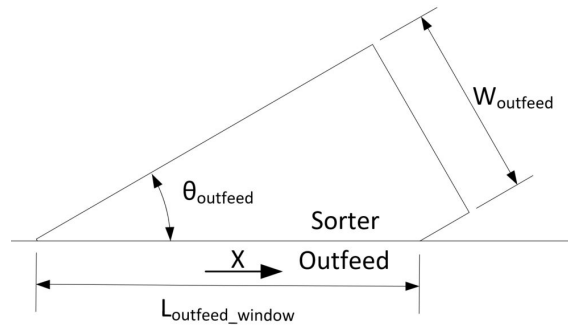


Figure 3.4: Main attributes of an outfeed

$$L_{sorter} = N_{outfeeds} * \frac{W_{outfeed}}{\sin(\theta_{outfeed})} \quad (3.2)$$

Note: this equation does not include margins between the outfeeds.

3.4.1 Outfeeds

Outfeeds come in different types, listed below. The type of outfeed determines the constraints on the position, orientation and motion of the MHU when it enters the outfeed.

- Driven
 - Roller

- Belt
- Non-driven (gravity)
 - Roller
 - Slider (metal, wood, plastic)

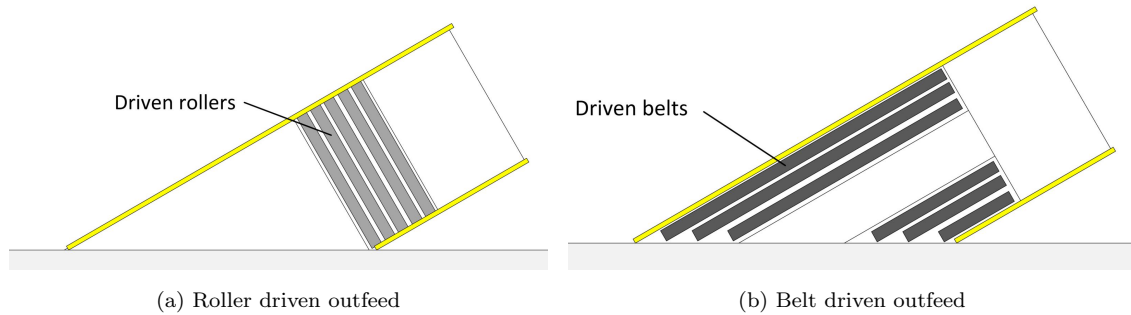


Figure 3.5: Critical outfeed types

The outfeed width is determined by three aspects; the physical dimensions of the parcels, the sort strategy (explained in Section 1.1.2) and a margin due to inaccuracies in parcel behaviour. The largest parcel will be sorted sequentially to minimize the outfeed width. The outfeed width will thus be determined by the width of the largest parcel and the inaccuracies in its behaviour. The sort accuracy of large parcels is thus important since these determine the outfeed dimensions.

3.5 Material Handling Unit (MHU) analysis

One of the main challenges of the sorter is handling a large range of parcels and the varying characteristics that come with this. Parcel characteristics which influence dynamic behaviour are analysed in this section. Aspects influencing for example detectability are definitely important for the entire system, but not within the framework of this study. Moreover, parcel characteristics are described both quantitatively (mass, dimensions) and qualitatively (shape, packaging material).

3.5.1 Geometric shape

The geometric shape of a parcel influences the locations of the contact points with the carrier and slider. This in turn influences its behaviour. A classification of parcel shapes is shown in Figure 3.6. A variable shape means that the shape can change significantly during contact with material handling systems.

Shape	Example			
Cubic				
Flat				
Cylindrical				
Convex				
Other				
Variable				

Figure 3.6: Geometrical parcel shape classification

3.5.2 dimensions and weight

The dimensions and weight of parcels can vary from a 20 gram envelope ($L \times W \times H$: $100 \times 50 \times 1 \text{ mm}$) to a 70 kg fridge ($1500 \times 1000 \times 1000 \text{ mm}$). The maximal, minimal and average dimensions of parcels are given in Table D.3 in the confidential appendix.

3.5.3 Base shape

Even though some parcels seem to have a perfectly flat base shape (such as a cardboard box for example), there can be small deviations in the shape which can influence on its behaviour significantly (Figure 3.7). Moreover, the base shape can have various surface patterns, some typical patterns are shown in Figure 3.8.

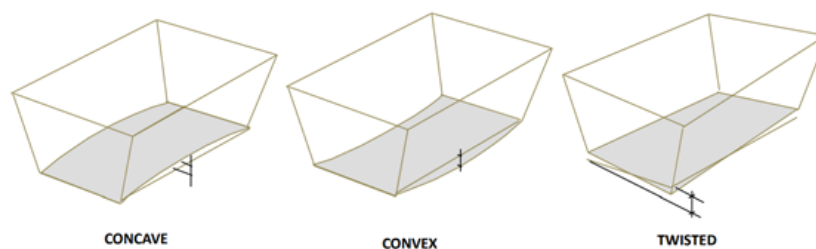


Figure 3.7: Base surface shape deviations [14]

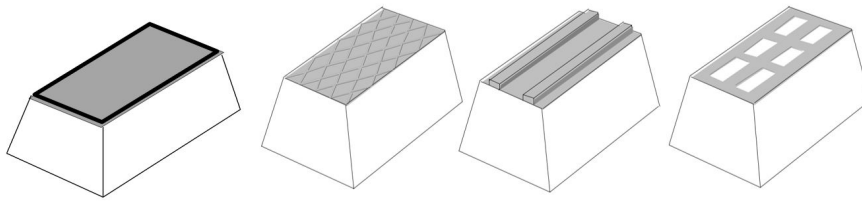


Figure 3.8: Examples of MHU base surface patterns [14]

The shape and stiffness of both the MHU and the carrier surface influence the pressure distribution on the base surface of the MHU. The scheme in Figure 3.9 can be used to classify the pressure distribution profile.

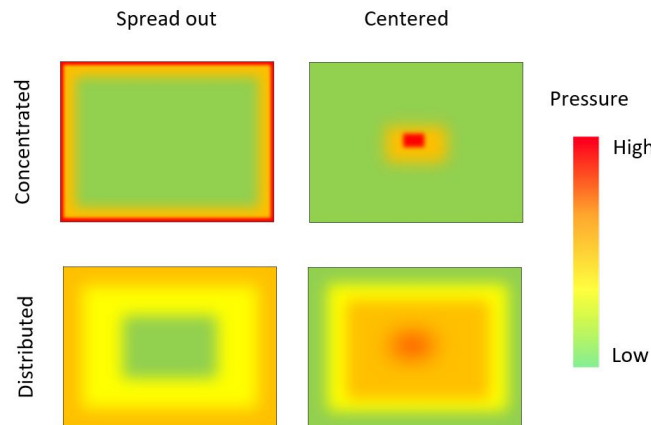


Figure 3.9: Pressure profile classification of parcel bottom surface

Note: The location of the COP is in the middle in all four Figures, yet does not have to be the case.

3.5.4 Packaging material

Packaging material can be distinguished into primary and secondary packaging (Figure 3.10). The primary packaging material comes into contact with the sorter equipment and thus has the greatest influence on the material behaviour. The secondary packaging material mainly influences the stiffness of the package (in case the primary packaging is flexible). Secondary packaging also influences the stability of the content. The main types of packaging materials used in the industry are given in Table 3.1.

The tensile strength of these materials is shown in Figure A.3. Yet, when these materials are processed into packing (such as a box for example) these properties become highly non-homogeneous and anisotropic and could thus deviate from the indicated values.

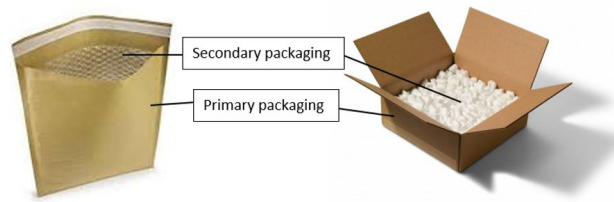


Figure 3.10: Primary and secondary packaging ([27] and [22] are used for illustration)

Primary packaging	Secondary packaging (padding)
Plywood / wood	
Metal	
Plastic	Foam pallets
Chipboard	Polyester fiber
Corrugated cardboard	Schredded cardboard
Paperboard (kraft paper)	Corrugated cardboard
Solid cardboard	Bubble wrap
Plastic foil	Padded bubble wrap
Woven fabric	
Plastic foam	

Table 3.1: Packaging materials [35], [37]

Apart from the packaging material, the parcels can have additional (external) features such as shown in Figure 3.11.

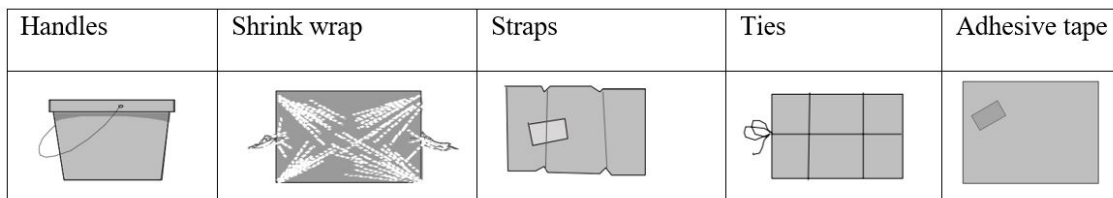


Figure 3.11: Additional (external) packaging features [15]

3.5.5 Content

The type of content in a parcel is not of interest. However, the state of the content (Figure 3.12) can vary, influencing two important parcel characteristics; content stability and the COM location. Content stability is categorized into four groups, based on the banking angle (in degrees) at which content starts sliding (Table 3.2). To put these angles in perspective, a bank angle of 45 degrees exerts a similar force on the content as a horizontal acceleration of about $7 m/s^2$.

The COM can theoretically have any position within the MHU, however, VI sets bounds on the COM location (Figure 3.13) to prevent problematic parcel behaviour.

Content stability	Stable MHU banking angle [°]
Fixed	≥ 45
semi fixed	20 – 45
semi-loose	5 – 30
loose	≤ 5

Table 3.2: MHU content stability classification scheme

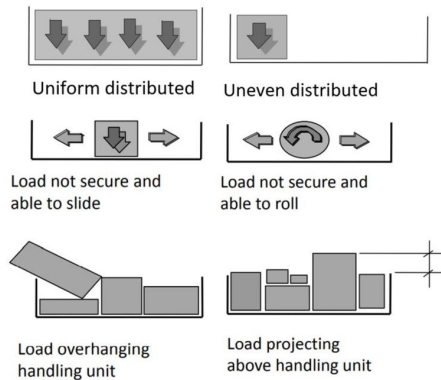


Figure 3.12: State of MHU content [15]

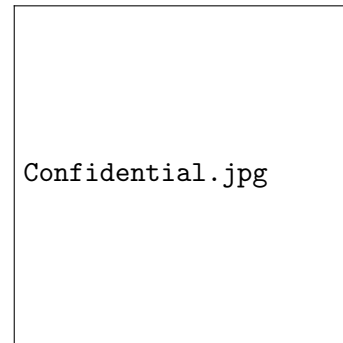


Figure 3.13: COM location envelope

Besides the COM, the mass distribution is also of importance. The mass distribution influences the moment of inertia of the body. The moment of inertia influences the rotation behaviour of the parcel. The classification scheme in Figure 3.14 is used to classify the moment of inertia. A qualitative scheme is used since no numerical bounds are set by VI on the moment of inertia.

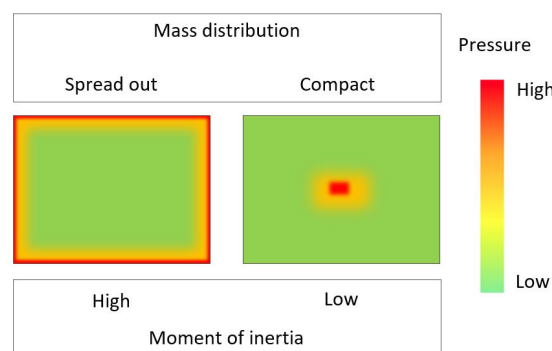


Figure 3.14: Moment of inertia classification scheme

Note: the location of the COM is in the middle in the figures, yet it is not constrained to this position.

3.5.6 Structural rigidity

Packages range in stiffness, from rigid products such as metal paint cans to soft clothing bags. It is not possible to classify the stiffness with a single value because the stiffness properties are highly non-homogeneous and isotropic. The classification scheme in Figure 3.15 is therefore used.


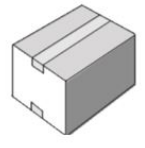


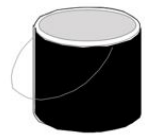



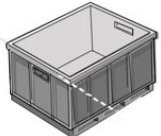


Rigid: No deformations can be observed after contact with MHE.	Semi-rigid: The overall shape of package is maintained after contact with MHE. Small local deformations can be observed.	Flexible: The package is bent or twisted when in contact with MHE, but the overall shape is maintained.	Soft: The package completely deforms after contact with MHE, the overall shape completely changes.
			
			
			

Figure 3.15: MHU structural rigidity classification [32]

3.6 Key Performance Indicators (KPIs)

A pre-study [1] defined eight key drivers for the development of the new sorter. Five of these key drivers are of interest to the current study. These key drivers serve as a foundation for defining the Key Performance Indicators (KPIs). The key drivers and how they can be impacted within the framework of the current study are explained below.

- **Accuracy:** minimize the difference between the expected parcel state and the actual parcel state when it enters the outfeed.
- **Capacity:** minimize the space (in the x-direction) used by each parcel throughout the sort process.
- **Gentle handling:** prevent damaging parcels during the sort process.
- **Cost:** the cost of the sorter approximately scales with its length. The length is determined by the width of each outfeed, determined by sort accuracy. Thus maximizing the sorting accuracy minimizes the sorter cost.

The system aspects are influenced by three variables related to the state of the parcel (Figure 3.16). These variables, together with the state of both the parcel and the sorter (in terms of damage) are the KPIs used in the current study.

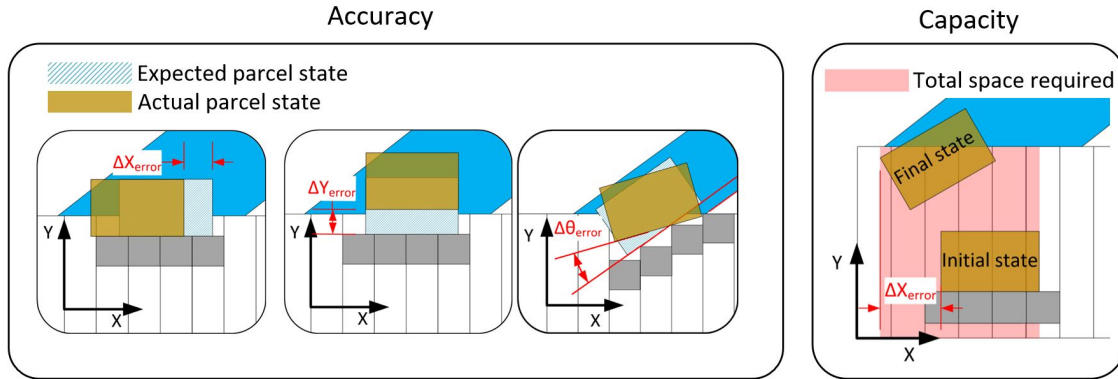


Figure 3.16: Illustration KPIs

The KPI related to the sorter capacity (x-displacement error) should be minimized throughout the whole sort process. The KPIs related to the outfeed width and downstream requirements are only of interest when the parcel enters the outfeed.

Even though the parcel's motion (velocity direction, velocity magnitude and angular velocity) is essential for the sort accuracy, it is not necessary to monitor this separately for this study. Since any deviation in the motion of the parcel can already be detected due to a deviation in the position or orientation. This concludes the KPIs in Table 3.3.

Domain	Variable	Description	When
Parcel	Δx_{error}	x-position error	Throughout entire process
	Δy_{error}	y-position error	When entering the outfeed
	$\Delta \theta_{error}$	Orientation error	
	Damage		Throughout entire process
Sorter	Damage		Throughout entire process

Table 3.3: KPIs

Moreover, there is also a difference between parallel and sequential sorting. When a parcel is sorted sequentially, the x-displacement error does not influence the sorting accuracy since the parcel is aligned with the outfeed. This is explained in greater detail in Section A.4.

3.7 Conclusion

The KPIs for the current study are derived (Table 3.3), answering sub-questions 1 (which was defined in Section 1.3). System requirements and parcel characteristics which influence

parcel behaviour are identified and analyzed (concluding sub-question 2). These variables are summarized in Table 3.4. These variable notations will be used to analyse the parcel behaviour in the next chapter.

	Input variables	Description	Range
MHU characteristics	L_{mhu}	MHU length	Confidential
	W_{mhu}	MHU width	Confidential
	H_{mhu}	MHU height	Confidential
	m_{mhu}	Mass of MHU	Confidential
	$I_{x,mhu}$	Moment of inertia of MHU around x-axis	No range defined
	$I_{y,mhu}$	Moment of inertia of MHU around y-axis	No range defined
	$I_{z,mhu}$	Moment of inertia of MHU around z-axis	No range defined
	x_{com}	COM position in x-direction	Confidential
	y_{com}	COM position in y-direction	Confidential
	z_{com}	COM position in z-direction	Confidential
		Structural rigidity	Rigid, semi-rigid, limp or soft
		Strength	Strong, average or weak
		Content stability	Fixed, semi-fixed, semi-loose or loose
	Pressure profile between slider and MHU	Centered or spread out Concentrated or distributed	
MHU input state	$y_{mhu,initial}$	Initial parcel position in y-direction (when fed to the sorter)	Confidential
	$x_{mhu,initial}$	Initial parcel position in x-direction (when fed to the sorter) with respect to the carriers	Confidential
	$\theta_{mhu,initial}$	Initial orientation (around z-axis)	Confidential
Sorter settings	$v_{transport}$	Transport speed of sorter (in x-direction)	Confidential
	v_y	Divert speed	Confidential
	$a_{\{slider\}}$	slider acceleration	Confidential
	$\alpha_{outfeed}$	Outfeed angle	Confidential
	W_{sorter}	Sorter width	Confidential
		slider/carrier pitch ¹⁾	Confidential
		Sort direction	Single sided and dual sided
	Sort strategy	Parallel and sequential	
1) The slider/carrier pitch is fixed since the new carriers should be retrofitable on older generation sorters.			

Table 3.4: (Uncontrollable) input variables

Note: the table included confidential ranges can be found in the confidential appendix

Chapter 4

Unwanted parcel behaviour analysis

Unwanted parcel behaviour is analysed in this chapter. First, all types of potential unwanted parcel behaviour are identified. Then the physical causes for each type of behaviour are analyzed. By a combination of experiments and theoretical analysis, a conclusion is drawn about which of the risks are significant and which can be discarded.

When analyzing parcel behaviour, it is necessary to focus on the unwanted behaviour of critical parcels and load scenarios. These "rare" scenarios become relevant due to the large number of parcels handled on the system. Some risks are discarded after analysis because they proved insignificant based on worst-case scenario tests.

The following sources were used as input for identifying unwanted parcel behaviour.

- Interviews with internal experts
- Previous test reports
- Site visit
- Literature review

Risks are separated and classified based on their physical causes and the outcome. This resulted in twenty individual unwanted parcel behaviour types (Figure 4.1).

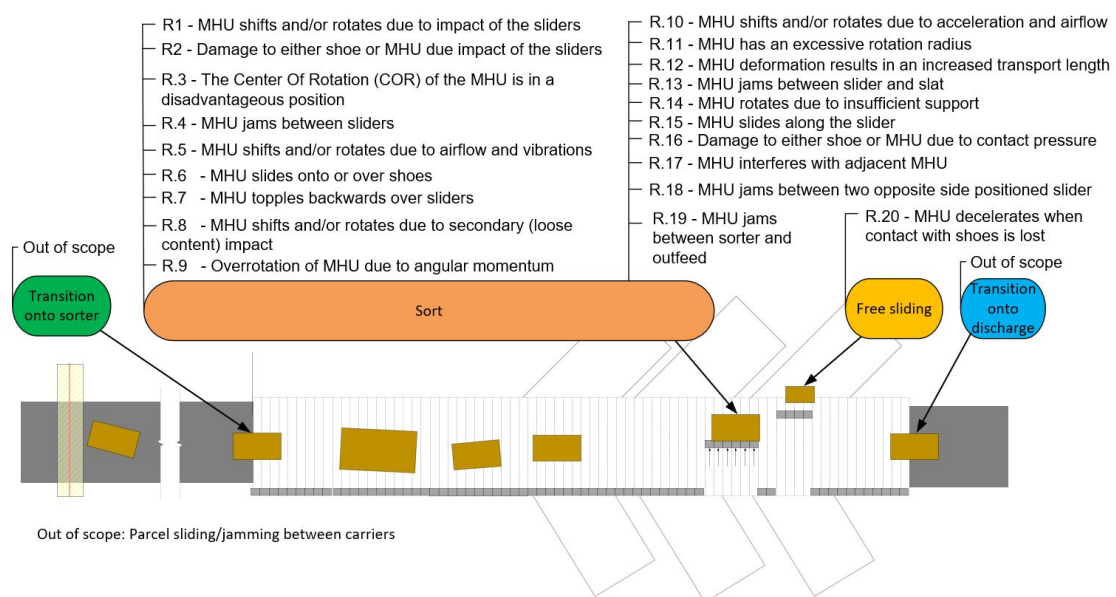


Figure 4.1: Identified potentially unwanted parcel behaviour types

4.1 Design parameters

The slider and carrier design are represented by their most important parameters. These parameters are referred to as design parameters and are shown in Figure 4.2 (and summarized in Table 4.1). This translation into parameters is done in order to gain insights into the influence of the slider and carrier design through inspecting equations (related to parcel behaviour). The friction coefficients are split into orientation and direction-dependent components. Moreover, the tangential slider friction coefficient (μ_{s_tan} in the figure below) is a function of the MHU angle. This angle is positive in the direction of the outfeed in which the parcel is sorted (Figure 4.3).

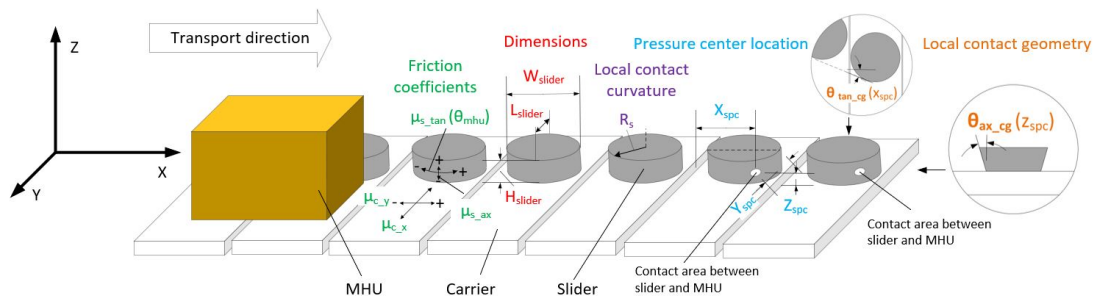


Figure 4.2: slider and carrier design: controllable variables

Note 1: A cylindrical slider shape is only used for explaining the design parameters, the slider shape is not constrained to any shape.

Note 2: the positive y -direction always points towards the outfeed in which the parcel will be sorted. The y -direction in this figure is thus opposite from all other figures used in this report.

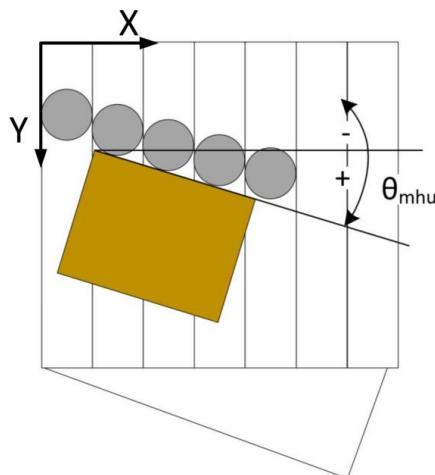


Figure 4.3: MHU angle definition

Component	Parameter type	Variable	Description
Carrier design	Friction coefficient	$\mu_{c.x}$	The CoF between the carrier and the MHU in the x-direction
		$\mu_{c.y}$	The CoF between the carrier and the MHU in the y-direction
slider design	Friction coefficient	$\mu_{s.tan}$	The CoF between the slider and the MHU in the tangential direction
		$\mu_{s.ax}$	The CoF between the slider and the MHU in the axial
	Dimensions	H_{slider}	slider height
		W_{slider}	slider width
		L_{slider}	slider length
	Pressure center location	x_{spc}	The COP exerted by the slider on the MHU in the x-direction
		y_{spc}	The COP exerted by the slider on the MHU in the y-direction
		z_{spc}	The COP exerted by the slider on the MHU in the z-direction
	Contact geometry	$\theta_{tan.cg}$	The slider geometry at the contact area with respect to the x-axis
		$\theta_{ax.cg}$	The slider geometry at the contact area with respect to the z-axis
Local contact curvature	R_{slider}	The local contact curvature of the slider	

Table 4.1: (Controllable) Design parameters

4.2 Research methodology

Two research methods were explored for quantitative analysis of the material behaviour; computer simulation and physical experimentation. Both methods are graded (Table 4.2) in four aspects considered important (Reliability/precision, cost, labour and flexibility).

Physical experiment-based research is chosen mainly due to the superior precision and the advantage that there is no need to build a model, which can be very time costly. The identified unwanted parcel behaviour modes (Figure 4.1) have varying physical causes, this would thus require building multiple models to cover all problems. Moreover, normally, the main advantage of computer simulation over physical experimentation is that there is no need to build the actual system. However, a test setup has already been built by VI. Another advantage of computer simulation is its flexibility to change certain variables and quickly find the system response, yet this does not weigh against the advantages of physical experimentation in this case.

To measure the system response (KPIs) on the test setup there are multiple measurement methods and instruments that can be used (Table 4.3). "Quantity and quality of

Research method	Computer simulation	Physical experiments
Reliability/ precision	-	+
Cost	0	0
Labor	-	+
Flexibility	+	0

Table 4.2: Comparison of research methods for quantitative analysis of parcel behaviour (grading +, 0, -)

measurement data” refers to the amount of data gained from the measurement. With the measurement tape for example it is only possible to determine the final state of the parcel, while the other instruments are capable of measuring the state throughout the test. A tracking camera is chosen since it is superior to the other measurement instruments in all aspects

Measurement method	Physical tracking	Optical tracking		Inertial tracking
Measurement instrument	Measurement tape	Video camera	Tracking camera	Inertial tracking unit
Description	Physical measuring initial and final state of package.	Motion tracking of package from video frame image analysis.	Multiple infrared camera tracks the position of markers placed on the package.	Place inertial tracking unit in package and track acceleration, derive position by mathematical means.
Accuracy	+	+	+	-
Convenience	-	-	+	-
Availability	+	+	+	+
Quality and quantity of measurement data	-	-/+	+	-

Table 4.3: Comparison of instruments to measure KPIs on test setup

The tracking camera measures the position (in three dimensions) of markers placed on the parcel with a frequency of 120 Hz (see Figure 4.4). It uses this information to determine the state of the parcel in all six degrees of freedom (position and orientation). The tracking camera has an accuracy of 0.5 mm, which is well within tolerance. The tracking data is exported as a comma-separated value (CSV) file for post-processing in Matlab. The y-position error is determined using the video recording instead of the measurement data. This is done because it is difficult to accurately determine this error from the data. Moreover, exploratory tests showed that this error is zero in nearly all cases.

4.2.1 General assumptions

The simple Coulomb friction model (only considering one friction coefficient instead of static and dynamic) is used to simplify the analysis. This assumption is acceptable since the theoretical analysis is mainly qualitative. Also, all parcels are assumed to have the same friction coefficient over the whole base surface. Besides, the assumption is made that no out-plane forces act on the parcel (unless stated otherwise). Therefore, the center of mass (COM) in the calculations is thus equal to the center of friction (COF) as is explained in Section 2.3.1.2.

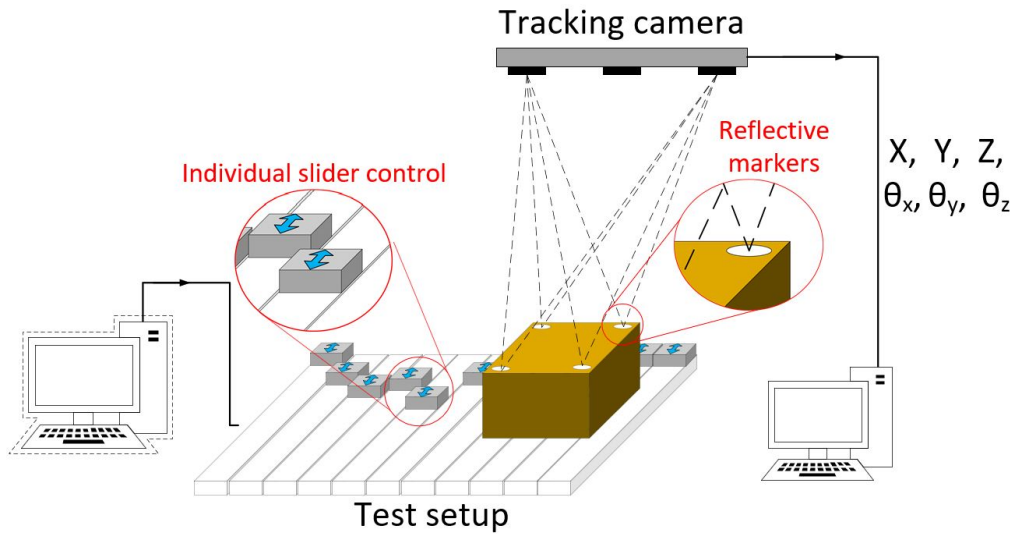


Figure 4.4: Test setup for simulating sort behaviour

For risks related to sequential sorting (rotation of parcels), only cubical shapes are analysed since this captures the majority of large parcels (small parcels are sorted parallel and are thus not rotated).

4.3 Shift and rotation due to the impact

The impact of the sliders on a parcel is one of the main issues for a regular sliding PDS. When the sliders start accelerating, one or multiple sliders will hit the parcel with an impact speed ($v_{impact} = \sqrt{2a_{slider}\Delta y_{error}}$, [24]). This impact could result in bouncing behaviour (loss of contact), which in turn results in KPI errors.

A model for this impact event is presented by Piatkowski [29] and is shown in Figure A.5. As described in Section 2.3.2, during the impact of packages, energy is mainly dissipated through plastic deformation. The impact event can be split into two separate successive events: impact (during contact) and free sliding (after contact). The velocity of the parcel after impact depends on the impact force. The impact force can be calculated using the kelvin model presented in Section 2.3.2.

Regarding the free sliding phase, the sliding distance can be determined by using conservation of energy (Equation 4.1). The difference in kinetic energy (before and after sliding) is equal to the work done by the friction force, since the carriers are horizontal, no work is done by the force resulting from gravity. Moreover, aerodynamic forces are neglected. From Equation 4.2 can be concluded that the only design parameter influencing

the free sliding distance is the carrier friction coefficient ($\mu_c = [\mu_{c,x}, \mu_{c,x}]^T$).

$$E_k = E_w \quad (4.1a)$$

$$\frac{1}{2}m_{mhu}(\Delta v_c)^2 = m_{mhu} * g * \mu_c * d_{slid_dis} \quad (4.1b)$$

Resulting in:

$$\begin{cases} d_{slid_dis-x} = \frac{(x_c)^2}{2g\mu_{c-x}} \\ d_{slid_dis-y} = \frac{(y_c)^2}{2g\mu_{c-y}} \end{cases} \quad (4.2)$$

For this problem, there can be a range of critical parcel types, some products are relatively stiff (plastic crates for example) and some are light (envelopes for example). A test is done to determine which product behaves worse upon impact. In the test (illustrated in Figure 4.5a), the sliders impact multiple parcels in a similar way, the sliders are stopped right after the impact event and the distance between the sliders and the MHU (sliding distance) is measured. The measurement results are represented in a box plot (Figure 4.5b), showing the median and spread of five measurements. A description of parcels used in this test can be found in the confidential appendix.

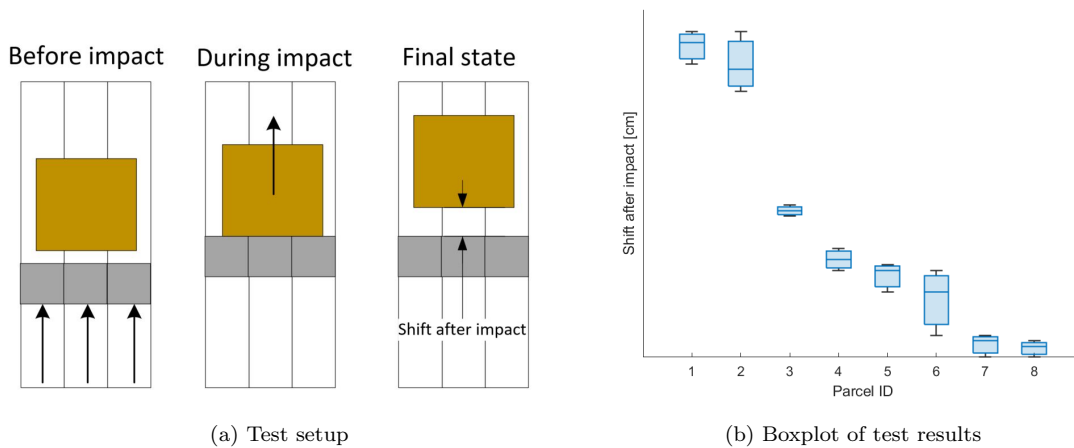


Figure 4.5: Test for determining what parcel behaves worst upon impact

Parcels 1 and 2, bounce the furthest after impact. Parcel 2 is expected to be the more critical of the two since it is this parcel could be sorted sequentially, which is not the case for parcel 1. Parcel 2 is therefore used to test the consequence of a position inaccuracy. Moreover, two more parcels are added to this test set for redundancy.

The test report can be found in Section D.6 (confidential appendix). The most important results are shown in Figure 4.6. These graphs show the orientation error (as illustrated in Figure 3.16) of each parcel as it moves across the sorter (in the y-direction). The initial orientation of the parcels in this test is 0° , and the required orientation is 30° , therefore, the measurement starts with an orientation error of -30° . A vertical line indicates the closest position where an outfeed could be. This corresponds to a parcel with an

initial position closest to the outfeed. The right-hand side of the plot corresponds to the furthest outfeed position. This corresponds to a parcel with an initial position furthest from the outfeed. Error bars indicate the standard deviation in parcel behaviour over five measurements.

From the graphs can be concluded that parcel 2, which has the worst characteristics in the view of impact and bounce, does not perform worst in this test. The parcel even behaves better with an initial offset than without. This is due to a reduced friction coefficient resulting from the bouncing behaviour, which reduces other problematic behaviour this parcel has (this specific behaviour will be discussed in Section 4.9). For the other two parcels, the offset slightly magnifies unwanted behaviour that can already be seen in the baseline measurement. Expected is that when the problems already present in the baseline measurements are reduced or mitigated, an offset (distance is confidential) will thus have little influence on the sort performance.

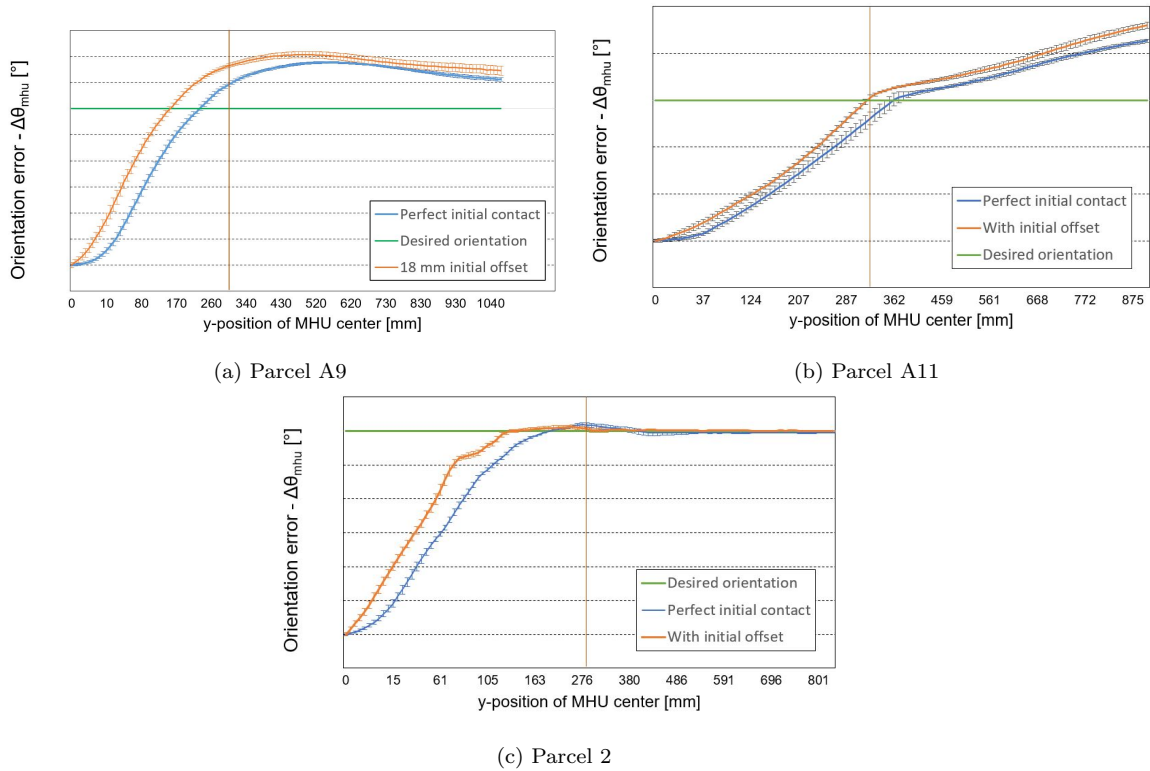


Figure 4.6: Initial impact test results - Orientation error ($\Delta\theta_{error}$) (vertical line indicates the first possible outfeed position)

Note: Numerical values have been removed from the graphs due to confidentiality

Therefore, sorting with the specified approach uncertainty (stated in Section 2 in the confidential appendix) is acceptable. No additional measures are required for this risk. Also, during the experiments, no damage occurred to the sliders or the parcels.

Both risks R1 and R2 can be discarded based on experiment results.

Note: R.1: MHU shifts and/or rotates due to the impact of the sliders. R.2: Damage to either slider or MHU due to impact of the sliders.

4.4 Drift due to airflow and vibrations

When parcels are transported to their designated outfeed, they could shift backwards (Figure 4.7). Even if the shift rate is low (in the range of mm/s), it can still add up to a significant distance after travelling an entire sorter length.

Two phenomena cause the shift; vibrations of the carriers and airflow. The vibrations are caused by moving parts in the sorter and propagating through the carriers to the packages on top. Vibrations can reduce the friction coefficient, depending on the: amplitude, frequency, contact stiffness and direction of the vibrations [30].

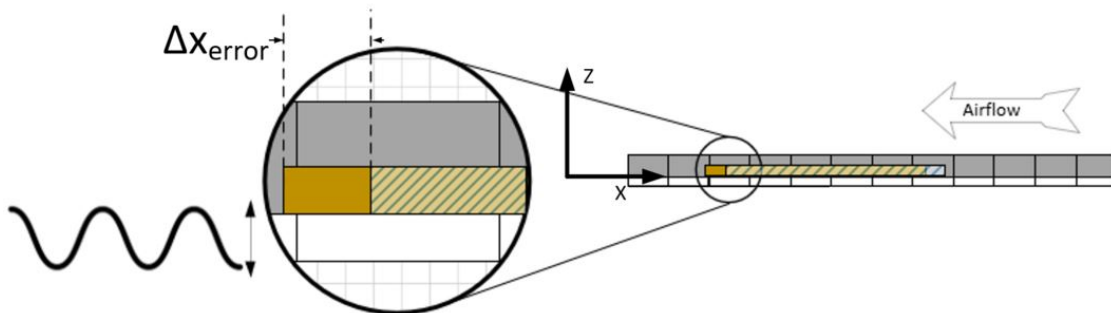


Figure 4.7: MHU drift due to airflow and vibrations

The influence of airflow can be split into two parts [32]:

- The airflow resistance of the body;
- The lift force on the parcel, especially the influence of the airflow between the bottom of the parcel and the carriers.

The effect of airflow on the parcels can be researched by simulation. Hafner [12] visualized the airflow around a plastic bag by using Computational Fluid Dynamics (CFD) simulations (Figure 4.8). A graph (Figure A.8) is derived from the simulation with the flow coefficients (drag coefficient and lift coefficient) for different flow directions. This method can be very valuable in gaining insights into the aerodynamic flow patterns and aerodynamic forces acting on the parcel. However, these results are only representative of a single shape. Finding the aerodynamic response of a large range of parcels can thus be very challenging and time-consuming, as is also pointed out in the study.

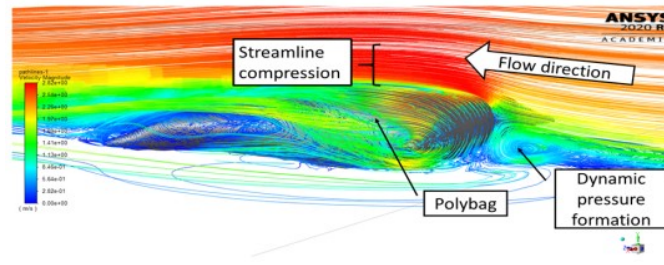


Figure 4.8: Aerodynamic simulation of MHU [12]

To get a more general understanding of the forces acting on the parcel due to airflow (shown in Figure 4.9), two general airflow equations are examined: those of lift and air resistance.

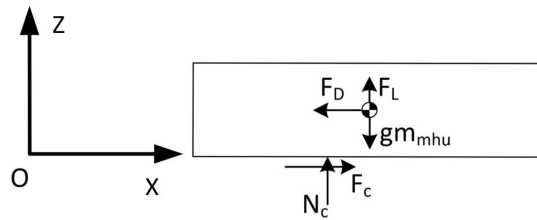


Figure 4.9: FBD of parcel on sorter when transported to outfeed

Aerodynamic lift [26]:

$$F_L = \frac{1}{2} d v^2 A_L C_L \quad (4.3)$$

where:

F_L = Lift force

d = Air density

v = velocity of airflow

A = Lift generating surface area

C_L = Lift coefficient

Aerodynamic drag [25]:

$$F_D = C_d \frac{\rho v^2}{2} A_d \quad (4.4)$$

where:

F_D = Drag force

d = Air density

v = velocity of airflow

A_d = Area of the object perpendicular to airflow

C_L = Lift coefficient

The equation of motion of the MHU can then be stated as:

$$(m_{mhu}g - F_L)\mu_{c,x}^- - F_D = m_{mhu} * \ddot{x} \quad (4.5)$$

The forces are due to the airflow scale with a factor of four and the friction force and inertia scale with a factor of eight (Figure 4.10). It is thereby expected that this problem will be most significant for small parcels. Experiments should thus be done with small lightweight parcels. An envelope with an upward folded front edge increasing its lift and drag coefficient is expected to be critical. However, there is currently no test setup available to perform experiments and draw conclusions on this problem.

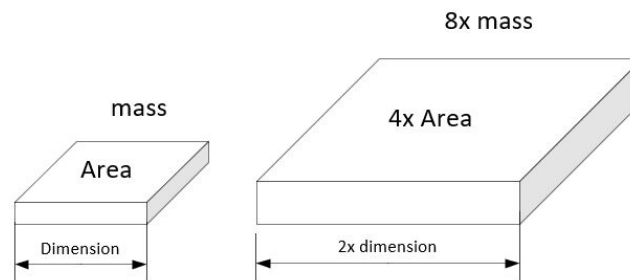


Figure 4.10: Relation between dimensions, surface area and mass of MHU's

No conclusions can be drawn on risks R5 and R.10 at this stage, additional testing is required when a test setup is available.

Note: *R.5: MHU shifts and/or rotates due to airflow and vibrations. R.20: MHU shifts and/or rotates due to acceleration and airflow*

4.5 Slide onto or over the sliders

During the sort action, there is a risk that MHUs fold up against or slide onto the slider. There are four potentially undesired consequences related to this risk:

1. A positional error with respect to sliders (in the y-direction) potentially resulting in a missort.
2. An increased frontal area of the package resulting in a high deceleration (due to aerodynamic drag) during the free sliding phase.
3. Friction with slider resulting in an increased deceleration during free sliding phase
4. A reduced acceleration of the parcel COM, resulting in a reduced velocity when leaving the sorter.

Within this specific problem, two cases are distinguished based on the initial contact between the slider and package: wall contact (Figure 4.11a) and corner contact (Figure 4.11b). The larger the slider height, the more parcels will be in the second category.

4.5.1 Wall contact

When a parcel makes initial wall contact, there is already an error with respect to the slider, which is referred to as the steady state overhang (Figure 4.11a). Although this

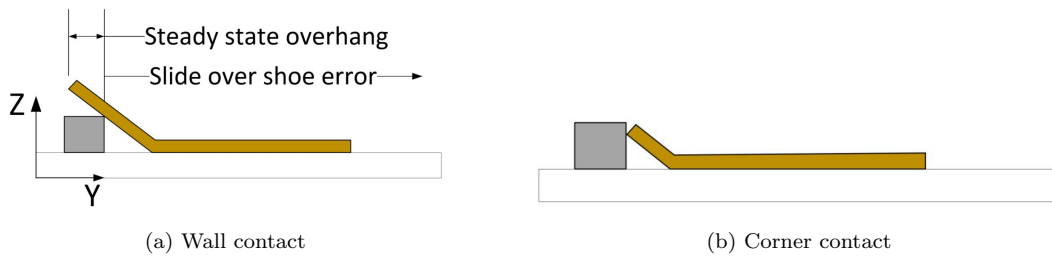


Figure 4.11: Initial contact mode for parcels with risk of sliding onto the sliders

steady state overhang is influenced by the slider height, it is considered out of scope. Increasing the slider height would result in the need for a higher scanning height. But it is possible to reduce this steady state overhang with a higher scanner on itself (by changing the slider trajectory based on it). Increasing the slider height to reduce this steady state overhang would thus have no additional benefits.

From some exploratory experiments, it became clear that critical MHUs can behave in three ways when the initial state is as shown in Figure 4.12a. Either the state of the parcel doesn't change throughout the sorting process, this is allowed and presents no problems. Another possibility is that the front flap is folded (Figure 4.12b). This is also allowed if it prevents the parcel from sliding onto the slider. The third case is that the parcel slides onto the sliders, potentially resulting in one of the four risks mentioned above.

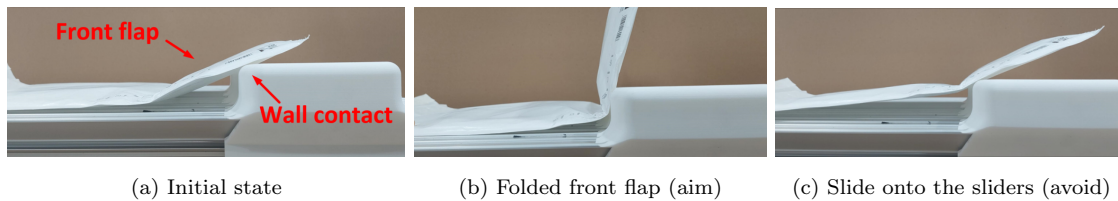


Figure 4.12: Behaviour of a flexible package with sloping front flap during sorting

The (flexible) package is presented as two rigid sections connected by a hinge with stiffness (see k_{mhu} in Figure 4.13). From analyzing the equation of motion (Section A.6 in the appendix) can be concluded that the slider friction ($\mu_{s,ax}$) should be maximized and the carrier friction ($\mu_{c,y}$) should be minimized to prevent sliding onto the slider. When the front flap of the MHU is folded, the contact normal of the slider starts pointing in the direction of movement, this prevents the MHU from sliding onto the slider further. Folding occurs when the following condition is satisfied:

$$N_s * \frac{H_{slider}}{\beta} > k_{mhu} \quad (4.6)$$

A higher slider will satisfy this condition for a larger range of packages (with varying k_{mhu} values). Maximizing the slider height thus also reduces this problem.

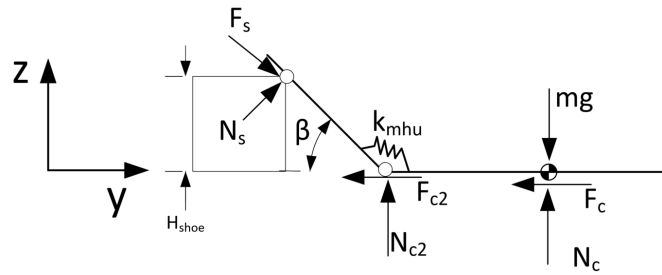


Figure 4.13: FBD of flexible MHU sliding onto the sliders (wall contact)

4.5.2 Corner contact

The second case is when a package initially makes corner contact with the slider (Figure 4.11b). In this case, the local slider geometry (θ_{ax_cg}) also becomes important (as shown in the model in Figure 4.14)

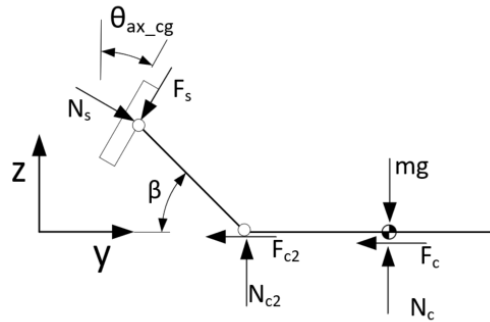


Figure 4.14: FBD of flexible MHU - sliding onto sliders

In this case, it is possible to fully prevent sliding if the following condition is satisfied:

$$\mu_{s_ax} \geq \tan^{-1}(\beta - \theta_{ax_cg}) \tag{4.7}$$

Findings from exploratory tests and a previous test performed by VI confirm the risk of parcels sliding onto or folding against the sliders (Figure 4.15). In these tests, this folding caused a missort in some cases.

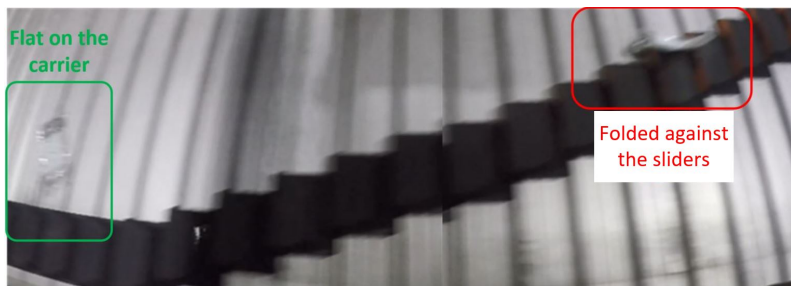


Figure 4.15: MHU folding up against the sliders (frames from video from a previous test performed by VI) [14]

Experiments show that risk R.6 is real, design improvements thus have to be implemented to reduce this risk.

Note: R.6: MHU slides onto or over sliders

This risk can be minimized by satisfying the design parameter objectives given in Table 4.4.

	Initial package state $< H_{slider}$ (corner contact)	Initial package state $> H_{slider}$ (wall contact)
Design variable	Objective	Objective
μ_{s_ax}	Maximize	Maximize
θ_{ax_cg}	Maximize	
H_{slider}		Maximize
μ_{c_y}	Minimize	Minimize

Table 4.4: Design parameter objectives risk R.6

4.6 Backward toppling over the sliders

When parcels are accelerated there is a risk of toppling backwards over the sliders. Whether this happens mainly depends on the COM location and the acceleration of the sliders. The FBD in Figure 4.16b illustrates a parcel with the worst possible COM position (within the boundaries shown in Figure 3.13). The critical acceleration before the parcel starts toppling can be calculated with Equation 4.8. A worst-case situation would be with a slider height of zero. This results in a critical acceleration of 5 m/s^2 , which is higher than the required acceleration stated in Table D. confidential appendix).

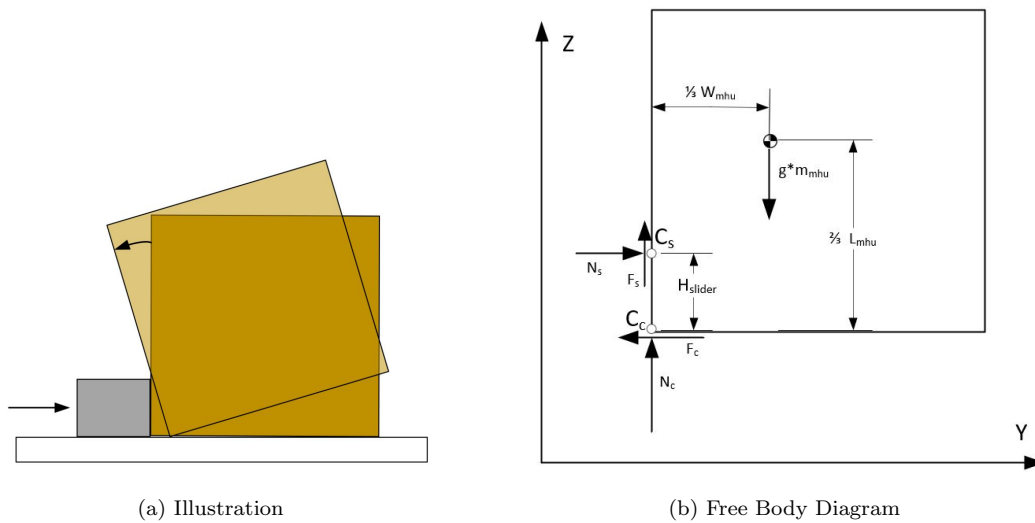


Figure 4.16: Backward toppling

$$a_{critical} = g * \frac{W_{mhu} + 3\mu_{c,y}H_{slider}}{2L_{mhu} - 3H_{slider}} \quad (4.8)$$

So it is clear that the parcel will start toppling backwards in a worst-case scenario. Yet, as long as the center of mass x-position does not move past the tipping point (indicated with C_c in Figure 4.16b) it will rotate back to a stable position after the acceleration stops. A test is done to find out how far the parcel topples backwards during maximal acceleration up to maximal speed. A block with a low height was put in front of the sliders during the test to imitate a minimal slider height. The other important input variables were in critical settings (see Table D.13 in the confidential appendix).

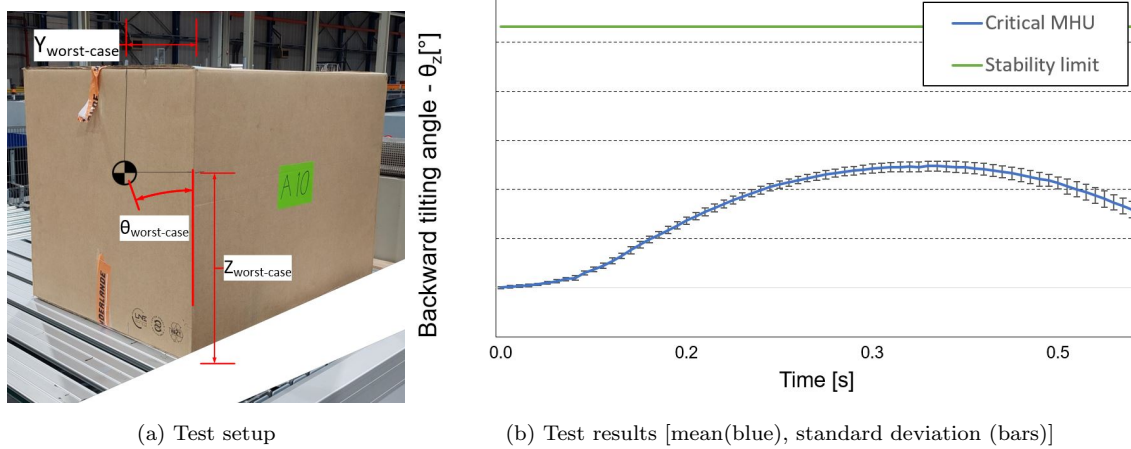


Figure 4.17: Critical parcel backwards toppling test

Note: Numerical values have been removed from the graphs due to confidentiality

The results show that the parcel tilts backwards due to acceleration (as expected). Yet, over five repetitions it does not tilt further than the tipping point (Figure 4.17a). The risk of parcels toppling backwards thus proves to be insignificant if the COM position is within the defined boundaries.

Risk R.7 can be discarded based on experiment results.

Note: R.7: MHU topples backwards over sliders

4.7 Shift and rotation due to secondary impact

When a parcel is accelerated, the content could start sliding due to its inertia. At some point, the content will impact the side of the parcel. This impact event could result in an uncontrolled situation, resulting in a shift and/or rotation. A model of loose content during the acceleration of a parcel is shown in Figure 4.18. The impact force resulting from the impact event depends on the speed. This impact speed can be calculated by

rewriting Equation 4.2. This results in Equation 4.9.

$$\Delta v_{content_on_mhu} = v_y - \sqrt{2 * g * \mu_{content} * d_{sliding_distance}} \quad (4.9)$$

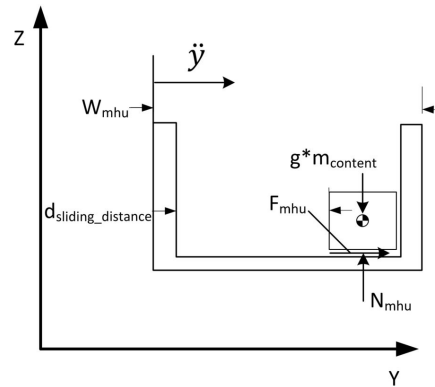
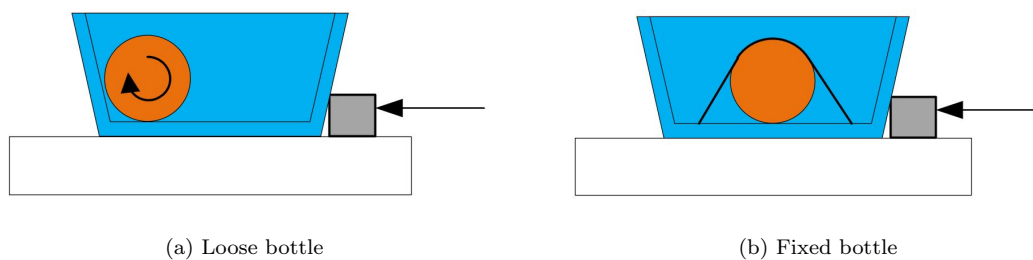


Figure 4.18: FBD of sliding content due to inertia

Two input variables thus influence the impact speed, the parcel width and the friction coefficient between the parcel and its content. The lowest friction coefficient possible is rolling friction. A critical load situation is considered to be a bottle of water in a hard plastic tote. The other test settings are stated in Section 4 in the confidential appendix.



(a) Loose bottle

(b) Fixed bottle

Figure 4.19: Illustrations of MHUs used for secondary impact test

The results of the test are shown in Figure 4.20. The tote carrying a loose bottle (orange line) behaves significantly better in both the orientation and x-displacement. The impact of the bottle "pushes" the parcels towards the sliders reducing the overrotation error. From these test results is concluded that secondary impact due to loose content is not problematic and thus requires no additional design measures.

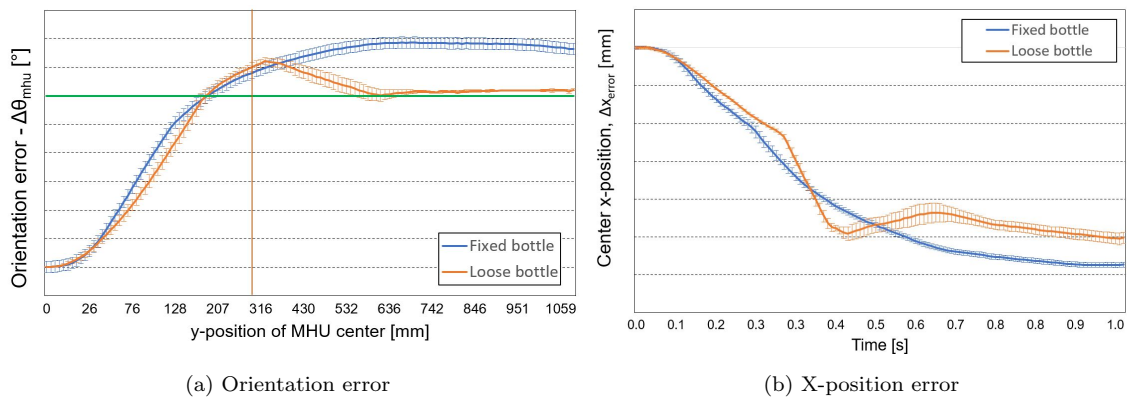


Figure 4.20: Secondary impact test results

Note: Numerical values have been removed from the graphs due to confidentiality

Risk R8 can be discarded based on experiment results.

Note: R.8: MHU shifts and/or rotates due to secondary (loose content) impact

4.8 Excessive rotation radius

Parcels that are required to be sorted sequentially need to be rotated to match the outfeed angle. The objective is to rotate the parcel in the smallest possible distance (in the y-direction). Additional space results in a wider sorter. The risk that presents itself is that the parcel cannot rotate fast enough; in other words, the parcel might have an excessive rotation radius.

This could have two consequences. Either the parcel is sorted into the outfeed with an insufficient rotation, or it could impact the sliders from the state in Figure 4.21, causing it to over-rotate.

Two possible contact modes during the rotation of a parcel can be distinguished: corner contact and wall contact. Corner contact (for which the model is shown in Figure 4.23a) results in a normal force pointing in the direction perpendicular to the slider surface (θ_{tan_cg}). Wall contact (for which the model is shown in Figure 4.23b) results in a normal force facing perpendicular to the MHU. During the sorting process, if the parcel remains in contact with the sliders, wall contact will be maintained. Yet, if the parcel rotates insufficiently, the contact mode could transition to corner contact as illustrated in Figure 4.22. Since both contact modes are currently possible, both are analysed.

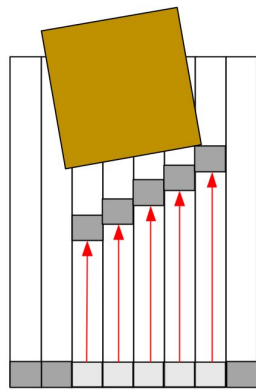
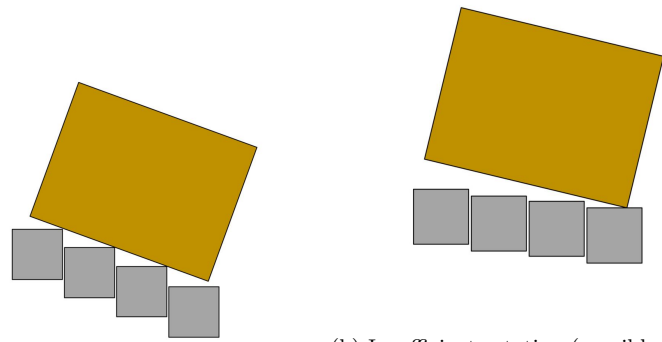


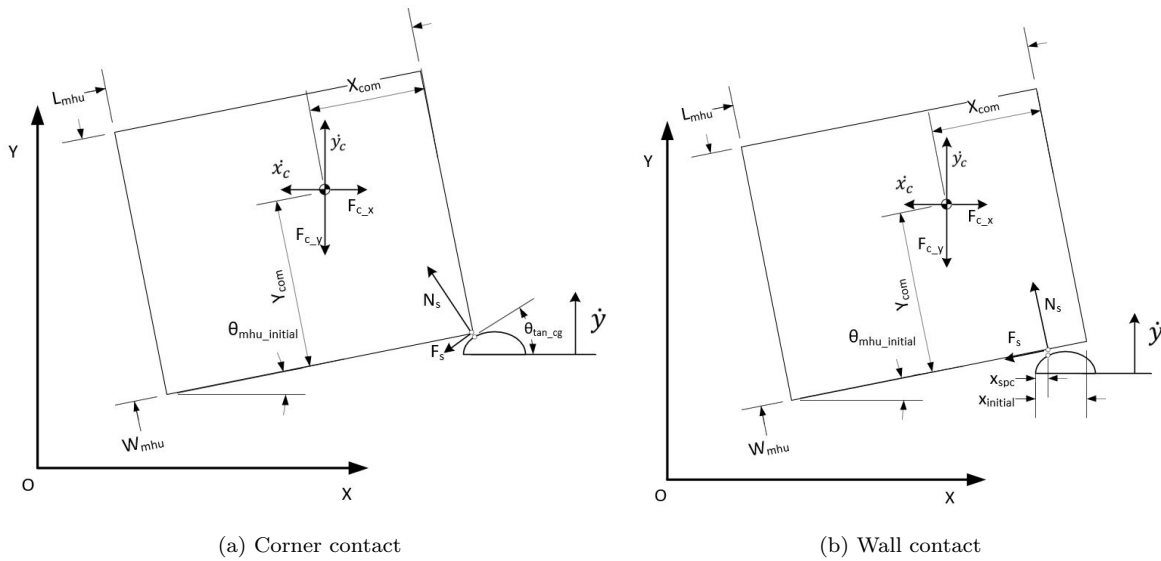
Figure 4.21: Parcel with an insufficient rotation radius



(a) Sufficient rotation (wall contact) (b) Insufficient rotation (possibly corner contact)

Figure 4.22: Contact modes during parcel rotation

Both the corner contact model and the wall contact model assume that only the furthest downstream slider is pushing the parcel. This is certainly not always the case. In many cases, multiple (or all) sliders exert a force on the parcel during rotation. However, if this is the case, the parcel is in contact with the sliders and thus rotates as desired, making it unnecessary to analyse.



(a) Corner contact (b) Wall contact

Figure 4.23: FBD of parcel during rotation

The direction of the friction force exerted by the slider (F_s) depends on the direction of motion of the contact point [21]. As explained in Section 2.3.1.2, the natural COR of a body is around its COP. The direction of motion of every point on a body is perpendicular to this COR. The motion of the contact point on the parcel will thus move to the right, as indicated with " $V_{c,mhu}$ " in Figure 4.24. The friction force will thus, according to Coulombs friction model, point to the left. This statement holds for all situations where $\theta_{mhu} < \beta$ which covers all parcels with a problematic (high) rotation radius.

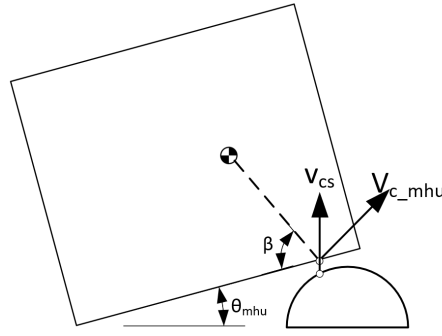


Figure 4.24: Direction of motion of the contact point on the MHU and on the slider

The equations of rotation for both corner and wall contact can now be formulated as follows:

Wall contact:

$$\ddot{\theta}_z I_z = N_s * \left(x_{com} - \frac{(x_{initial} - x_{spc})}{\cos(\theta_{mhu})} \right) - N_s * \mu_{s_tan} * y_{com} - \tau_f \quad (4.10)$$

Corner contact:

$$\ddot{\theta}_z I_z = N_s * x_{com} * \cos(\theta_{tan_cg} - \theta_{mhu}) - N_s * \mu_{s_tan} * y_{com} * \sin(\theta_{tan_cg} - \theta_{mhu}) - \tau_f \quad (4.11)$$

where the planar frictional torque can be calculated with Equation 4.12. Here, r_o is the vector from the COR to the local area where friction is computed. The \times symbol signifies the cross-product. Thus an object which is supported near its edges (wide pressure distribution) has a large friction torque.

$$\tau_f = - \int_{contactarea} \mu(x, y) p(x, y) [r_o \times \frac{\mathbf{v}(x, y)}{|\mathbf{v}(x, y)|}] dA \quad (4.12)$$

The slider pressure center height (z_{spc}) also influences the rotation radius. The slider pressure center height influences the location of the pressure center between the parcel and carrier (indicated as Δd_{mhu_pc} in Figure 4.25). A higher slider thus effectively increases y_{com} , making the rotation behaviour of the parcel even worse.

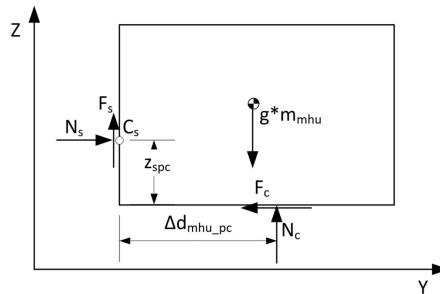


Figure 4.25: FBD - shift of pressure center due slider height

Figure 4.26 shows the results from of a test done with a parcel. The test report can be found in Section D.6 (confidential appendix). As can be seen in the figure, the parcel has

a lower rotation rate than the sliders resulting in an orientation error at the first outfeed position (indicated in orange).

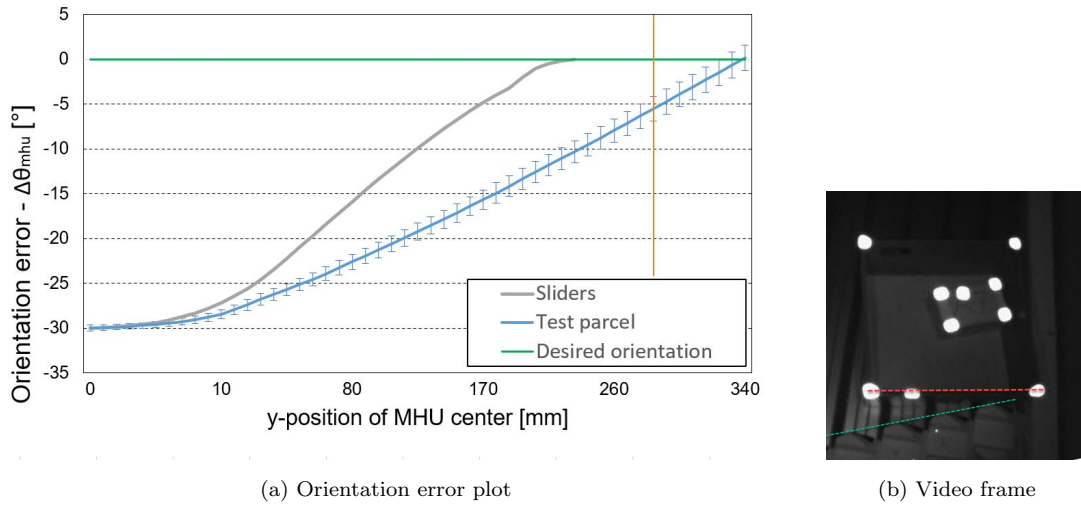


Figure 4.26: MHU with excessive rotation radius test results

Note: Numerical values have been removed from the graphs due to confidentiality

Experiments show that risk R.11 is real, design improvements thus have to be implemented to reduce this risk.

Note: R.11: MHU has an excessive rotation radius

Design parameter	Objective	Boundary condition
x_{spc}	Maximize	
$\mu_{s_tan}^+$	Minimize	$-30^\circ \leq \theta_{mhu} < 30^\circ$
θ_{tan_cg}	Minimize	$0 \text{ mm} \leq x_{spc} \leq W_{slider}$
$\frac{\mu_{d_y}}{\mu_{d_x}}$	Maximize	
z_{spc}	Minimize	

Table 4.5: Design parameter objectives R.11

4.9 Over-rotation due to angular momentum

In case a parcel is required to be sorted sequentially it is first rotated and then translated to the outfeed. After the rotation, the parcel could experience an overrotation (Figure 4.28a) due to its angular momentum. Over-rotation could have three negative effects (Figure 4.27). The parcel can rotate back towards the sliders resulting in impact, with slide and/or rotation as a consequence. The parcel can also be sorted with an overrotation (as shown in Figure 4.27b). Finally, even worse than the other two scenarios, the parcel could rotate counterclockwise. This rotation will be analysed in greater detail in Section 4.12.1.

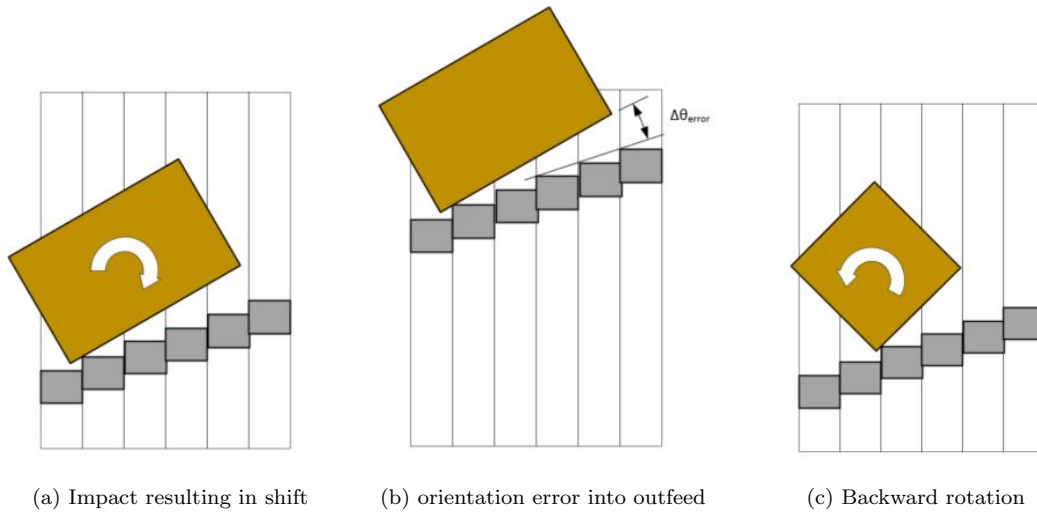


Figure 4.27: Potential negative consequences of over-rotation

The magnitude of this overrotation can be approximated by using conservation of energy (Equation A.6).

$$E_k = E_w \tag{4.13a}$$

$$\frac{1}{2} I_{z_mhu} \omega_{mhu}^2 = \theta_{mhu} * \tau \tag{4.13b}$$

$$\theta_{mhu} = \frac{\frac{1}{2} I_{z_mhu} \omega_{mhu}^2}{\tau} \tag{4.13c}$$

The friction torque (τ_f) can be calculated using Equation 4.12.

Figure 4.28b shows a model of the parcel after overrotation. From this model can be concluded that the clockwise rate of rotation (back to the sliders) is increased by minimizing both slider pressure center location (x_{spc}) and the slider friction coefficient ($\mu_{s_tan}^-$).

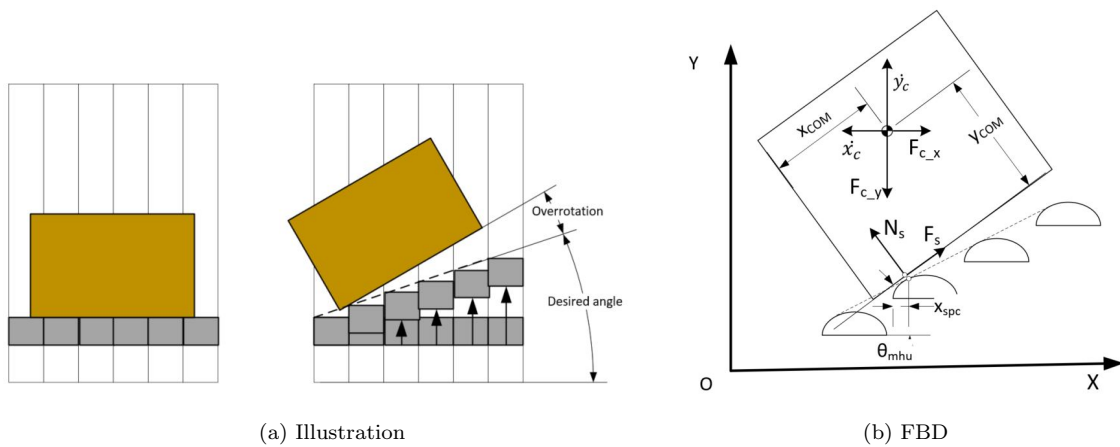


Figure 4.28: Overrotation of MHU

During an exploratory test, this problem proved significant. Figure 4.29 shows the results of a test done with a parcel (see Figure D.12 in the confidential appendix). The parcel is rotated and overshoots to 9° , after which it starts converging back to zero slowly. The closest possible outfeed position is highlighted in orange.

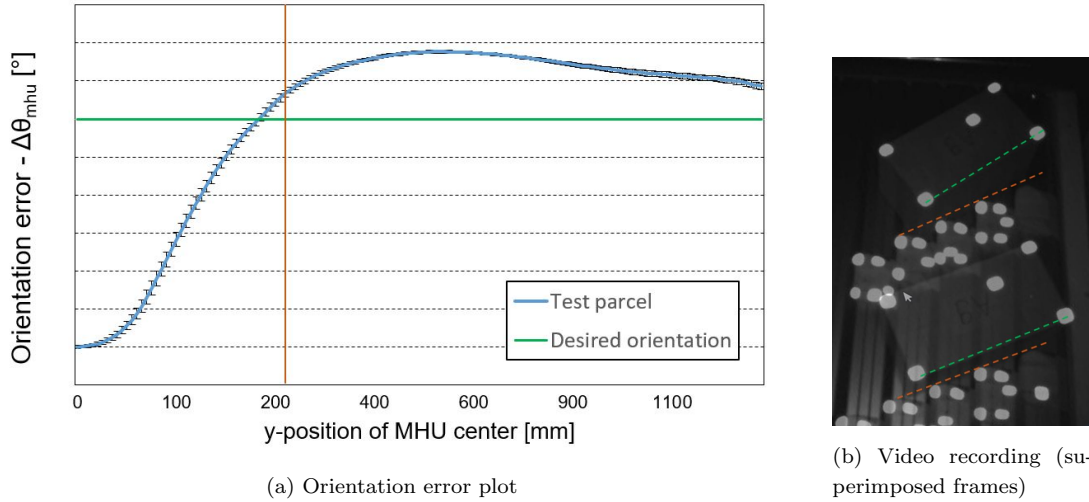


Figure 4.29: Overrotation due to angular momentum

Note: Numerical values have been removed from the graphs due to confidentiality

Experiments show that risk R.9 is real, design improvements thus have to be implemented to reduce this risk.

Note: R.9: Over-rotation of MHU due to angular momentum

Design parameter	Objective	Boundary condition
μ_{c-x}	Maximize	
μ_{c-y}	Maximize	
ω_{slider}	Minimize	
$\mu_{s,tan}^+$	Minimize	$30^\circ \leq \theta_{mhu} < 60^\circ$
x_{spc}	Minimize	

Table 4.6: Design parameter objectives risk R.9

4.10 Disadvantageous COR position

The position of a parcel after rotation can vary depending on its COR. The physical length increase due to rotation is inevitable and is thus not seen as an error. However, an additional length increase due to unused carrier space, as indicated in Figure 4.30, can be minimized or even fully prevented.

The equations of motion (in the x-direction) of a parcel during rotation can be derived from the models shown in Figure 4.23.

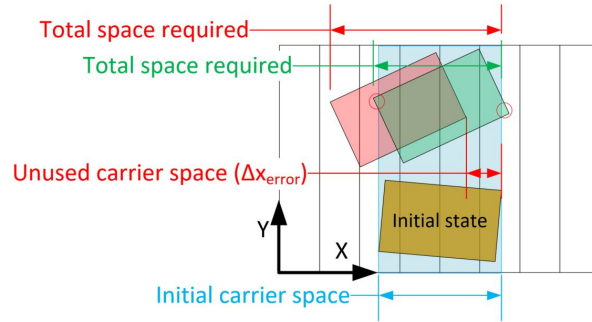


Figure 4.30: Varying final positions depending on the COR location

$$\text{Wall contact : } m_{mhu}\ddot{x}_c = N_s \sin(\theta_{mhu}) + N_s * \mu_{s_tan}^+ \cos(\theta_{mhu}) - \mu_{c_x} * m_{mhu} * g \quad (4.14)$$

$$\text{Corner contact : } m_{mhu}\ddot{x}_c = N_s \sin(\theta_{cg_tan}) + N_s * \mu_{s_tan}^+ \cos(\theta_{cg_tan}) - \mu_{c_x} * m_{mhu} * g \quad (4.15)$$

The displacement in the x-direction can thus be minimized by minimizing the slider friction (μ_{s_tan}) and the local slider geometry (θ_{cg_tan}). Figure 4.31a shows the x-displacement of a parcel on the upstream and downstream displacement sides for the test described in test report in Section D.6 (confidential appendix). As indicated in the figure, since both sides have a displacement in the same direction, a part of the carrier is unused when the parcel enters the outfeed. Due to this, the total space required to perform the sort action thus increases.

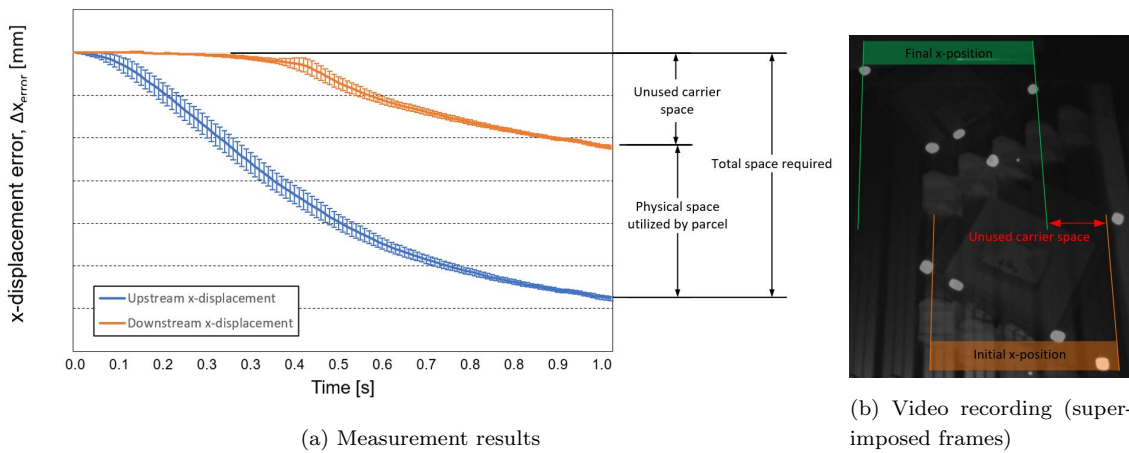


Figure 4.31: Disadvantageous center of rotation test results

Note: Numerical values have been removed from the graphs due to confidentiality

Experiments show that risk R.3 is real. Design improvements thus have to be implemented to reduce this risk.

Note: *R.3: the COR of the MHU is in a disadvantageous position.*

Design parameter	Objective
$\mu_{s_tan}^+$	Minimize
θ_{tan_cg}	Maximize
$\frac{\mu_{d_y}}{\mu_{d_x}}$	Minimize

Table 4.7: Design parameter objectives R.3

4.11 Length increase due to deformation

Soft packages can deform upon contact with the sliders (as explained in Section 3.5.6). This deformation can result in a length increase (as shown in Figure 4.32). The amount of deformation is linked to the size of the MHU. Large MHUs thus show the greatest absolute deformation. The deformation of these types of MHUs depend on:

- The size of MHU
- Content
 - Type of content (size, weight, packaging type)
 - Orientation of content
- Flexibility of the external packaging
- Sort profile (how the sliders enclose the parcel)

Exploratory tests were done. The percentage increase in transport length was measured. The amount of deformation was highly unpredictable (low repeatability in outcome) due to the variability of some of the test parameters (particularly the orientation of the content).

Although this problem proved significant, large-size deformable parcels will not be handled on the sorter, according to VI.

Exploratory experiments show that risk R.12 is real. Yet, it is out of scope since critical parcel types for this risk will not be handled on the system.

Note: *R.12: MHU deformation results in an increased transport length*

Design parameter	Objective
$\frac{\mu_{d_y}}{\mu_{d_x}}$	Minimize

Table 4.8: Design parameter objectives R.12

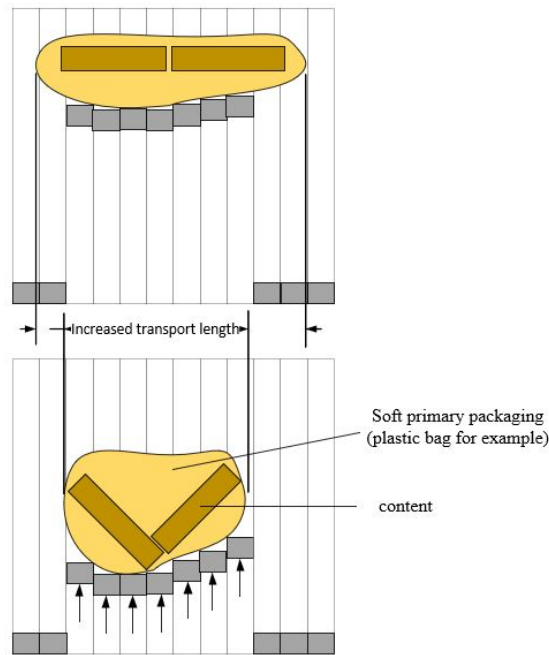


Figure 4.32: Illustration of increased transport length resulting from MHU deformation

4.12 Unwanted rotation due to insufficient support

During the sort action, there is a risk that parcels will rotate due to insufficient support of the sliders. Two situations can be distinguished: sequential sorting of large parcels and parallel sorting of small parcels.

4.12.1 Sequential sort

When a parcel is sorted sequentially it will only be supported by the sliders along its length side (as shown in Figure 4.33). To prevent rotation, the COM x-position (x_{com}) should be equal to or greater than the contact point x-position ($x_{c.s}$). For a critical COM position, this results in a maximal parcel orientation angle which is lower than the desired sort angle (stated in the confidential appendix). Additional solutions are required since this is not possible in the current situation.

$$\theta_{mhu} \leq \theta_{com} = \tan^{-1}\left(\frac{x_{com}}{y_{com}}\right) \quad (4.16)$$

4.12.2 Parallel sort

Small parcels which fit in the outfeed in any orientation do not have to be rotated. For these parcels, there are two sorting strategies. Either divert the parcel without rotation or rotate the parcel to a stable orientation before diverting. The slider design changes depending on the strategy chosen. Diverting a parcel without any rotation is advantageous since it will result in no displacement in the x-direction. This strategy is therefore chosen.

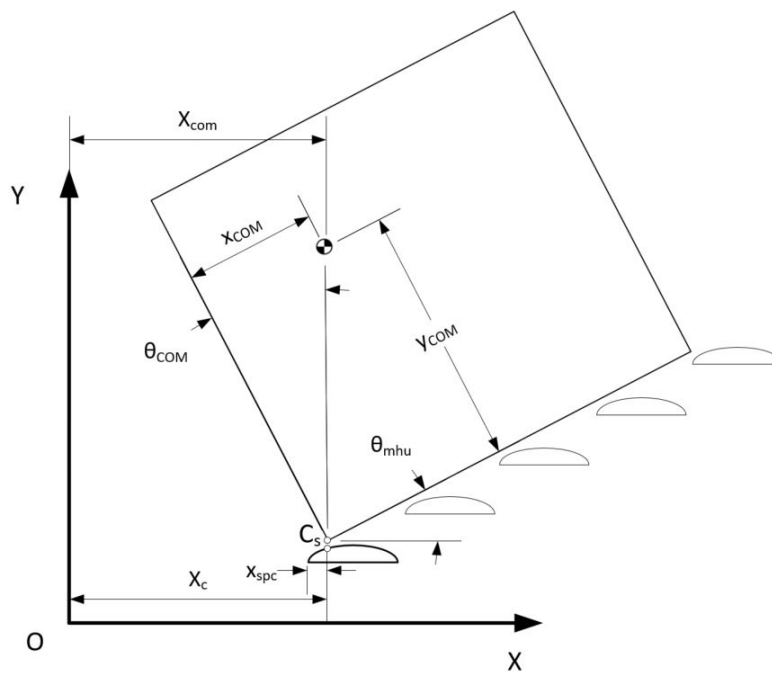


Figure 4.33: FBD of sequential sorted parcel - reduce unwanted rotation

For small parcels, a similar condition for maintaining stability as for the large parcel (described above) is applicable. If the parcel COM position is in between the x-positions of the most outer contact points, stable pushing is maintained. From this statement, stable support regions are introduced (Figure 4.34). These are the edges of the parcel that are in physical reach of the sliders (facing the sliders) and lay beyond its COM x-position. Stable pushing (pushing without unintended rotation) is maintained as long as there is at least one contact point in both stable support regions. From this rule, the conclusion can be drawn that any MHU with a transport length greater than three sliders can always be pushed in a stable manner regardless of the slider shape.

The "optimal" slider shape highly depends on the parcel shape. In other Sections, mainly cubical parcel shapes were assumed. However, this problem focuses on small parcels whose shape and orientation tend to be more random (observation during a site visit). Therefore, any convex-shaped parcel in random orientation is assumed to be possible for this problem. Convex shapes are expected to make up the bulk of the parcels handled by the system.

The effectiveness of a slider shape can be assessed based on the lowest parcel transport length which it can push in a stable manner. For a flat slider (Figure 4.35), which is currently used for parallel sorting, this limit is at a transport length equal to three sliders. Any parcel smaller than the critical transport length requires additional sliders on the

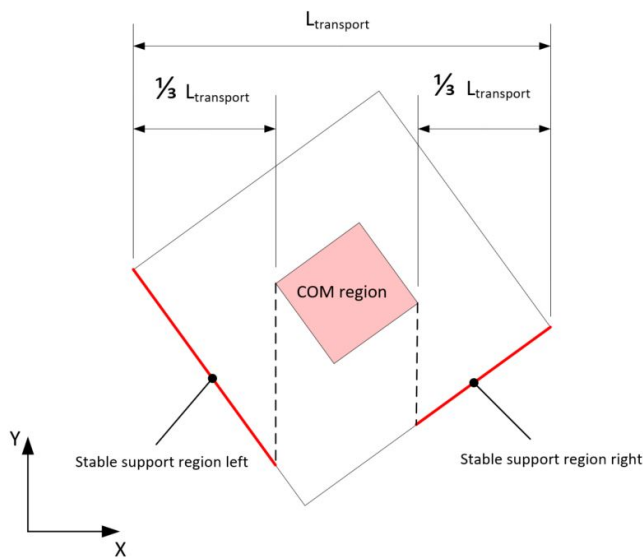


Figure 4.34: Definition stable support regions

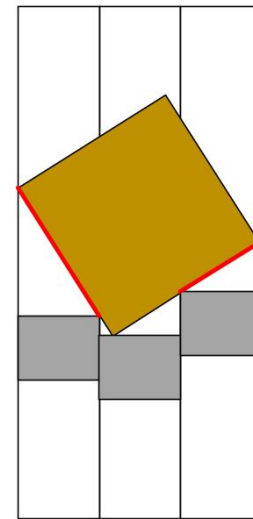


Figure 4.35: Stable pushing transport length limit for flat slider

upstream and downstream side for redundancy. The downside of this is a loss of capacity since it requires larger gaps between the parcels. The flat slider shape is far from optimal because the contact point location (x_{spc}) ranges between 0 and W_{slider} depending on the MHU shape and orientation. The goal is to bring this x_{spc} on the upstream side to 0 and the downstream side to W_{slider} for all parcel shapes and orientations. However, this is not possible since the slider can only have a limited deformation (which will be explained in Section 4.16.1). A compromise between the two objectives is a x_{spc} which is centered for all parcel shapes and orientations.

The theoretical analysis concludes that risk R.14 is real, design improvements thus have to be implemented to reduce this risk.

Note: R.14: MHU rotates due to insufficient support.

	Design parameter	Objective	Boundary condition
Large parcels (sequential sort)	x_{spc}	Minimize	
	$\mu_{s.tan}$	Minimize	$30^\circ \leq \theta_{mhu} \leq 60^\circ$
Small parcels (parallel sort)	x_{spc}	Center	for all θ_{mhu}
	$\mu_{s.tan}$	Maximize	$0 \leq x_{spc} \leq W_{slider}$ $-90^\circ \leq \theta_{mhu} \leq 90^\circ$
Both	$\frac{\mu_{d-y}}{\mu_{d-x}}$	Minimize	

Table 4.9: Design parameter objectives R.14

4.13 Slide along the sliders

When a parcel is pushed under an angle, there is a risk of sliding (as indicated in Figure 4.36a). This would result in an x-direction error. For the case where there is no slide in the x-direction ($\dot{x}_{mhu} = 0$), which is desired, the following calculation can be used:

$$F_x = 0 \quad (4.17a)$$

$$F_s \cos(\theta_{mhu}) - N_s \sin(\theta_{mhu}) = 0 \quad (4.17b)$$

$$F_s = N_s \mu_{s,tan}^- \quad (4.17c)$$

This results in the following relation:

$$\mu_{s,tan}^- \geq \tan(\theta_{mhu}) \quad (4.18)$$

For the highest sequential divert angle, the friction coefficient thus requires to be at least:

$$\mu_{s,tan}^- \geq 0.57 \quad \text{for } \theta_{mhu} = 30^\circ \quad (4.19)$$

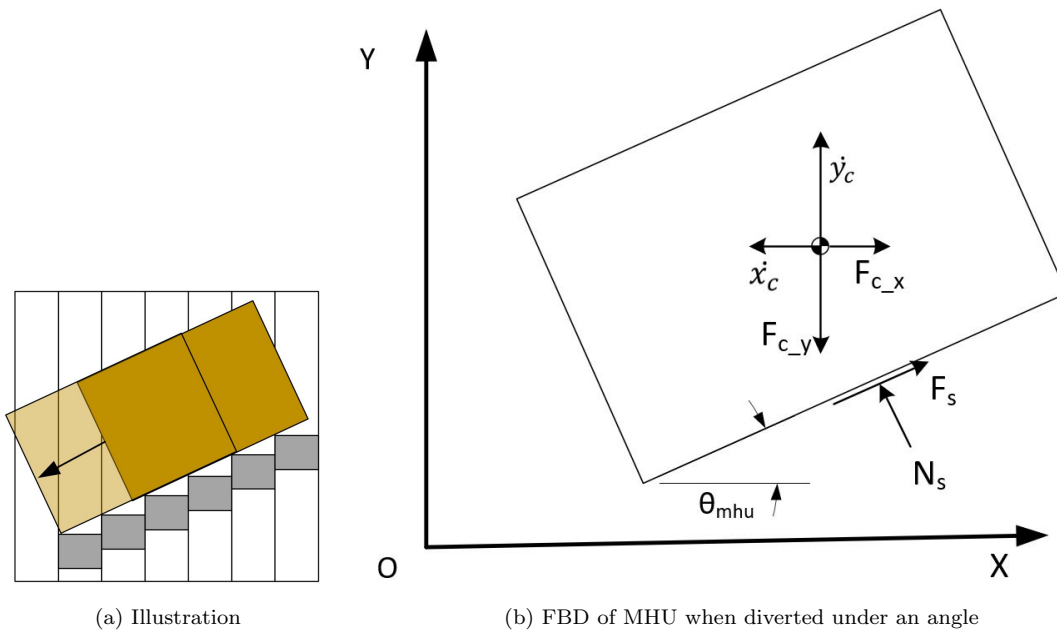


Figure 4.36: MHU sliding along the sliders

Theoretically, when the COF is above 0.57 (Condition 4.19) there will be no slide. Yet, vibrations (caused by moving parts) in the sorter and dirt on the slider or parcel can reduce this COF. Moreover, uncontrolled MHU behaviour resulting in temporary loss of contact with the sliders (bounce) also reduces the COF. Therefore, more stable parcel behaviour is expected when the slider COF ($\mu_{s,tan}^-$) is maximised (instead of constraining a minimal value of $\mu_{s,tan}^- \geq 0.57$).

In case the parcel does start sliding ($\dot{x}_{mhu} \neq 0$), the ratio between the carrier friction in the x and y-direction also starts playing a role.

Theoretical analysis concludes that risk R.15 is real, design improvements thus have to be implemented to reduce this risk.

Note: *R.15: MHU slides along the sliders*

Design parameter	Objective	Boundary condition
$\mu_{s_tan}^-$	Maximize	$0 \leq \theta_{mhu} \leq 30$
$\frac{\mu_{d_y}}{\mu_{d_x}}$	Minimize	

Table 4.10: Design parameter objectives risk R.15

4.14 Damage due to contact pressure

The sliders exert a normal pressure on the parcel during pushing (Figure 4.37). If this pressure exceeds the tensile strength of the packaging material, the parcel could be damaged.

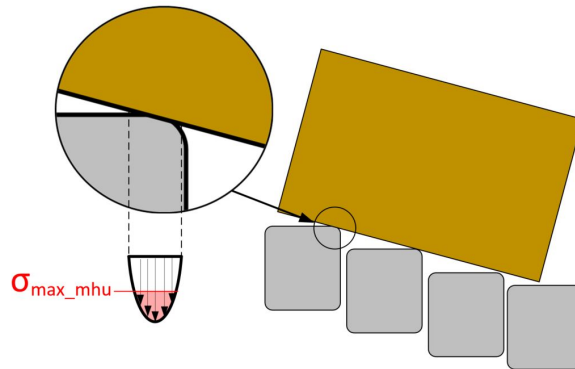


Figure 4.37: Potential damage due to contact pressure illustration

The average pressure over the contact area depends on the pushing force and the area in contact (Equation 4.20). However, the pressure distribution across the contact area is generally not constant. The shape and e-modulus of both components influence the pressure distribution across the contact area. High e-moduli result in greater differences in pressure distributions and thus higher peaks in local pressure. Sharp edges for example result in local pressure peaks. Below are two examples to illustrate the influence of shape on pressure distribution.

$$p_o = \frac{A_{real}}{F} \quad (4.20)$$

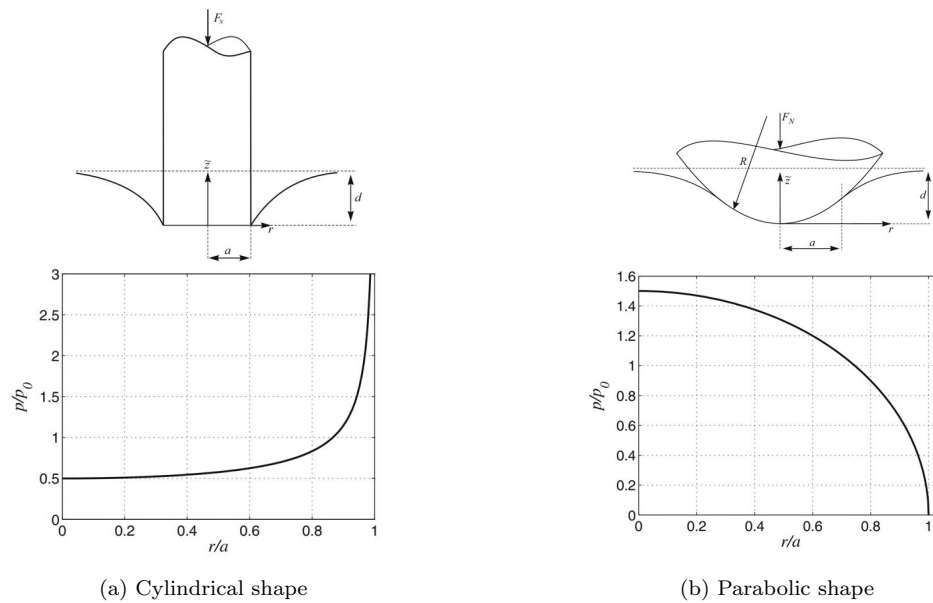


Figure 4.38: Normal pressure distributions [31]

The local pressure peak around the edges can thus be more than three times the average pressure (Figure 4.38a). It is therefore important to design a blunt slider shape.

There are two standardized tests which are often used to measure packaging material strength: the puncture resistance test and the Mullen burst test. Both tests measure the strength of a flat piece of packaging material. However, on the sorter, the packages will be pushed on their bottom edge, which has significantly higher stiffness and strength (Figure 4.39). These two tests are thus not realistic to gain the necessary insights.

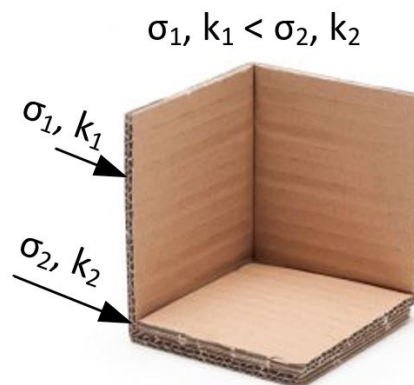


Figure 4.39: Variation in MHU strength and stiffness

4.14.1 Minimal contact radius

A customized version of the puncture resistance test is created. In this test, wooden cylindrical shapes (Figure 4.40b) are pushed into different packaging samples in a similar

way the slider would. The highest possible load (which could be applied in reality) is applied to the packaging samples using a bolt and spindle mechanism and a load sensor for the force measurement. This process is repeated three times for each combination of packaging sample and pressure cylinder, after which the damage to the packaging samples is inspected. The pressure cylinders have ranging radii (10 to 45 mm) and heights (30 and 60 mm). A cylindrical shape (with a fillet edge) is chosen because it distributes the pressure evenly (no local peak pressure) and it can easily be translated into a design constraint for the slider (as a minimal contact radius).

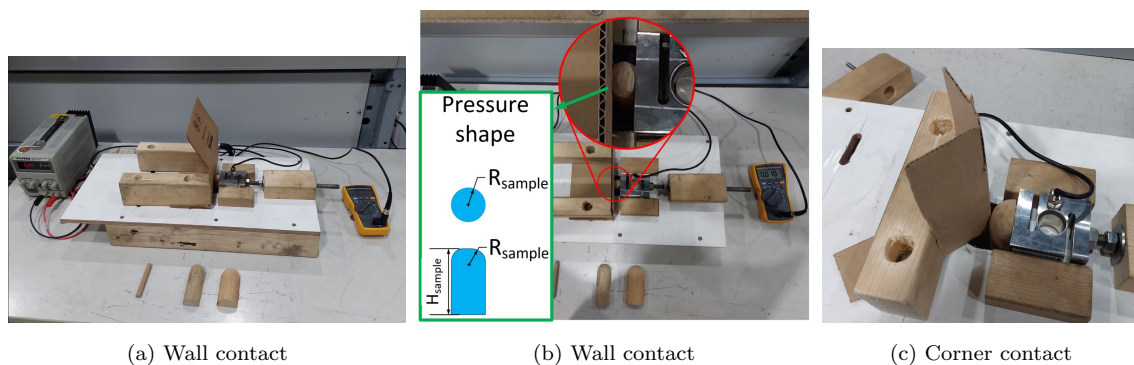


Figure 4.40: Test setup - effect of slider shape on parcel damage

The packaging material samples are chosen using CES Edupack. This is an engineering material selection tool. Paper and cardboard proved to be critical packaging material types (Figure A.4). Four types of packaging samples were used in the tests (these are stated in the confidential appendix).

In the case of wall contact, all packaging samples were able to withstand the peak force, even for the smallest pressure cylinder. Pictures of the samples, both during loading and after release, are shown in the confidential appendix. A minimal contact radius equal to the smallest cylinder would thus be sufficient to prevent damage to parcels. Moreover, as was expected, the pusher height has no influence on the damage (so increasing the slider height does not reduce this problem).

With corner contact, the weakest parcel (parcel 2) was not able to withstand the required pushing force. Moreover, an increase in pusher height showed no improvement. So, there is a possibility that parcels get damaged when pushed on the corners. Yet, this cannot be further reduced with slider design.

From the test results can be concluded that the slider shape must have a contact radius equal to or greater than the smallest pressure cylinder (see Section 4 in the confidential Appendix for this dimension). The height must be at least 30 mm.

Parcel ID	Dimensions [LxBxH]	Type	Wall thickness [mm]	Maximum pressure [N]	Equivalent parcel mass [kg]	Maximum pressure [N] (Corner load)	Equivalent parcel mass [kg] (Corner load)
1	150x100x100	Corrugated cardboard - single wall	2	See numerical values in the confidential appendix			
2	200x200x110	Corrugated cardboard - single wall	3				
3	430x350x350	Corrugated cardboard - double wall	4				
4	100x100x130	Craft paper	0.5				

Table 4.11: Results pressure tests

Experiments show that R.16 can be a real risk. However, the risk is mitigated if the constraints in Table 4.12 are taken into account.

Note: R.16: Damage to either slider or MHU due to contact pressure

Design parameter	Objective
R_{slider}	Confidential
H_{slider}	$> 30 \text{ mm}$

Table 4.12: Design parameter constraints R.16

4.15 Deceleration during free sliding

During the final stage of the sort action, the sliders decelerate to prevent colliding with the side of the sorter. When the sliders start decelerating, the parcel slides freely into the outfeed. A model of this behaviour is shown in the top view Figure 4.41. The $|X|, |Y|$ coordinate system is fixed while the x, y coordinate system moves with the carriers.

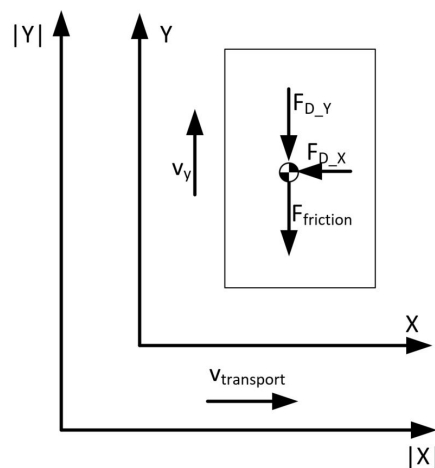


Figure 4.41: FBD of the free-floating parcel after contact with sliders is lost

The forces acting on the parcel influence its trajectory when leaving the sorter. The trajectories resulting from the different forces acting on the parcel are illustrated in Figure

4.42. The drag in the x-direction counteracts the deceleration due to friction. Moreover, the drag in the x-direction is larger than in the y-direction, since the velocity in the x-direction is greatest. Due to this, there can be different critical cases. The first case is a parcel with a high friction force and negligible drag forces. The second case is a parcel with high drag forces and negligible friction force. A parcel with a combination of both will likely not be critical since the forces counteract one other.

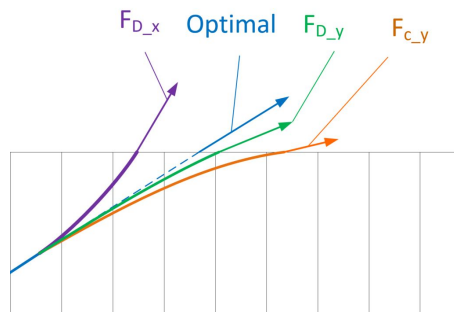


Figure 4.42: Alternative trajectories of a parcel resulting from different forces

The sliding distance of a parcel during free sliding has already been calculated in Section 4.3 (Equation 4.2). This equation can be used to calculate the positional error in the x-direction resulting from the deceleration of the parcel (see Figure 4.43). The expected free-sliding distance is stated in Table D.7 in the confidential appendix. The x-position error is within an acceptable margin with this free sliding distance. Deceleration due to friction is thus not a significant problem.

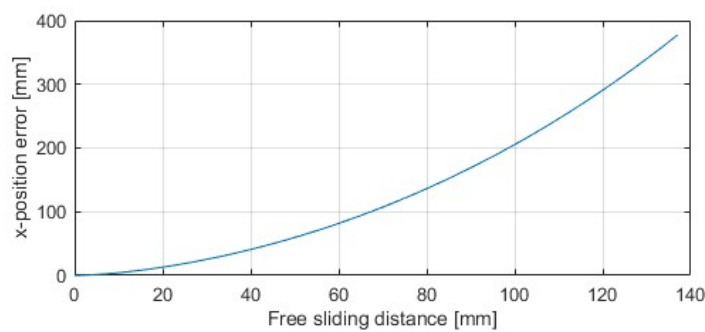


Figure 4.43: X-position error resulting from deceleration due to friction ($\mu = 0.6$)

Deceleration due to drag has similar causes as discussed in Section 4.4. However, there is currently no test setup available to perform experiments and draw conclusions on this problem.

No conclusions can be drawn on risk R.20 at this stage, additional testing is required when a test setup is available.

Note: R.20: MHU decelerates when contact with sliders is lost

4.16 Non-performance related constraints and objectives

The aspects of the design related to performance (parcel behaviour) are all analyzed. Yet, there are also other aspects which need to be considered for the design. The most important aspects are: control (of the slider trajectory), noise, wear and energy use. The constraints and objectives related to these aspects are given below. A rationale is attached to each constraint or objective as an explanation and justification.

4.16.1 Control related constraints and objectives

1. Limit the slider weight ($m_{slider} < m_{slider_max}$, m_{slider_max} is stated in Table 3 in the confidential appendix)

Rationale: the inertia of the slider influences its ability to accelerate and decelerate. The slider weight is a constraint to reach desired specifications

2. Maximize the slider stiffness

Rationale: any slider deformation will be unpredictable since many parcel characteristics are unknown (weight, friction coefficient, COM location). Any slider deformation that will occur thus introduces uncertainty in positioning the slider in the desired location (to make contact with the parcel). Deformation and, thus slider stiffness need to be limited to maximize the predictability of contact point location.

3. Minimize the slider pressure center in z-direction (minimize z_{spc})

Rationale: the majority of MHUs are stiffest near their base surface (z_{spc}) as illustrated in Figure 4.39. High stiffness is beneficial for robust control.

4. Minimize pressure center distances (minimize z_{spc} , y_{spc} and center x_{spc})

Rationale: z_{spc} , y_{spc} and x_{spc} influence the moment which needs to be counteracted by the slide bearings. Minimizing these design parameters reduces the slide friction forces, which benefits the slider position control.

4.16.2 Noise-related constraints and objectives

1. Minimize the slider height and mass (minimize m_{slider} and H_{slider})

Rationale: at the head and tail pulley, the carriers and sliders revolve around a chain wheel pulley. The chain, at the base of the carriers, travels at a constant speed around this pulley (at radius R_1). The carrier and slider travel on a greater radius (R_2), and there will thus be a sudden speed increase, which causes vibrations resulting in noise emissions. Minimizing the slider height and mass minimizes noise emissions

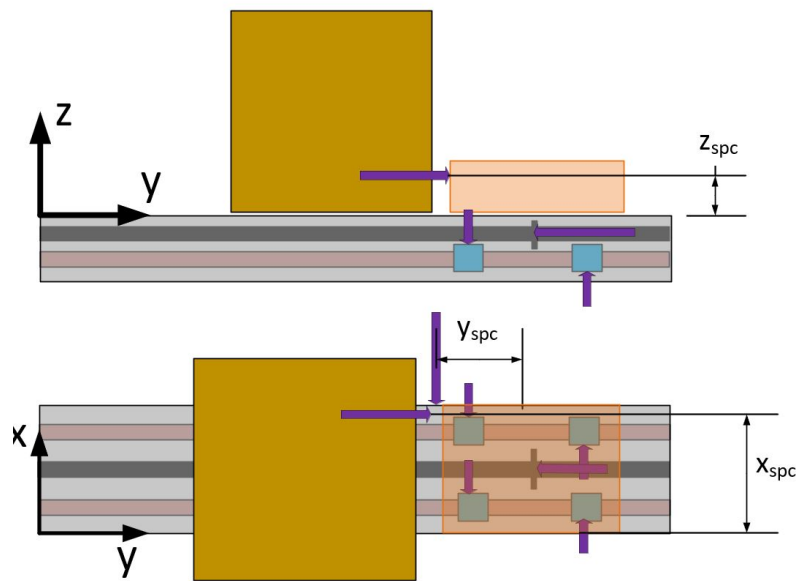


Figure 4.44: Relation between the slider pressure center location and the slide bearing forces/ moment forces in the slider

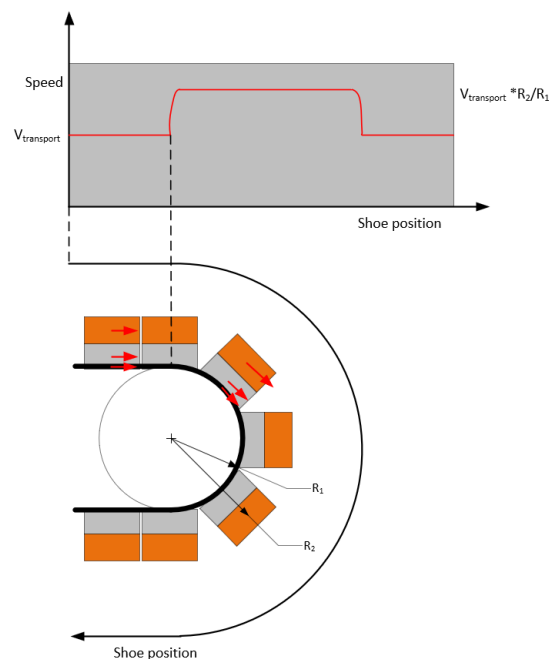


Figure 4.45: Relation between slider height and noise emission at the end take up

4.16.3 Wear related constraints and objectives

1. Maximize slider height and local contact radius (*maximize R_{slider} and H_{slider}*)
Rationale: wear on the slider pusher surface can be minimized by maximizing the contact area with parcels. Increasing the contact area decreases the overall stress, decreasing the wear rate [31].

2. Minimize pressure center distances (*minimize z_{spc} , y_{spc} , center x_{spc}*)

Rationale: these parameters influence the normal force on the slide bearings, as is explained in Section 4.16.1. Minimizing these normal forces reduces the wear rate of the bearings.

4.16.4 Energy use related constraints and objectives

1. Minimize the slider weight (*m_{slider}*)

Rationale: the slider weight influences energy use at acceleration.

4.17 Conclusion

The unwanted parcel behaviour analysis started with the identification of 20 separate modes (Figure 4.1). The physical causes for this behaviour are analyzed by a combination of theoretical analysis and physical testing (Section 4.2). Seven risks proved to be most significant at this stage of the design process (see Table A.1). The design parameter objective of these risks are summarized in Table B.1 and B.2. These design parameter objectives will be translated into a physical concept design in the next chapter.

Five risks proved insignificant since even critical load situations showed no significant problems. Therefore, these require no additional solutions. Also, for the three risks, there was no conclusive answer on their significance because additional testing is required for which a test setup is not available yet. Future tests should give insights into the significance of these risks.

Finally, four risks are out of scope currently. These modes, which are all risks related to the jamming of parcels, are mainly influenced by fine design details rather than the overall design. Measures for mitigating these risks should be implemented into the design after its overall shape and materials are chosen.

Chapter 5

Conceptual solutions

From the parcel behaviour analysis in the previous chapter, seven risks remain. First, these risks are translated into seven functions (Figure 5.1). The process of finding solutions for these functions is split into two parts (as illustrated in Figure 5.1). In the first part, solutions originating from brainstorming are analysed and assessed. In the second part, the conceptual design is derived from the parameter objectives found in the previous chapter. Both the solution from brainstorming and the concept design are meant to be implemented together to maximize performance improvement.

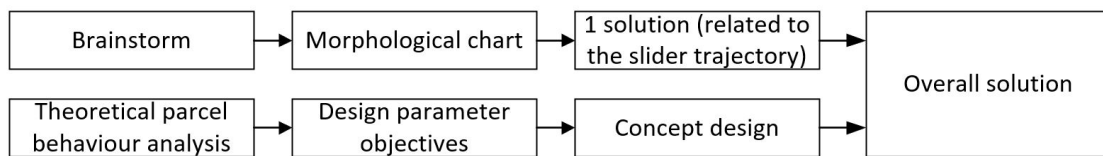


Figure 5.1: Conceptual solution process

The overall solution aims to accomplish the functions in Table 5.1. These functions focus on reducing the problems found in Chapter 4.

Reference	Function
F.1	Reduce the space required for rotation
F.2	Reduce overrotation due to angular momentum
F.3	Reduce overrotation of the MHU due to angular momentum
F.4	Increased rotation rate
F.5	Reduce unwanted rotation
F.6	Reduce slide along sliders
F.7	Prevent damage due to contact pressure

Table 5.1: Functions of the conceptual solution(s)

5.1 Morphological chart

The second part of this chapter focuses on the generation of a concept design based on the design parameter objectives derived in Chapter 4. This design methodology is particularly

suiting for gaining insights and finding solutions or compromises for conflicting design objectives. However, the solution space using this methodology is rather limited. Therefore, a second design methodology based on brainstorming is also used. This methodology explores a much larger solution space. The solutions from the brainstorm are structured in a morphological chart, which is shown in Figure B.1 and B.2, showing different solutions per function. Some solutions can be found for multiple functions; these solutions thus solve multiple problems.

The solutions are graded based on implementation cost and expected effectiveness. One solution is chosen for further analysis. This solution is related to a new slider trajectory for rotating parcels. This solution does not require additional hardware, making it much more cost-effective than other solutions. Furthermore, the solution serves multiple functions.

5.1.1 Improved slider trajectory

In the currently proposed sort strategy, there is certain unwanted behaviour related to the rotation of parcels (Section 4.8, 4.9 and 4.12). Based on the analysis of these problems, an improved slider trajectory is derived. This new trajectory reduces the angular velocity during the sorting process. This decrease in angular velocity is expected to significantly improve the parcel rotation behaviour. A detailed description of this slider trajectory is given in Section D.7 in the confidential appendix.

5.2 Concept design (resulting from parameter objectives)

The slider concept design comprises of its shape and friction coefficients. Specific materials to facilitate these friction coefficients are not chosen. The design is split into three parts which are analyzed separately: the shape in the XY-plane, the shape in the YZ-plane and the tangential friction coefficients. The design of each aspect is based on the design parameter objectives related to that specific aspect.

5.2.1 Slider shape (in XY-plane)

Three design parameter objectives relate to the XY-plane slider shape; the pressure center (x_{spc}) contact geometry ($\theta_{tan.cg}$) and the contact curvature (R_s). The slider shape in the XY-plane is designed on the basis of these design parameter objectives, summarized in Table 5.2.

The most crucial function fulfilled by the XY-plane slider shape is reducing unwanted rotation of small parcels due to insufficient support (analyzed in Section 4.12.2). The XY-plane slider shape is essential for this function since no other solution can accomplish it. As derived in Section 4.12.2, an optimal slider shape would have a centered contact point for every parcel shape and orientation. A possible slider shape for this would be a single

	Reference	x_{spc}	$\theta_{tan.cg}$	R_s	
Performance related	F.1		Max		
	F.2				
	F.3	Min			
	F.4	Max	Max		
	F.5	Sequential sort	Min		
		Parallel sort	Center (for all θ_{mhu})		
	F.6				
F.7				Confidential	
Control related		Min. range			
Wear related		Min. range		Max	
Noise related					
Energy use related		Min. range			
Boundary condition		$0 \leq x_{spc} \leq W_{slider}$	$-90^\circ \leq \theta_{tan.cg} \leq 90^\circ$		

Table 5.2: Design parameter objectives related to the slider shape in the XY-plane

point slider (Figure 5.2). However, the downside of a single contact point slider is that it cannot support parcels that partially overlap the carrier (as illustrated in Figure 5.2). The optimal slider shape should thus have a centered contact point (x_{spc}) for any parcel shape and orientation and be capable of supporting parcels that only partially overlap the carrier. This leaves the design space indicated in Figure 5.3. Three potential slider shapes within this design space are shown in Figure 5.4.

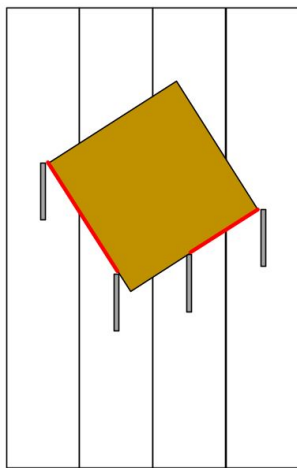


Figure 5.2: Single point slider shape

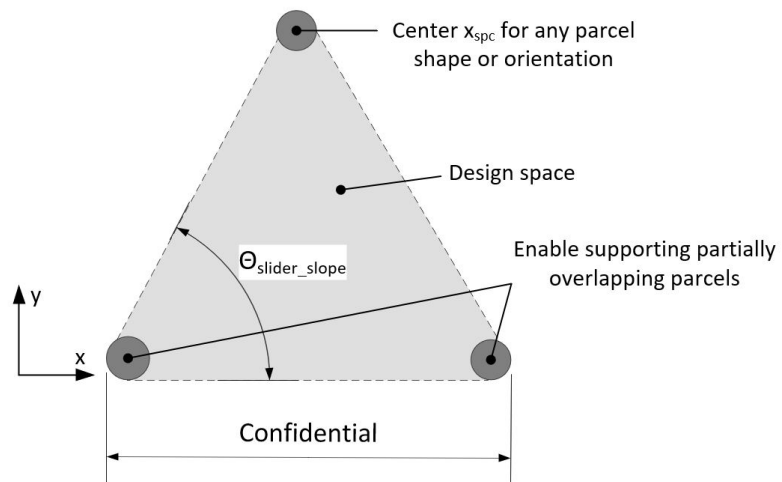


Figure 5.3: Design space slider shape

All three shapes focus on the same two objectives, center the contact point for parcels which overlap at least half the carrier width and enable corner contact for parcels which span less than half the carrier width. The minimal transport length parcel which can be diverted in a stable manner with these slider shapes is reduced to $\frac{3}{2}W_{slider}$ (see Figure 5.4). This is an improvement of factor two with respect to a flat slider shape (see Figure

4.35).

A risk related to the slider shapes shown in Figure 5.4 is jamming parcels between adjacent sliders. This risk is analyzed in greater detail in Section D.8 (confidential appendix). To minimize this risk, the contact geometry angle ($\theta_{tan.cg}$) should be minimized. This angle is the lowest for slider shape "a" since the constant contact angle. This triangular slider shape is therefore chosen.

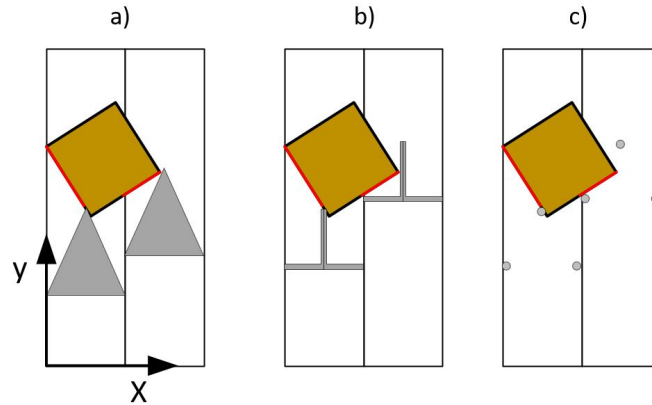


Figure 5.4: Stable pushing transport length limit for optimal slider shape

The final slider shape is shown in Figure 5.5. The slider is triangular-shaped, the exact angle is shown in Figure D.16 in the confidential appendix. The angle is chosen as a compromise between offering reliable support of small parcels and preventing parcels from jamming between sliders (see Section D.5 in the confidential Appendix for this analysis). Moreover, the shape ensures a predictable (centered) contact point, minimizing the moment forces in the slider and slide mechanisms. Finally, the contact curvature across the whole slider is restricted to the minimum (R_{min}) determined in the test described in Section 4.14.1. This prevents damaging parcels due to contact pressure.

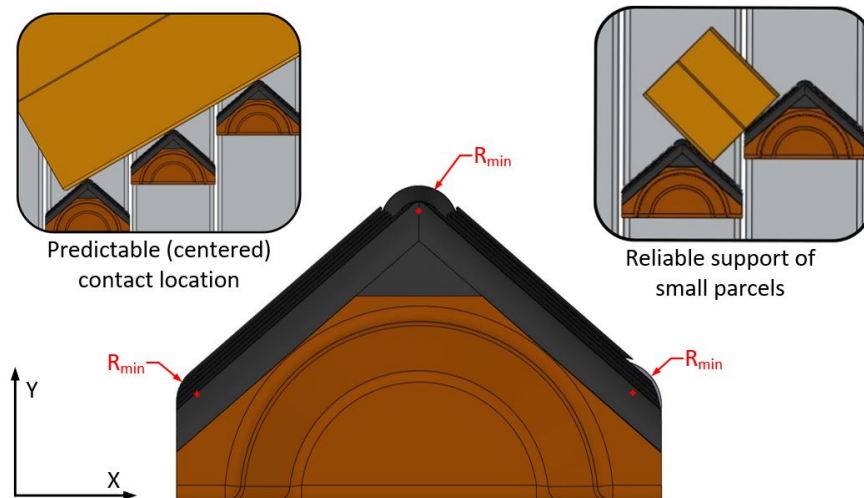


Figure 5.5: Concept design - XY-plane shape (topview)

5.2.2 Slider shape in YZ-direction

Three design parameter objectives relate to the YZ-direction slider shape; the pressure center (z_{spc}) contact geometry ($\theta_{ax.cg}$) and the slider height (H_{slider}). The slider shape in the YZ-plane is designed on the basis of these design parameter objectives, summarized in Table 5.3.

	Reference	H_{slider}	z_{spc}	$\theta_{ax.cg}$
Performance related	F.1			
	F.2	Max		Max
	F.3			
	F.4		Min	
	F.5			
	F.6			
	F.7	>30 mm	Min	
Control related		Min (m_{slider})	Min	
Wear related			Min	
Noise related		Min		
Energy use related		Min (m_{slider})	Min	
Boundary condition			$0 \leq z_{spc} \leq H_{slider}$	$-90^\circ \leq \theta_{ax.cg} \leq 90^\circ$

Table 5.3: Design parameter objectives related to the slider shape in the YZ-plane

The overall shape (shown in Figure 5.6) slightly banks backwards to maintain a low pressure center with parcels. This low pressure center is beneficial for parcel behaviour and minimizes load on the slide bearings. The top edge is rounded with the minimal contact radius determined in Section 4.14.1 to prevent damaging parcels. The slider height (shown in Figure D.16 in the confidential appendix) is chosen as a compromise between avoiding sliding of packages onto the sliders and reducing weight. Finally, the groves are a solution to the conflict illustrated in Figure B.4 and force products down, preventing (mainly flexible) packages from sliding onto or folding up against the sliders. These groves' shape and size are chosen intuitively; their optimal shape could be a future research topic.

5.2.3 Tangential slider friction coefficient

There are various conflicting objectives for the tangential slider friction coefficient (see Table 5.4). However, when looking at the direction-based components, it can be found that nearly all objectives require a high friction coefficient in one direction and a low friction coefficient in the other direction. Multiple solutions are considered to facilitate this (see the morphological chart in Figure B.3).

A rotary ratchet and pawl is chosen as solution since this is a passive and robust solution regardless of the packaging material. The concept design based on this rotary ratchet and pawl mechanism is shown in Figure 5.7 and is named the friction diode.

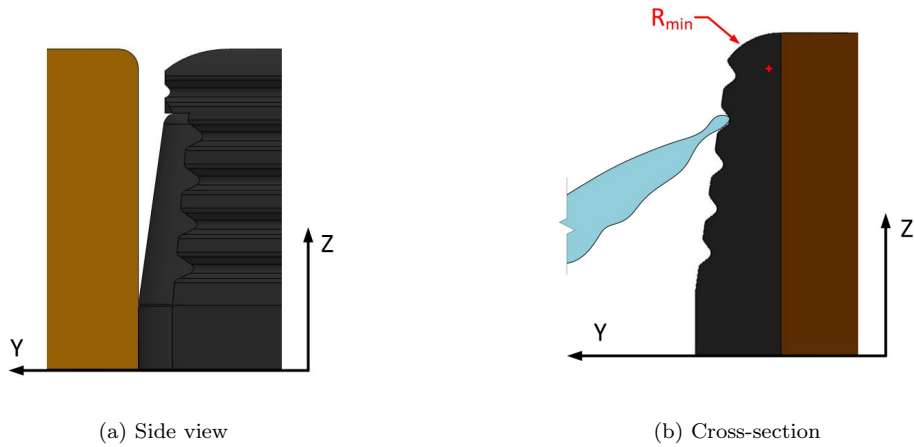


Figure 5.6: Concept design YZ-plane shape

	Reference	μ_{s_tan}	Boundary condition	
Performance related	F.1	Min +	$-30^\circ \leq \theta_{mhu} \leq 30^\circ$	
	F.2			
	F.3	Min -	$30^\circ \leq \theta_{mhu} \leq 60^\circ$	
	F.4	Min +	$-30^\circ \leq \theta_{mhu} \leq 30^\circ$	
	F.5	Sequential sort	Min -	$30^\circ \leq \theta_{mhu} \leq 60^\circ$
		Parallel sort	Max	$0 \leq x_{spc} \leq W_{slider}$ $-90^\circ \leq \theta_{mhu} \leq 90^\circ$
	F.6	Max -	$0^\circ \leq \theta_{mhu} \leq 30^\circ$	
F.7				
	Control related			
	Wear related			
	Noise related			
	Energy use related			
	Boundary condition			

Table 5.4: Tangential slider friction coefficient objectives

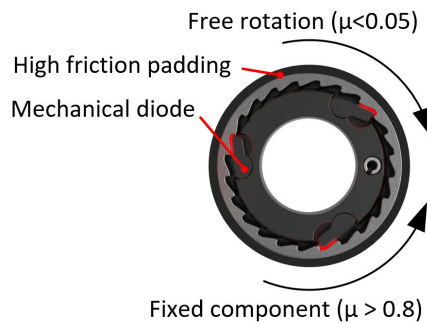


Figure 5.7: Mechanical friction diode concept illustration

From a friction perspective the slider is comprised of three parts (Figure 5.8b); a high friction material over the majority of the slider surface (section 1), a friction diode (section 2) and a low friction material (section 3).

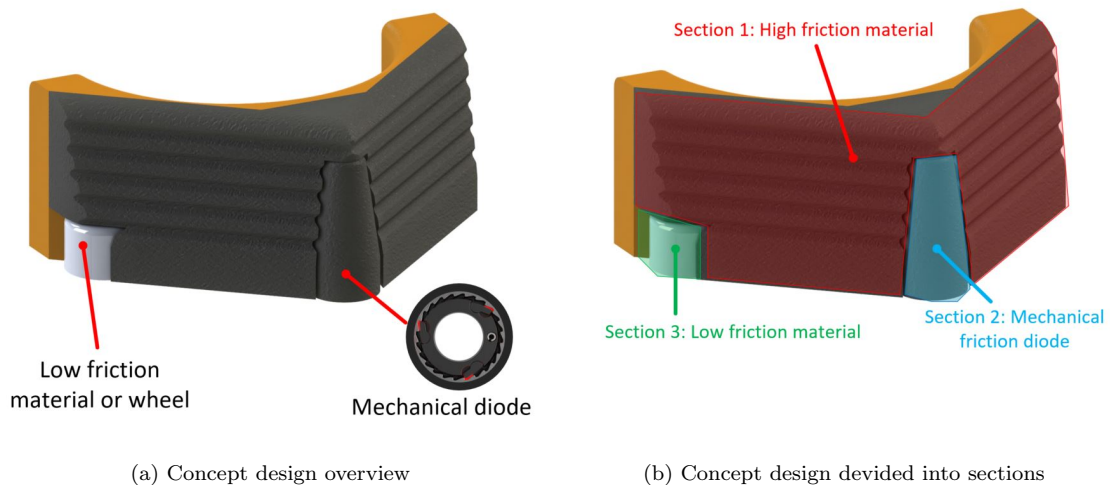


Figure 5.8: Overview final slider concept design

”Section 1” comprises of a material with a high friction coefficient in all orientations and directions. This section comes into contact with parcels between 45° and 90° when in wall contact and nearly all cases of corner contact. The high friction coefficient in all directions prevents small parcels from rotating.

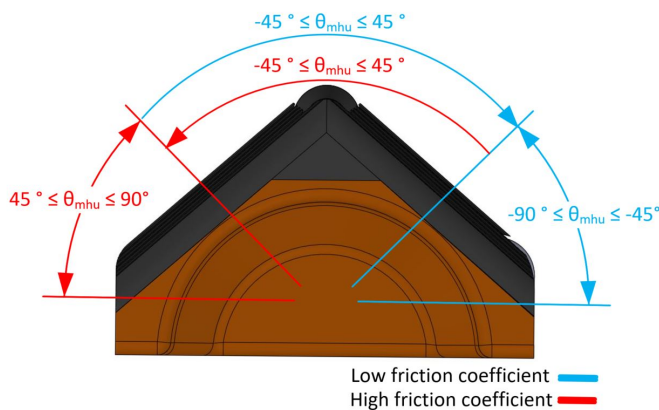


Figure 5.9: Ranging friction coefficient concept design (top view)

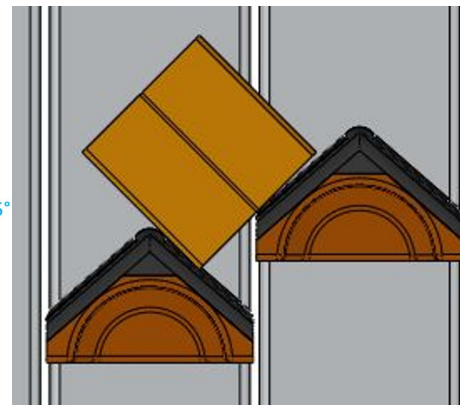
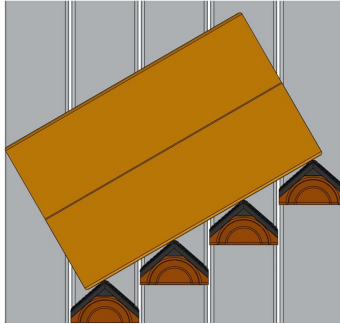


Figure 5.10: Support small parcel

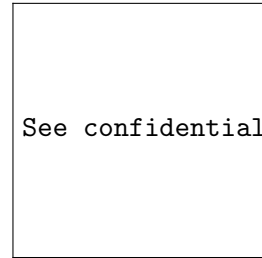
”Section 2” comprises of the friction diode (presented in Figure 5.7). A parcel that will contact the slider with an angle between -45° and 45° will thus experience a high friction coefficient in the negative x-direction and a low friction coefficient in the opposite direction. Firstly, this enables sorting parcels under an angle without sliding (risk R.15, Figure 4.38) as shown in Figure 5.11a. Secondly, the low friction coefficient in the positive x-direction improves the rotation rate of the parcel and reduces the x-displacement due to rotation, reducing risk R.3 and R.11 (Section 4.8 and 4.10).

Finally, ”section 3” consists of a material with a low friction coefficient in all directions. This part comes in contact with parcels with an angle between -45° and -90° as shown in

Figure 5.11b. This component, together with the friction diode satisfies Condition D.10 in the confidential appendix for adding additional support sliders (explained in Section D.8 in the confidential appendix).



(a) sequential sort topview



(b) Friction coefficient measures related to the new slider trajectory

Figure 5.11: Friction diode features

5.3 Carrier design

For the carrier friction coefficient objectives shown in Table 5.5, there are many conflicting objectives. Due to the number of conflicting objectives and the lack of a solution for these conflicts, finding a well-founded compromise at this stage is difficult. Therefore, the following steps are recommended for VI. First, test the remaining risks which could not be tested yet (see Table A.1). The concept design should be updated based on the results of these tests. When the concept design is updated it can be produced and tested (this will be described in further detail in Section 7.2). Finally, depending on the conclusions that can be drawn from these tests, the carrier design can be used to reduce the remaining unwanted parcel behaviour (using Table 5.5). Figure B.3 shows different solutions for achieving anisotropic friction in case this would be required.

	Reference	$\mu_{c,x}$	$\mu_{c,y}$
Performance related	F.1	>	
	F.2		Min
	F.3	Max	Max
	F.4	<	
	F.5	>	
	F.6	>	
	F.7		
Control related			
Wear related			
Noise related			
Energy use related		Min	Min
Boundary condition			

Table 5.5: Carrier design parameter objectives

Note: The greater than and less than signs (<, >) indicate that the objective is to maximize the ratio between the variables.

5.4 Conclusion

The final slider concept design (Figure 5.8a) focuses on decreasing the seven risks which proved to be most significant from the parcel behaviour analysis. The different aspects of the slider in terms of shape and friction coefficients have been carefully chosen based on design parameter objectives. Using this methodology gives a clear overview of any conflicting design objectives. For the conflicting design objectives which were present, solutions have been derived. Such as for example the friction diode (Figure 5.7).

On top of the concept design, also additional solutions were explored. The most promising solution (from the morphological chart in Figure B.1 and B.2) is chosen to analyze in greater detail. The effectiveness of the concept design and the additional solution will be explored in the next chapter.

Table 5.6 gives an overview of the relations between the solutions found in this chapter and the function they accomplish.

		F.1	F.2	F.3	F.4	F.5		F.6	F.7
						Sequential sort	Parallel sort		
slider design	Tangential slider friction coefficient	+		-	+			+	
	XY-plane slider shape	0				-	+		+
	YZ-plane slider shape and friction coefficient		+		+				
Carrier design	Friction coefficients	+/-	+/-	+/-	+/-	+/-	+/-	+/-	
New slider trajectory				+	+	+		+	

Table 5.6: Relation between functions and solutions (positive impact "+", negative impact "-", to be determined "+/-", neutral "0")

Note 1: *The tangential friction coefficient negatively impacts the overrotation in two ways. Firstly, it increases the rotation rate of the parcels, increasing the overrotation due to their angular momentum. Secondly, the design does not take the design parameter objective for reducing overrotation into account, since other functions were given a higher priority here.*

Note 2: *The low pressure center (due to the shape in the YZ-plane) benefits the parcel rotation rate.*

Chapter 6

Results

From the parcel behaviour analysis in chapter 4, seven unwanted behaviour modes remained. Solutions for these seven problems have been generated in chapter 5. The effectiveness of these solutions will be assessed in this chapter on the basis of experimental test results.

6.1 Prototype

One of the major aspects of the concept design that requires testing and assessment is the friction diode (shown in Figure 5.7). A prototype (Figure 6.1) is therefore created which can be mounted on the test setup. The prototype consists of a metal component with a diameter of 30 mm which has a ratchet and pawl mechanism inside, enabling rotation in only one direction. A rubber tape around the circumference provides a high friction coefficient.



Figure 6.1: Mechanical friction diode prototype

6.2 Reduce overrotation due to angular momentum

As explained in Section 4.9, there is a risk that parcels overshoot when rotated. This issue can be reduced by decreasing the angular velocity of the sliders during sorting. A new slider trajectory, with a decreased angular velocity, is proposed (Section 5.1.1). This trajectory is implemented in the test setup and compared to the current sort trajectory.

Figure 6.2 shows the performance improvement (%) in terms of the orientation error using the new trajectory. This is calculated using Equation 6.1. The overshoot is significantly reduced for a y -position greater than 500 mm. However, below 500 mm the new trajectory behaves significantly worse. The trajectory used in this test could thus only be used if there is sufficient distance to the outfeed. This depends on the initial y -position of

the parcel. A possibility is to customize the trajectory, based on the y-distance available.

$$\frac{|\Delta\theta_{error_old}| - |\Delta\theta_{error_new}|}{|\Delta\theta_{error_old}|} * 100\% \quad (6.1)$$

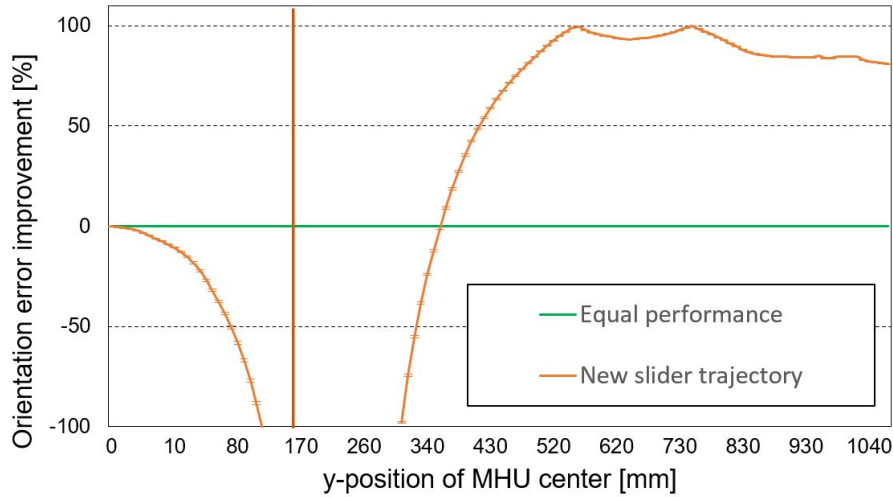


Figure 6.2: Increased rotation radius results

The overrotation could be further reduced by decreasing the tangential slider friction μ_{s_tan} , yet this could result in an increase of risk R.14. Another possibility is to increase the carrier friction coefficient, yet this is also in conflict with other risk reduction objectives (Table 5.5).

6.3 Increased rotation rate

An excessive rotation radius of parcels proved to be a problem, as explained in Section 4.8. Analysis of this problem concluded that one of the major design parameters influencing this problem is the tangential slider friction ($\mu_{s_tan}^+$), which should be minimized. The friction diode prototype satisfies this objective. To find the effectiveness of this solution, it is tested and compared to the current slider design.

Figure 6.3 shows the performance improvement (%) in terms of the orientation error (calculated using Equation 6.1). As expected, the friction diode greatly improves the first stage of the sort action. Reducing the y-distance required to rotate the parcel from its initial orientation (0°) to its desired orientation (30°) by 27 %. This reduction becomes even larger when the parcel has an initial orientation of -30° , as can be seen in figure 13 in the confidential Appendix. In this case, the y-distance required for this rotation (which is 60° in total) is reduced by 35 %. Loss of contact between the sliders and parcel due to the under rotation (which occurs with the current slider design) is also completely eliminated (for the specific parcel that is tested) with friction diode.

Yet, when using the friction diode, the parcel orientation still diverges after reaching the desired orientation. This is partially caused by the increased rotation rate that the prototype design enables (this results in the problem explained in Section 4.9). The new slider trajectory proved to be an effective solution for this overrotation (Figure 6.2). This solution can, therefore also be combined with the friction diode to improve the behaviour of this parcel further.

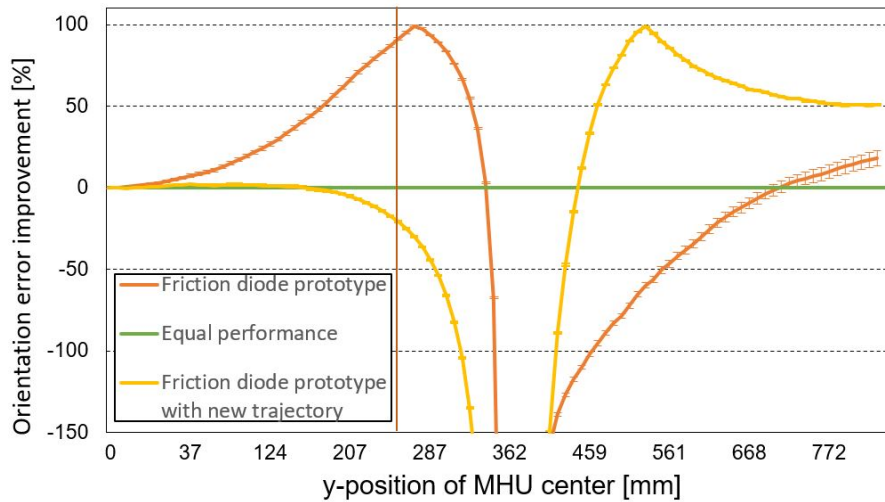


Figure 6.3: Increased parcel rotation rate results

The remaining error is primarily due to insufficient support for this parcel. Measures to reduce this problem are analyzed in the next Section.

6.4 Reduce unwanted rotation

As explained in Section 4.12, there is a risk of unwanted rotation of parcels during sorting. An improved slider shape has been derived to reduce the rotation of small parcels. However, with the test setup, it is currently not yet possible to position the sliders based on the parcel contour. Yet, this feature is required to test the effectiveness of the XY-plane slider shape in preventing small parcels from rotating. However, based on the theoretical analysis, the transport length of parcels which could be sorted in a stable manner is reduced from $3W_{slider}$ to $\frac{3}{2}W_{slider}$. The parcel length distribution for parcels in the market segment "smalls" is shown in Figure 18 in the confidential Appendix. From this figure can be derived that with the new slider design, an additional 63% of all parcels in this segment can be pushed in a stable manner.

6.5 Reduce space use during rotation

A disadvantageous COR position can result in additional space use (see Figure 4.31). From the analysis of this problem (in Section 4.10) was concluded that the tangential slider friction ($\mu_{s,tan}^+$) should be minimized to reduce this problem. The friction diode

prototype satisfies this objective. To find the effectiveness of this solution, it is tested and compared to the current slider design.

The test results are shown in Figure 6.4. The graphs show a parcel's upstream and downstream displacement throughout the sort action for both the current slider and the prototype. When the has an orientation of 0° (Figure 6.4) the prototype reduces the x-displacement throughout the sort action by 22 % (from 287 mm to 223 mm). For an initial parcel orientation of -30° , this reduction is 39 % (from 242 mm to 149 mm), as can be seen in Figure 16 in the confidential Appendix.

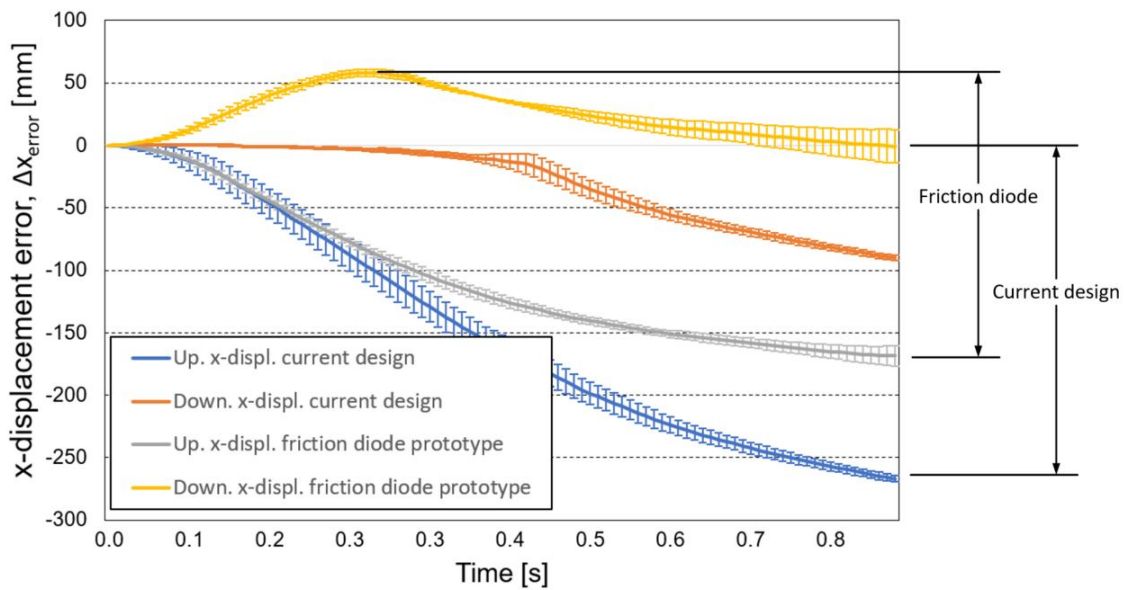


Figure 6.4: Improved center of rotation results ($\theta_{mhu_initial} = 0^\circ$)

6.6 Reduce sliding along the sliders

The current slider design already has a relatively good friction coefficient to prevent sliding. A comparison between the friction diode and the current slider thus gives little insight. So instead a comparison is made between the friction diode (low friction in only one direction) and a low-friction material slider (low friction in both directions), to highlight the importance of a sufficient friction coefficient in the negative x-direction.

Figure 6.5 shows the x-displacement of the center of a parcel throughout the sort action for both the friction diode slider and a low-friction material slider. With the low friction slider, the parcel keeps sliding in the x-direction, up to a total displacement of 241 mm. This highlights the importance of a sufficient friction coefficient in the negative x-direction ($\mu_{s_tan}^-$).

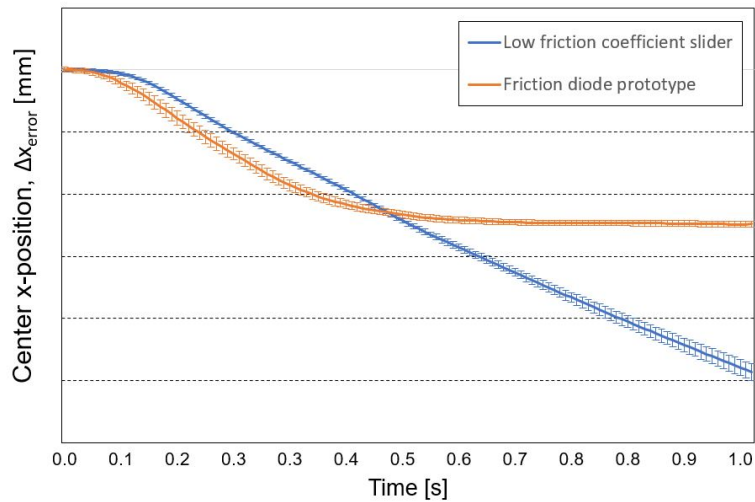


Figure 6.5: Reduced sliding along the sliders results

Note: Numerical values have been removed from the graphs due to confidentiality

6.7 Conclusion

A prototype is created to assess the effectiveness of different features of the concept design. Every design aspect that is tested showed improvement with respect to the current slider design. These improvements and their impact on important system properties are given below. The calculations and assumptions used to calculate these percentages are shown in Section A.10.

- Improved rotation behaviour, maintaining better contact with the sliders during the sorting process (less over- or under-rotation). This enables sorting parcels in the desired orientation more accurately. This can potentially reduce margins, which can reduce the sorter length by up to 14% (see Section A.10.1). Moreover, an increased parcel rotation rate could reduce the sorter width up to 16% (Section A.10.2).
- More efficient rotation of parcels results in up to 16 % less space required for the rotation of parcels. This could result in smaller gaps between parcels, yielding a potential capacity increase up to 16 % (Section A.10.3).
- Increased capacity due to improved support of small parcels, allowing smaller gaps for these parcels.
- Enable sorting square parcels with an unfavourable COM location without unwanted rotation, which was not possible before.

Chapter 7

Conclusion and recommendations

This chapter concludes the steps taken and methodologies used to come to the main findings of this study. Also, recommendations are given to both Vanderlande Industries and the scientific community for potential future actions to maximize the impact of this study.

7.1 Conclusion

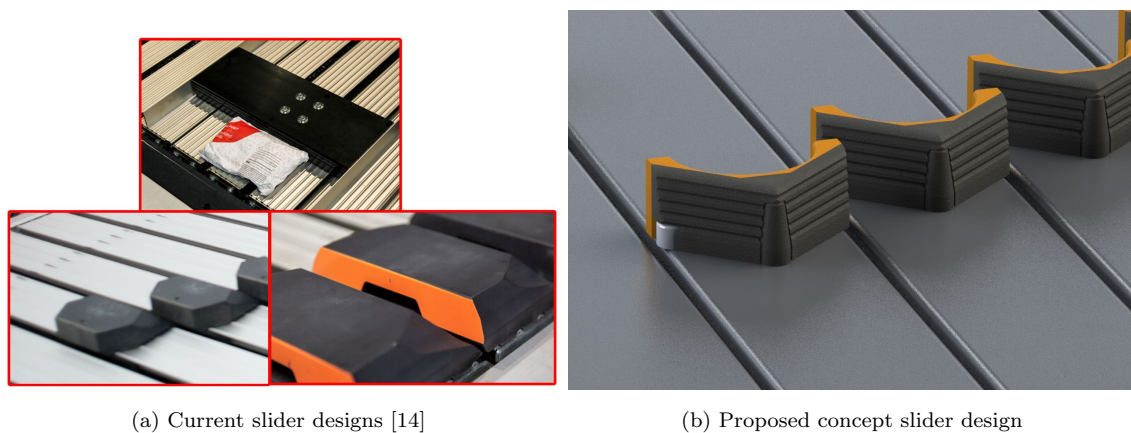
The aim of this project was to research the influence of the slider and carrier design on the performance of the sorter. Also, these insights should yield a new slider and carrier design which improves the sorter performance. These steps have been taken to achieve this.

Four main drivers for developing the new sorter have been translated into KPIs for the current study. These KPIs (Table 3.3) represent important aspects of the physical parcel state during the sorting process and when entering the outfeed. Important sorter variables and settings which could affect these KPIs have been identified and analyzed. Moreover, also parcel characteristics, which impact performance, have been studied and the most influential ones have been listed. These variables, which influence the parcel behaviour, but can not be controlled, are referred to as input variables. These input variables are summarized in Table 3.4.

Based on multiple input sources, 20 separate unwanted parcel behaviour modes were identified (Figure 4.1). Parcel behaviour is divided into these separate modes based on their cause and outcome. The physical causes for each type of unwanted behaviour have been analyzed individually. This was done by a combination of theoretical analysis and physical testing (Section 4.2). The slider and carrier designs were translated into design parameters which could be used in the theoretical analysis. These parameters represent the aspects of the design that have the most influence on parcel behaviour. The tests were performed on the test setup described in Section 3 in the confidential Appendix.

During these tests, the KPIs were extracted by measuring the physical state of the parcel using a tracking camera (Figure 4.4). On the basis of these KPI values, seven risks proved to be most significant (see table A.1). To reduce these risks, objectives and constraints were derived for each influential design parameter. These design parameter objectives are summarized in Table B.1 and B.2.

In order to minimize these risks, a design was created based on the design parameter objectives. The different aspects of the slider in terms of shape and friction coefficients have been carefully chosen in order to satisfy the most objectives possible. This resulted in the slider design shown in Figure 7.1b. Using this methodology gave a clear overview of any conflicting design objectives. In case of any conflicts, the first step was to find solutions to still satisfy both objectives. Such as the friction diode (Figure 5.7) and the horizontal groves in the pusher surface (Figure B.4). In case no solution was found for the conflict, preference was given to the risk with the least alternative design parameter solutions.



(a) Current slider designs [14]

(b) Proposed concept slider design

Figure 7.1: Current and new slider design

On top of the concept design, also additional solutions were explored for further performance improvement. The two most promising solutions (from the morphological chart in Figure B.1 and B.2) have been analyzed in greater detail and necessary design measures are taken in order to incorporate these features.

Finally, a prototype was created and tested in order to assess the effectiveness of the solutions. In these tests, the current slider design is compared to the concept design.

- Improved rotation behaviour, maintaining better contact with the sliders during the sorting process (less over- or under-rotation). This enables sorting parcels in the desired orientation more accurately. This can potentially reduce margins, which can reduce the sorter length by up to 14% (see Section A.10.1). Moreover, an increased parcel rotation rate could reduce the sorter width up to 16% (Section A.10.2).
- More efficient rotation of parcels results in up to 16 % less space required for the rotation of parcels. This could result in smaller gaps between parcels, yielding a potential capacity increase up to 16 % (Section A.10.3).
- Increased capacity due to improved support of small parcels, allowing smaller gaps for these parcels.

- Enable sorting square parcels with an unfavourable COM location without unwanted rotation, which was not possible before.

In conclusion, as the research has shown, an improved performance have been achieved with the new concept design while also reducing the number of slider configuration required.

7.2 Recommendations

7.2.1 Roadmap for slider and carrier design

First, it is important that VI tests the three risks which are primarily driven by aerodynamic forces (R.5, R.10 and R.20). These tests can be done when a setup is available that also moves in the x-direction (which is not the case for the setup currently used). Besides, the concept solutions related to the slider trajectory should be implemented and assessed. This regards the trajectory of support sliders and parcel contour-based parallel sorting. Based on the conclusion that can be drawn from the activities above, the concept design can be updated and improved. When the overall concept design of the slider is definite, measures to prevent jamming should be implemented (R.4, R.13, R18, R.19).

The finished concept design can be produced. Rapid prototyping is particularly suitable to produce the required shape. A surface treatment will be necessary (with some kind of rubber-like material) to give the slider its required friction properties. Finally, this design should be tested and further optimized.

7.2.2 Parcel behaviour in outfeeds

One of the main aspects of the new sorter is accuracy, sorting as many parcels into the right outfeed as possible. In the current study, this is maximized by improving the parcel behaviour on the sorter. However, the behaviour of parcels when they entered the outfeed is not analyzed. An analysis of the behaviour of the parcel in the outfeed could yield further accuracy improvement. Firstly, this could be done by improving the outfeed design. Secondly, the sort trajectory of the sliders could also be optimized based on findings of parcel behaviour in the outfeeds. An example of this could be that light products are highly impacted by aerodynamics in the outfeed, requiring throwing them further back or forth in the outfeed to compensate for this unwanted behaviour in the outfeed.

7.2.3 Dataset on parcel characteristics

The analysis of the parcel characteristics in this study is mostly qualitative because little data to work with was available. For future development or optimization studies, it can be valuable if a large dataset on parcel characteristics would be available. Competitor Siemens already seem to have a data set like this [32], yet this is not publicly available. Such a

dataset enables a statistical design approach which results in more realistic requirements and load scenarios. A critical parcel could then be chosen for example based on statistical relevance instead of taking a parcel which is the worst case in all aspects (as was currently often done). This approach might have resulted in very rare and insignificant scenarios as a foundation for system requirements. The data could be gathered by implementing sensors and cameras in the first actual system that will be delivered to a client.

7.2.4 Future studies

A solution found in this study which could be further explored is the proposed friction diode (Figure 5.7). Robotic manipulators often require single-direction friction as was the case for the slider. A popular solution for this is so-called gecko adhesion [2], which uses Van der Waals forces to stick to a surface when loaded in a specific direction. Though this solution is only applicable when the product to be handled has a smooth surface. The friction diode is capable of achieving this same principle for rough surfaces. Yet, no robotic applications of the proposed friction diode have been found. This leaves the possibility of exploring other applications where this mechanism could be a useful solution.

Bibliography

- [1] Mohamed Alost. “The smart carrier: design of a novel approach to the next generation of line sorters”. In: (2019).
- [2] Kellar Autumn and Anne M Peattie. “Mechanisms of adhesion in geckos”. In: *Integrative and comparative biology* 42.6 (2002), pp. 1081–1090.
- [3] II William A Bastian, Garrett Clark, and II Eric C Halvorson. *Cross belt slat sorter*. US Patent 9,409,716. Aug. 2016.
- [4] Jon Cohen. *The Importance of Packaging in Logistics*. <https://www.shiproyal.com/rsc-the-importance-of-packaging-in-logistics/>. Sept. 2019.
- [5] Larissa Custodio and Ricardo Machado. “Flexible automated warehouse: a literature review and an innovative framework”. In: *The International Journal of Advanced Manufacturing Technology* 106.1 (2020), pp. 533–558.
- [6] Mark R Cutkosky and Paul K Wright. “Friction, stability and the design of robotic fingers”. In: *The International Journal of Robotics Research* 5.4 (1986), pp. 20–37.
- [7] Michael Erdmann. “On a representation of friction in configuration space”. In: *The International Journal of Robotics Research* 13.3 (1994), pp. 240–271.
- [8] National Postal Forum. *Top 5 Sortation Challenges Facing Parcel Operations*. <https://sps.honeywell.com/us/en/support/blog/automation/top-5-sortation-challenges-facing-post-parcel-operations>. May 2017.
- [9] Jakobus M van den Goor. *Conveyor*. US Patent 5,435,429. July 1995.
- [10] Suresh Goyal. “Planar sliding of a rigid body with dry friction: limit surfaces and dynamics of motion”. PhD thesis. Cornell University Ithaca, NY, 1989.
- [11] Suresh Goyal, Andy Ruina, and Jim Papadopoulos. “Planar sliding with dry friction part 1. limit surface and moment function”. In: *Wear* 143.2 (1991), pp. 307–330.
- [12] F Hafner. “Prozess zur Beschreibung des Fly-Out Verhaltens von Polybags innerhalb eines Sortiersystems”. In: *Masterarbeit, Graz* (2021).
- [13] Russell Charles Hibbeler. *Engineering mechanics: dynamics*. Pearson Educación, 2004.
- [14] Vanderlande Industries. *Company document*.
- [15] Vanderlande Industries. *PRODUCT HANDLING UNITS*. 11224-620-PD222. 2007.
- [16] Mordor Intelligence. *COURIER, EXPRESS, AND PARCEL (CEP) MARKET – GROWTH, TRENDS, COVID-19 IMPACT, AND FORECASTS (2022 - 2027)*. 2021. URL: <https://www.mordorintelligence.com/industry-reports/courier-express-and-parcel-cep-market>.
- [17] Intelligrated. *Sorting out your sortation options*. n.d.

- [18] Maarten de Jager. “Increasing the flexibility of a push divert sorter by designing an individual actuated slider-carrier system with local intelligence: A feasibility study”. In: (2018).
- [19] Francesco Jovane, Yoram Koren, and CR Boer. “Present and future of flexible automation: towards new paradigms”. In: *CIRP Annals* 52.2 (2003), pp. 543–560.
- [20] Ping Lu et al. “The use of anisotropic texturing for control of directional friction”. In: *Tribology International* 113 (2017), pp. 169–181.
- [21] Kevin M Lynch and Frank C Park. *Modern robotics*. Cambridge University Press, 2017.
- [22] Smithsonian magazine. *Scientists Turn Packing Peanuts Into Battery Components*. URL: <https://www.smithsonianmag.com/innovation/scientists-turn-packing-peanuts-into-battery-components-180954697/>.
- [23] Filipe Marques et al. “A survey and comparison of several friction force models for dynamic analysis of multibody mechanical systems”. In: *Nonlinear Dynamics* 86.3 (2016), pp. 1407–1443.
- [24] James L Meriam, L Glenn Kraige, and Jeff N Bolton. *Engineering mechanics: dynamics*. John Wiley & Sons, 2020.
- [25] NASA. *Drag Equation*. 2022. URL: <https://www1.grc.nasa.gov/beginners-guide-to-aeronautics/drag-equation/>.
- [26] NASA. *Lift Formula*. 1996. URL: https://www.grc.nasa.gov/WWW/K-12/WindTunnel/Activities/lift_formula.html.
- [27] Hunt Office. *Jiffy Assorted Sizes Gold AirKraft Bubble Lined Protective Envelopes Bag Pack of 50*. URL: <https://huntoffice.co.uk/jiffy-brown-assorted-airkraft-bags-pack-of-50-37378.html>.
- [28] Tomasz Piatkowski. *Analiza i modelowanie procesu sortowania strumienia małowabarytowych ładunków jednostkowych*. Wydawnictwa Uczelniane Uniwersytetu Technologiczno-Przyrodniczego, 2010.
- [29] Tomasz Piatkowski. *Analiza i modelowanie procesu sortowania strumienia małowabarytowych ładunków jednostkowych*. Wydawnictwa Uczelniane Uniwersytetu Technologiczno-Przyrodniczego, 2010.
- [30] Mikhail Popov, Valentin L Popov, and Nikita V Popov. “Reduction of friction by normal oscillations. I. Influence of contact stiffness”. In: *Friction* 5.1 (2017), pp. 45–55.
- [31] Valentin L Popov, Markus Heß, and Emanuel Willert. *Handbook of contact mechanics: exact solutions of axisymmetric contact problems*. Springer Nature, 2019.
- [32] Michael Schadler et al. “Characteristics of ‘polybags’ used for low-value consignments in the mail, courier, express and parcel industry”. In: *Logistics Journal: Reviewed Publications 2022* (2022).

- [33] Statista. *Global parcel shipping volume between 2013 and 2026 (in billion parcels)*. 2021. URL: <https://www.statista.com/statistics/1139910/parcel-shipping-volume-worldwide/>.
- [34] David E Stewart. “Rigid-body dynamics with friction and impact”. In: *SIAM review* 42.1 (2000), pp. 3–39.
- [35] Yuehuan Su et al. “Characterizing the environmental impact of packaging materials for express delivery via life cycle assessment”. In: *Journal of Cleaner Production* 274 (2020), p. 122961.
- [36] Halvor T Tramsen et al. “Inversion of friction anisotropy in a bio-inspired asymmetrically structured surface”. In: *Journal of The Royal Society Interface* 15.138 (2018), p. 20170629.
- [37] UPS. *Internal Packaging*. URL: <https://www.ups.com/re/en/help-center/packaging-and-supplies/packing-materials/internal-packaging.page>.
- [38] Zhi-Wei Wang. “Dropping damage boundary curves for cubic and tangent package cushioning systems”. In: *Packaging Technology and Science: An International Journal* 15.5 (2002), pp. 263–266.
- [39] Zhi-Wei Wang. “On evaluation of product dropping damage”. In: *Packaging Technology and Science: An International Journal* 15.3 (2002), pp. 115–120.
- [40] P.J. Werkman. “Optimisation of parcel sortation profile”. In: (2018).
- [41] PAN XIANGWU. *Logistics sorting and steering device*. China Patent CN109516151. 2018.

Appendix A

Figures and calculations

A.1 Literature figures

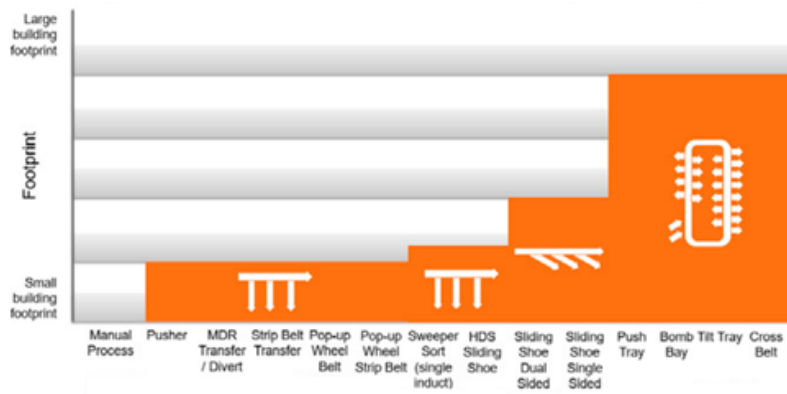


Figure A.1: Typical footprint of different linear and loop configuration sorters

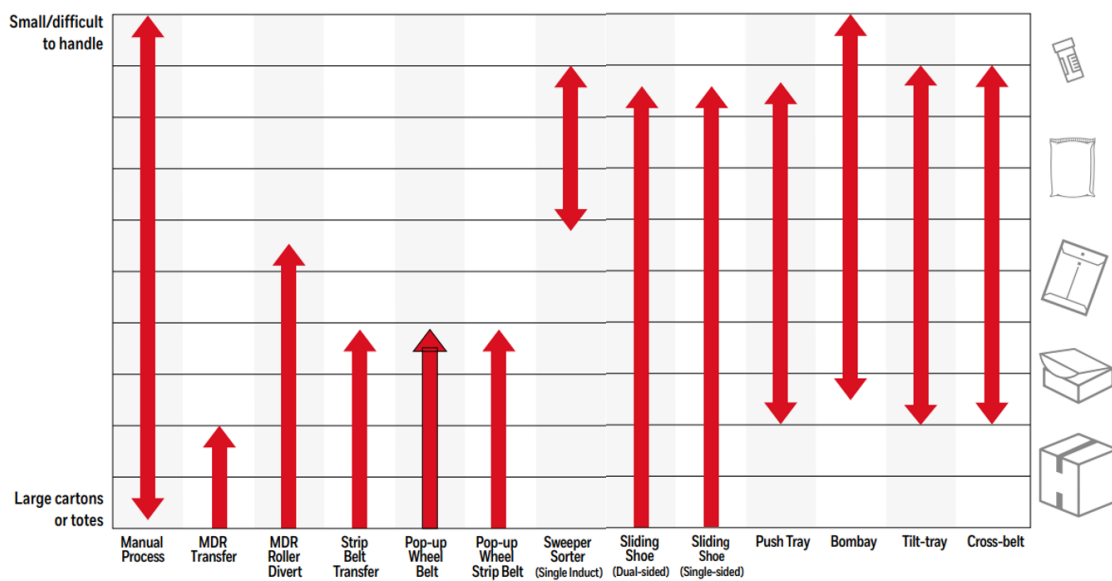


Figure A.2: Typical compatibility of different sorter types with varying products types [17]

A.2 Yield strength of commonly used packaging types

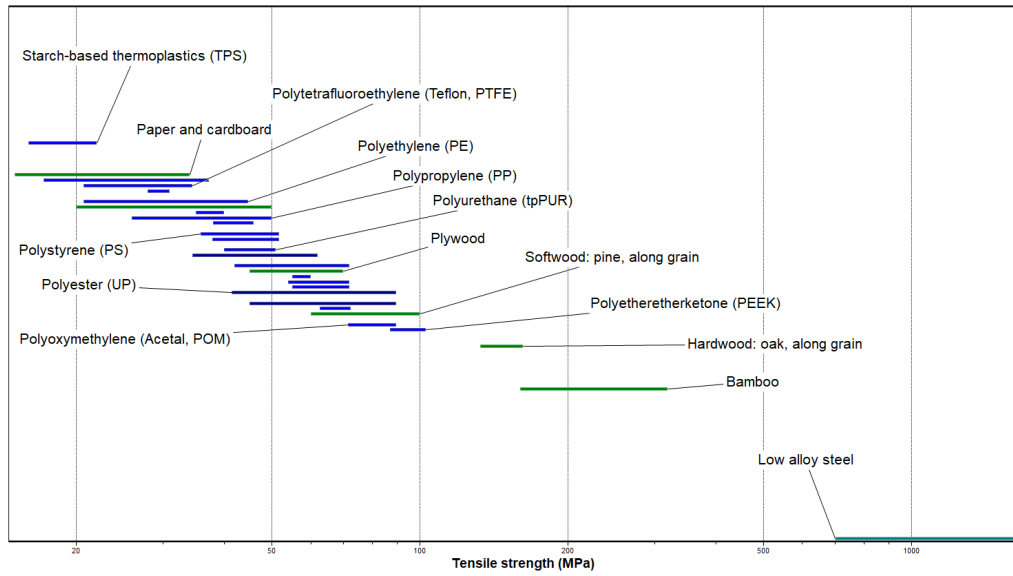


Figure A.3: (Tensile) strength of packaging materials (from CES Edupack)

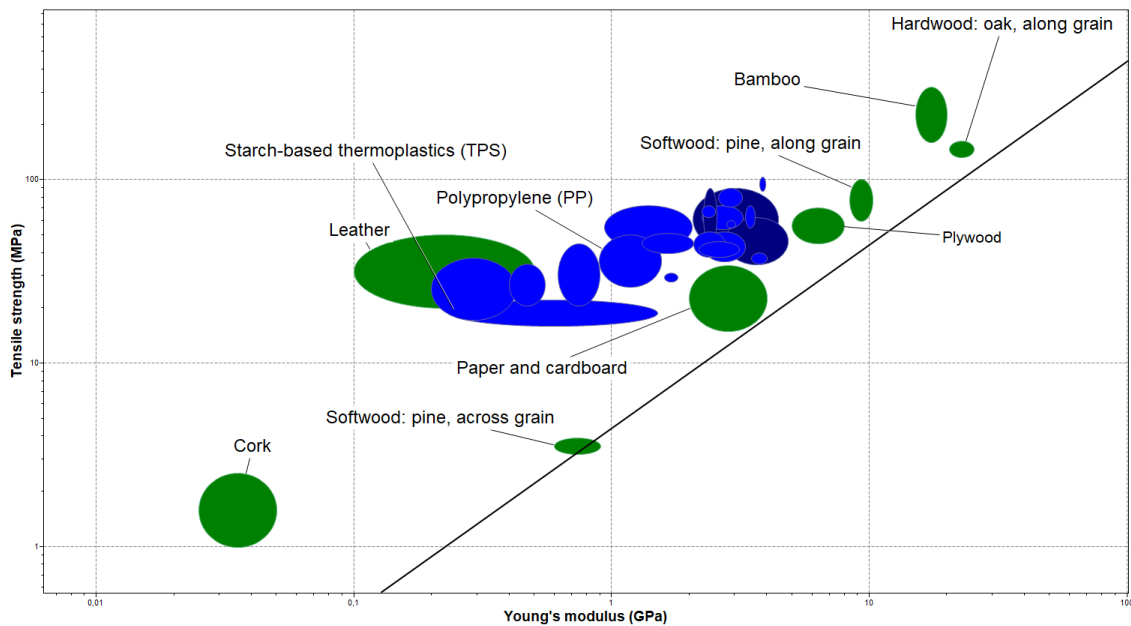


Figure A.4: Packaging material comparison graph (Youngs Modulus and yield strength)

A.3 Physical impact model

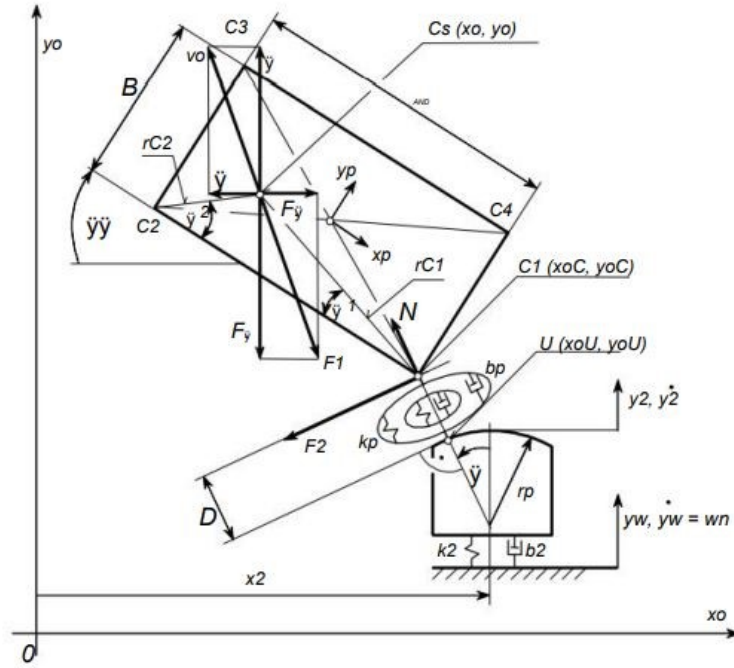


Figure A.5: Physical model of slider impact on parcel [29]

where:

- m_p, m_2 = mass of package and slider ($m_p \gg m_2$)
- k_p, b_p, k_2, b_2 = coefficients of stiffness and damping of the package and slider support
- y_2 = position of slider
- y_w = displacement given to the slider by actuators
- x_o, y_o = position of center of mass of package
- ζ, η = Components of the velocity of the center of mass of the package
- T = moment of friction forces between the package and carriers
- F_ζ, F_η = components of the friction force of the package on the carriers

A.4 Absolute outfeed protrusion error calculation

The absolute outfeed protrusion is the distance a parcel protrudes from the outfeed measured perpendicular from the outfeed side (as illustrated in Figure A.6).

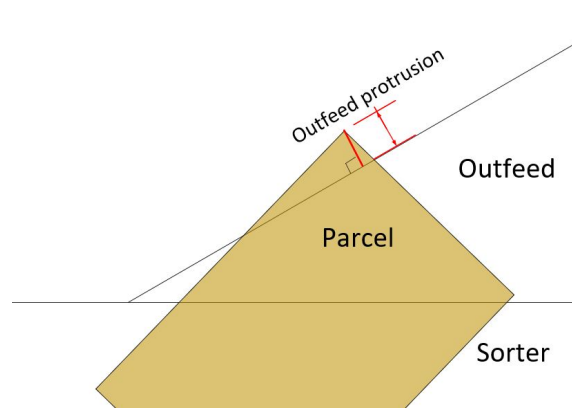


Figure A.6: Definition of the absolute outfeed protrusion distance

This absolute protrusion distance with a certain x-position error depends on the outfeed angle and sort angle. In the picture below, the blue contour is the initial position of a parcel. The orange contour is the parcel when shifted in the x-direction (error). The green parcel is the final location of the parcel in contact with the sliders. The effect of the x-position error (x_{error}) on the outfeed width error can be magnified or eliminated depending on the sort angle (θ_{sort}). " Δd " can first be calculated with:

$$\Delta d = \frac{x_{error}}{\cos(\theta_{sort})} \quad (A.1)$$

Then the outfeed protrusion error (highlighted in red) can be calculated with the following:

$$W_{outfeed_error} = \sin(\alpha_{outfeed} + \theta_{sort}) * \frac{x_{error}}{\cos(\theta_{sort})} \quad (A.2)$$

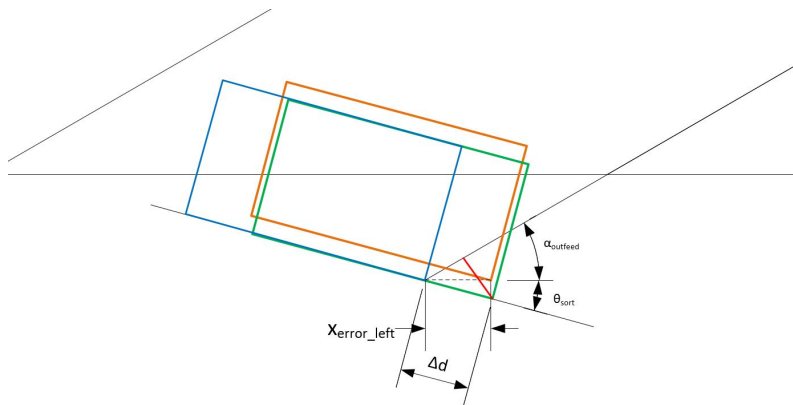


Figure A.7: Morphological chart (part 2)

When the sort angle (θ_{sort}) is equal to the outfeed angle, the x-error (x_{error}) cancels out; this is thus the case for sequential sorting. Thus in other words, the x-position error does not influence the sort accuracy in case of sequential sorting.

A.5 Drag coefficients of a plastic package

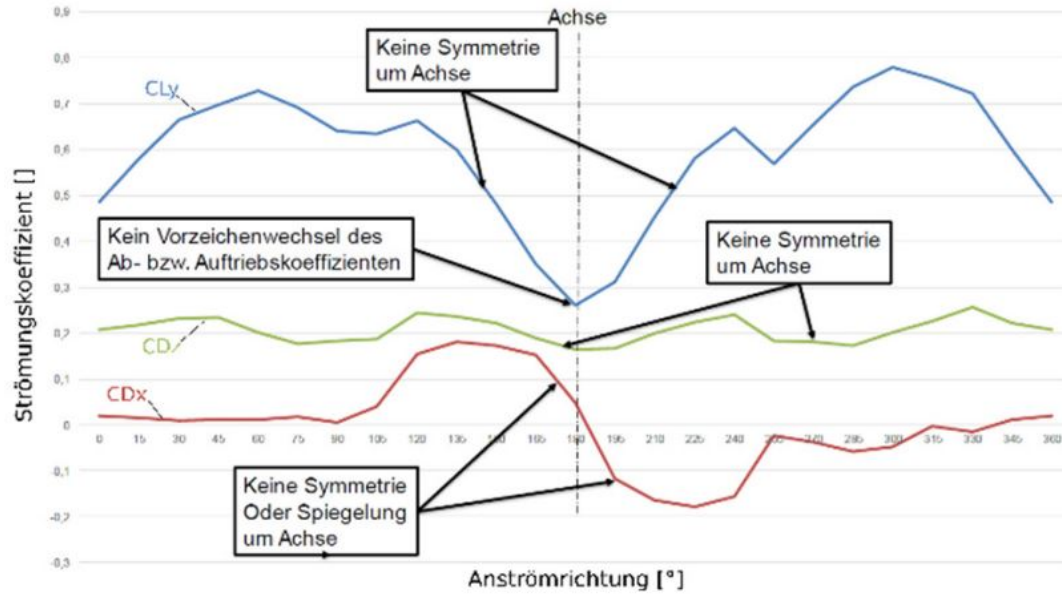


Figure A.8: Airflow coefficients of a polybag for different flow directions [12]

A.6 Calculation sliding onto slider

Equation A.4 for estimating whether a parcel will slide onto the slider or not are derived using the model presented in Figure 4.13.

$$-F_c - F_{c2} + N_s * \sin(\beta) + F_s * \cos(\beta) = m_{mhu} * \ddot{x} \quad (\text{A.3})$$

$$-m_{mhu} * g * \mu_{c,y} - \sin(\beta) * N_s \mu_{s,ax} * \mu_{c,y} + N_s * \sin(\beta) + N_s * \mu_{s,ax} * \cos(\beta) = m_{mhu} * \ddot{x} \quad (\text{A.4})$$

A.7 Calculation backward toppling

The critical acceleration before a parcel starts toppling can be calculated by setting the angular acceleration (α_x) equal to zero (since there is no rotation around the x-axis in a stable state):

$$M_c = I_x * \alpha_x \quad (\text{A.5a})$$

$$N_s * H_{slider} + m_{mhu} * g * W_{mhu} - a_{critical} * m_{mhu} * \frac{2 * H_{mhu}}{3} = 0 \quad (\text{A.5b})$$

$$a_{critical} = \frac{3 * N_s * H_{slider}}{2 * m_{mhu} * W_{mhu}} + \frac{g}{2} \quad (\text{A.5c})$$

And the Equation of motion in the y-direction is following:

$$F_y = m_{mhu} * a_{critical} \quad (A.6a)$$

$$N_s - F_c = m_{mhu} * a_{critical} \quad (A.6b)$$

$$N_s - m_{mhu} * g * \mu_{c-y} = m_{mhu} * a_{critical} \quad (A.6c)$$

Substituting these equations gives the following equation:

$$a_{critical} = g * \frac{W_{mhu} + 3\mu_{c-y}H_{slider}}{2L_{mhu} - 3H_{slider}} \quad (A.7)$$

A.8 Calculation free sliding deceleration

The motion of such a parcel which is decelerated due to friction is illustrated in Figure A.9. The final parcel state (when it left the sorter) has three potential error states: speed (Δv_{error}), direction ($\Delta \alpha_{error}$) and position (Δx_{error}).

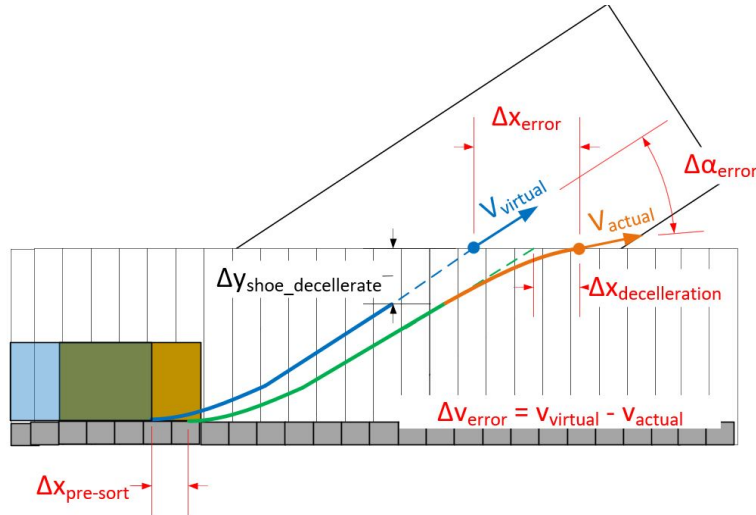


Figure A.9: Parcel trajectory error due to deceleration after contact with sliders is lost

The deceleration is considered until the parcel is fully clear of the sorter. The sliding distance can be calculated by the conservation of energy. The difference in kinetic energy (before and after sliding) is equal to the work done by the friction force, since the decks are horizontal, no work is done by the force resulting from gravity. Aerodynamic drag is neglected.

$$E_k = E_w \quad (A.8)$$

$$\frac{1}{2}m(\Delta v)^2 = mg\mu d_{sliding_distance} \quad (A.9)$$

$$\Delta v = \sqrt{2g\mu d_{sliding_distance}} \quad (A.10)$$

So the velocity direction error is:

$$\Delta\alpha_{error} = \tan^{-1}\left(\frac{v_i}{v_{sorter}}\right) - \tan^{-1}\left(\frac{\Delta v - v_i}{v_{sorter}}\right) \quad (\text{A.11})$$

$$\begin{aligned} \Delta t_{error} &= \Delta t_{normal} \Delta t_{decelerated} \\ \Delta t_{error} &= \frac{d_{sliding_distance}}{v_i} - \frac{d_{sliding_distance}}{\frac{v_i + v_f}{2}} \end{aligned}$$

Where:

$$v_f = v_i - \Delta v$$

and

$$\Delta x_{error} = \Delta t_{error} * v_{sorter}$$

Then:

$$\Delta x_{error} = v_{sorter} * \left(\frac{d_{sliding_distance}}{v_{initial}} - \frac{d_{sliding_distance}}{\frac{v_{initial} + (v_i - \sqrt{2g\mu d_{sliding_distance}})}{2}} \right)$$

The x-position error (Δx_{error}) resulting from the deceleration is plotted in Figure 4.43 with respect to the deceleration distance of the sliders.

A.9 Conclusion (table) material behaviour analysis

Number	Potential risks in parcel behaviour	Discard			Take into account
		Within margin	Inconclusive	Out of scope	
R.1	MHU shifts and/or rotates due to impact of sliders	X			
R.2	Damage to either slider or MHU due to impact of sliders	X			
R.3	The COR of the MHU is in a disadvantageous position				X
R.4	MHU jams between the sliders		X		
R.5	MHU shifts and/or rotates due to airflow and vibrations			X	
R.6	MHU slides onto sliders				X
R.7	MHU topples backwards over sliders	X			
R.8	MHU shifts and/or rotates due to secondary (loose content) impact	X			
R.9	Overrotation of MHU due to angular momentum				X
R.10	MHU shifts and/or rotates during sorting due to airflow			X	
R.11	MHU has an excessive rotation radius				X
R.12	MHU deformation results in an increased transport length			X	
R.13	MHU jams between slider and slat		X		
R.14	MHU rotates due to insufficient support				X
R.15	MHU slides along the sliders				X
R.16	Damage to either slider or MHU due to contact pressure				X
R.17	MHU interferes with adjacent MHU	X			
R.18	MHU jams between two opposite side positioned sliders		X		
R.19	MHU jams between sorter and outfeed		X		
R.20	MHU decelerates when contact with sliders is lost			X	

Table A.1: Conclusion parcel behaviour analysis

Note 1: A detailed justification for the parcel behaviour conclusions can be found in Section D.7 (confidential appendix)

A.10 Sorter performance increase calculations

A.10.1 Length decrease due to reduced rotation overshoot

If the sorter does not manage to push parcels into the outfeed in the required orientation, the outfeed width has to be increased ($W_{outfeed_margin}$). The new sort trajectory reduced the orientation error by about 8° and this is not even a critical parcel yet (so this reduction could even be bigger). For a parcel with maximum dimensions $W_{mhu} = 900 \text{ mm}$ and $L_{mhu} = 1000 \text{ mm}$, the outfeed margin can be calculated as follows:

$$W_{outfeed_margin} = \sin(\Delta\theta_{error}) * L_{mhu} = 139 \text{ mmm} \quad (\text{A.12})$$

This is an outfeed width increase of 13,9 %. So, if all parcels handled by the sorter would be similar to parcel A9 used in test 6.2, the sorter length could be decreased by 14% with the new trajectory.

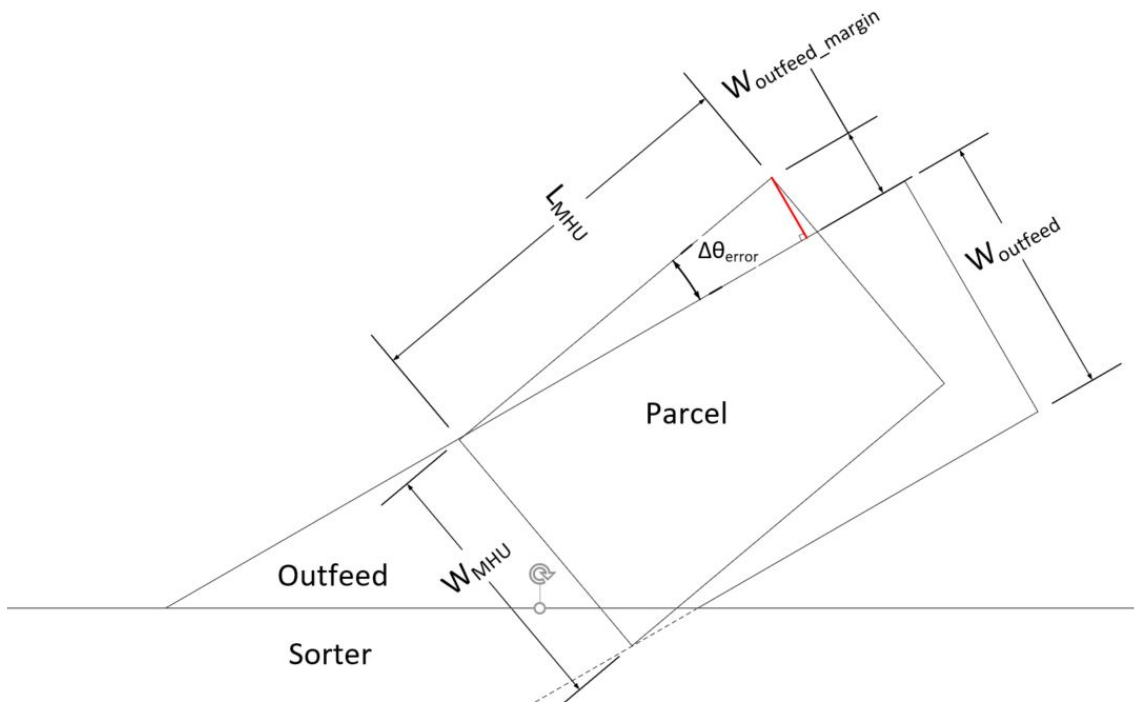


Figure A.10: Parcel length distribution for small parcels

A.10.2 Sorter width decrease due to reduced rotation radius

The prototype reduces the distance (in y-direction) required to rotate the parcel from 0 to 30 degrees by 99 mm 6.3. When the parcel has an initial orientation of -30° , the reduction is 195 mm. On an average sorter width of 1200 mm this could result in a 8,5 % and 16 % width decrease.

A.10.3 Improved COR location

The parcel in Figure D.18 (confidential appendix) uses 927 mm in the x-direction throughout the sort action with the current slider design. With the friction diode, this distance is reduced by 16 % (to 775 mm). In case the whole flow of products would consist of this parcel type in this orientation, the friction diode would thus have the potential to increase the throughput capacity by 16 %.

Appendix B

Conceptual design

B.1 Design parameter table

Design parameter objectives are derived in Chapter 4 for the seven most significant unwanted parcel behaviour types that were found. These objectives are summarized in Table B.1 and B.2.

	Reference	H_{slider}	L_{slider}	W_{slider}	$\mu_{s,tan}$	$\mu_{s,ax}$	x_{spe}	y_{spe}	z_{spe}	
Performance related	F.1				Min + $-30^\circ \leq \theta_{mhu} \leq 30^\circ$					
	F.2	Max				Max +				
	F.3				Min - $30^\circ \leq \theta_{mhu} \leq 60^\circ$		Min			
	F.4				Min + $-30^\circ \leq \theta_{mhu} \leq 30^\circ$		Max		Min	
	F.5	Sequential sort				Min - $30^\circ \leq \theta_{mhu} \leq 60^\circ$		Min		
		Parallel sort				Max $0 \leq x_{spe} \leq W_{slider}$ $-90^\circ \leq \theta_{mhu} \leq 90^\circ$		Center (for all θ_{mhu})		
	F.6				$0^\circ \leq \theta_{mhu} \leq 30^\circ$					
F.7		>30 mm								
Control related		Min (m_{slider})			$\theta_{mhu} = 60 \pm 5^\circ$		Minimize variation over all θ_{mhu}	Min	Min	
Wear related					$\theta_{mhu} = 30 \pm 5^\circ$					
Noise related										
Energy use related										
Boundary condition						$0 \leq x_{spe} \leq W_{slider}$	$0 \leq y_{spe} \leq \frac{1}{2}L_{slider}$	$0 \leq y_{spe} \leq \frac{1}{2}H_{slider}$		

Table B.1: Combined design parameter objective table (part 1)

	Reference	$\theta_{tan.cg}$	$\theta_{ax.cg}$	$\mu_{c,x}$	$\mu_{c,y}$	R_s	
Performance related	F.1	Max		>			
	F.2		Max		Min		
	F.3			Max			
	F.4	Max		<			
	F.5	Sort with rotation			>		
		Sort without rotation					
	F.6				>		
F.7						$\geq 25mm$	
Control related							
Wear related							
Noise related							
Energy use related				Min	Min		
Boundary condition		$-90^\circ \leq \theta_{tan.cg} \leq 90^\circ$	$-90^\circ \leq \theta_{ax.cg} \leq 90^\circ$				

Table B.2: Combined design parameter objective table (part 2)

B.2 Morphological charts

The morphological chart in Figure B.1 and B.2 show the solutions found in a brainstorm per function. This section does not consider solutions related to the design parameters (explained in Section 4.1). An example would be increasing the slider height as a solution for function "F.2". This solution is not considered here because it is already considered during the conceptual design process. The solutions are graded (+, ++, +/−, −, −−) on their implementation cost and expected effectiveness (in accomplishing the function). These aspects are indicated with a "C" and "E", respectively.




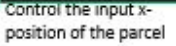

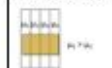
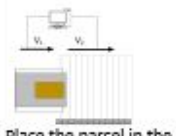





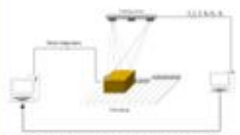
	Solution 1	Solution 2	Solution 3	Solution 4	Solution 5
F.1 Direct the COR of the MHU towards most advantageous position	<p>Limit motion freedom with a physical barrier between the carriers</p>  <p>C: - E: ++</p>	 <p>Add support shoes</p> <p>C: ++ E: ++</p>			
F.2 Reduce sliding of the MHU onto shoes	<p>Give the package a corrugate shape by support design to increase its bending stiffness.</p>  <p>C: ++ E: -</p>				
F.3 Reduce over rotation of the MHU due to angular momentum					
F.4 Reduce the rotation radius of the MHU	<p>Control the input x-position of the parcel</p> 	<p>Exert opposite force on the parcel to increase rate of rotation</p>  <p>Suction</p>	<p>Active friction control</p> 		<p>Change support pressure distribution</p>
	<p>Place the parcel in the optimal position with respect to the shoes</p>  <p>C: + E: -</p>	<p>Apply vacuum suction force</p>  <p>C: -- E: ++</p>	<p>Pre-position or slide shoe with high friction pad under the parcel</p>  <p>C: +/- E: +</p>	<p>Attach a high friction component to each carrier which can be lifted to contact the parcel.</p>  <p>C: - E: +</p>	<p>Lift parcel by means of incline surface</p>  <p>C: + E: +</p>
Reduce the rotation overshoot of the MHU due to impact	<p>Shoe trajectory</p>  <p>Increase shoe trajectory rotation radius</p> <p>C: ++ E: ++</p>		<p>Active adaptive control based on (measured) parcel orientation</p>  <p>C: -- E: +</p>		

Figure B.1: Morphological chart (part 1)

F.5	Reduce unwanted rotation due to insufficient support of the shoes – large sequential sorted parcels	Control the input x-position of the parcel	Shoe trajectory	Exert opposite force on the parcel to prevent rotation	Physical fencing
				Suction Active friction control	
		Place the parcel in the optimal position with respect to the shoes C:+ E:-	Increase rotation radius – minimize the time that the parcel is in an unstable position C:++ E:+	Apply vacuum suction force C:- E:++	Pre-position or slide shoe with high friction pad under the parcel C:+/- E:+
	Reduce unwanted rotation due to insufficient support of the shoes – small parallel				Attach a high friction component to each carrier which can be lifted to contact the parcel. C:- E:+
					Limit parcel rotation with fence inbetween carriers C:- E:++
F.6	Reduce slide of the MHU along shoes	Limit parcel rotation with fence inbetween carriers. C:- E:++			
F.7 Design rule is sufficient, no further improvement required.					

Figure B.2: Morphological chart (part 2)

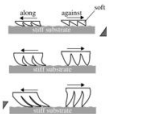
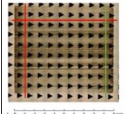
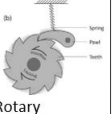
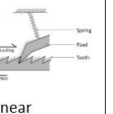
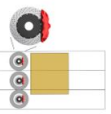
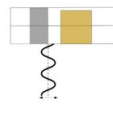
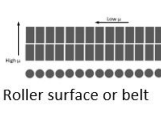
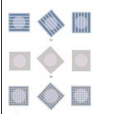
Anisotropic friction (180 degrees)	Method	Passive solutions		Active solutions	
	Solution	Surface texture	Mechanical diode		
		 Sawtooth-structured surface 1)	 Triangular flat dimple surface 2)	 Rotary	 Linear
				 Control friction by active breaking	 Friction control by vibrating the shoe (with inbalanced motor in shoe for example)
Anisotropic friction (90 degrees)	Method	Mechanical	Surface texture		
	Solution	 Roller surface or belt	 3)		

Figure B.3: Morphological chart - enable anisotropic friction coefficient 1): [36], 2) [20]

B.3 Groves in slider surface

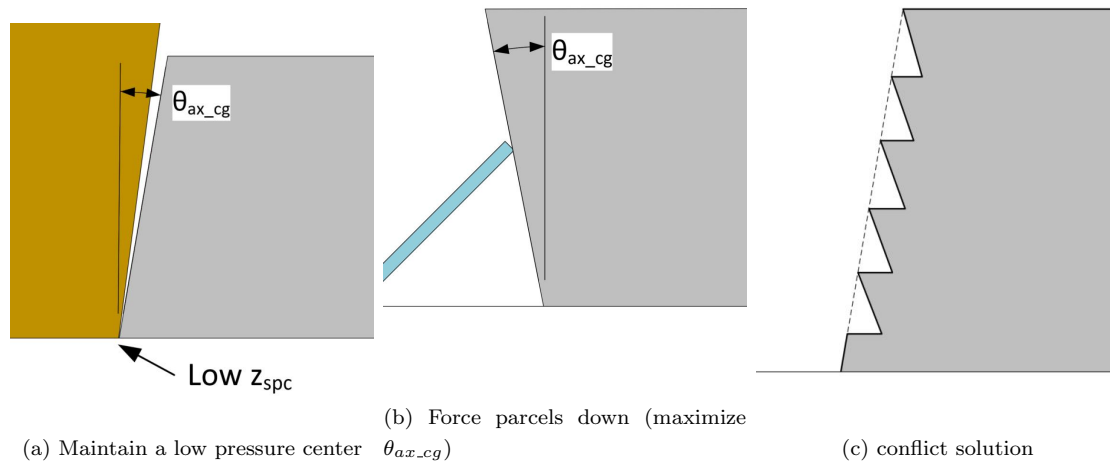


Figure B.4: Design rationale of groves in slider shape

Appendix C

Research paper

MASTER THESIS RESEARCH PAPER

Design optimization of a next-generation push divert sorter

D.K.J. van der Wielen,^{*†} Dr.ir W. van den Bos, Dr.ir. D.L. Schott,[†] and Ir. J.J.M.J.P. Meens[‡]

[†]Delft University of Technology, Faculty Mechanical, Maritime and Materials Engineering, Department of Maritime and Transport Technology, Mekelweg 2, 2628 CD Delft, The Netherlands

[‡]Vanderlande Industries, Rooseveltlaan 1, 5466 AC Veghel, The Netherlands

^{*}Corresponding author. Email: D.K.J.vanderwielen@student.tudelft.nl

Abstract

The performance of a Push Divert Sorter (PDS) is highly influenced by the design of components interacting with parcels. The shape and materials of these components influence the locations, directions and magnitude of forces acting on parcels, which influences their dynamic behaviour. The influence of the design of these components on the system performance is analyzed, and an improved design is proposed and assessed.

Keywords: Material handling, Automated sortation systems, Push divert sorter, Design optimization, parametric design

Worldwide parcel shipping volumes are continuously increasing [8]. Automated material handling equipment is key in accommodating this increase. The performance of this equipment requires continuous improvement. The need to handle a broad range of parcel types together with high throughput rates are major challenges the industry is facing. However, a research topic that has so far received little attention is the design of parcel interaction components. These are components that come into contact with parcels throughout the sorting process.

A new-generation PDS aims to push the boundary in terms of throughput capacity and parcel variety. To maximize the performance of this system, research is done on the influence of the design of parcel interaction components on the system performance. Moreover, for further performance improvement, the utilization of increased manipulation capabilities offered by the new sorter design is also explored.

The performance of automated sorting systems is influenced by the behaviour of parcels. Research into parcel behaviour on automated sorting equipment is mainly done by T. Piatkowski. Over a series of studies [4], [5], [6], [7] Piatkowski build models to analyse and simulate dynamic phenomena occurring on automatic sorting systems. However, this research is limited to a single cardboard box. Also, only impact events are analyzed, other parcel behaviour is not researched.

The behaviour of parcels on a PDS can be analyzed using theories of planar (two-dimensional) pushing mechanics. M. Mason laid the groundwork for this research topic, introducing the friction cone and defining methods for predicting the direction of rotation when an object is pushed [3]. K. Lynch built upon this work and introduced a method for analyzing the stability of an object being pushed by using graphical representations [2].

1. System analysis and design requirements

The system being researched has been proposed by M. de Jager [1] and comprises of a series of beam-like components referred to as carriers (see Figure 1a). Each carrier is equipped with a movable plastic block called the slider. The motion of each slider can be controlled individually by an electric motor as indicated in the figure. The carriers and parcels positioned on top, move in the indicated transport direction. Outfeed lanes are positioned on the side of the sorter. When a parcel nears its desired outfeed, the sliders start moving, pushing the parcel into the outfeed, this process is also referred to as sorting. This sorting process can be done in one of two ways. If a parcel fits into the outfeed in its initial orientation, it is sorted by a pure translation. If this is not the case, it is first rotated to align with the outfeed and then translated into the outfeed (Figure 1b).

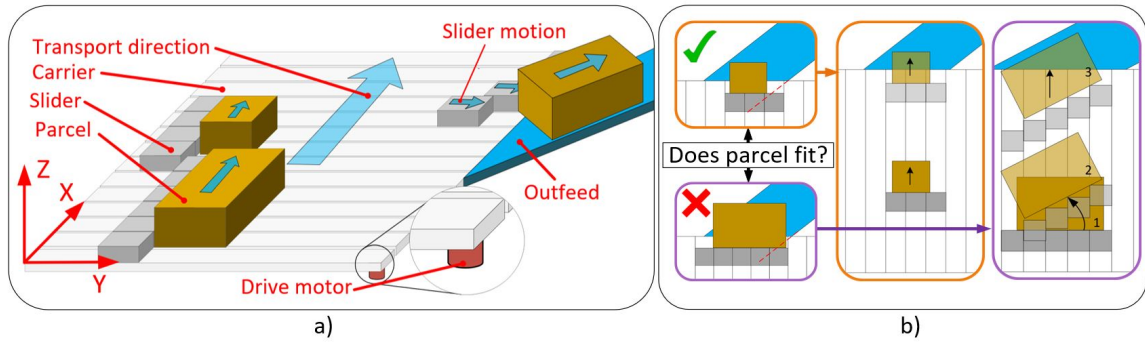


Figure 1. a) System overview, b) Sort strategies

The position and orientation of the parcels are only measured when they enter the system. It is thus not possible to correct any unexpected parcel behaviour once on the sorter. It is therefore important that the actual parcel state (position and orientation) is close to its expected state when entering an outfeed. Large deviations between the actual state and the desired state could result in the parcel being sorted into the wrong outfeed, or not fitting in the outfeed. Three KPIs which are considered to be important for maximizing the accuracy of the sorter are shown in Figure 2. These are the position in x and y-direction (Δx_{error} , Δy_{error}) and the orientation ($\Delta \theta_{error}$). These KPIs should be minimized at the moment a parcel enters the outfeed.

Besides accuracy, also the throughput capacity of the sorter is influenced by parcel behaviour. The total space required for a single parcel (highlighted in red in Figure 2) is influenced by the x-displacement during sorting (Δx_{error}). The amount of space required for a single parcel influences the density of parcels on the sorter, which influences its capacity. Finally, besides accuracy and capacity, it is also important that both parcels and the sorter are not damaged during the process. This concludes the following KPIs which should be minimized:

Table 1. Design KPIs

Domain	Variable	Description	When
	Δx_{error}	x-position error	Throughout entire process
	Δy_{error}	y-position error	
	$\Delta \theta_{error}$	Orientation error	
Parcel	Damage		Throughout entire process
Sorter	Damage		Throughout entire process

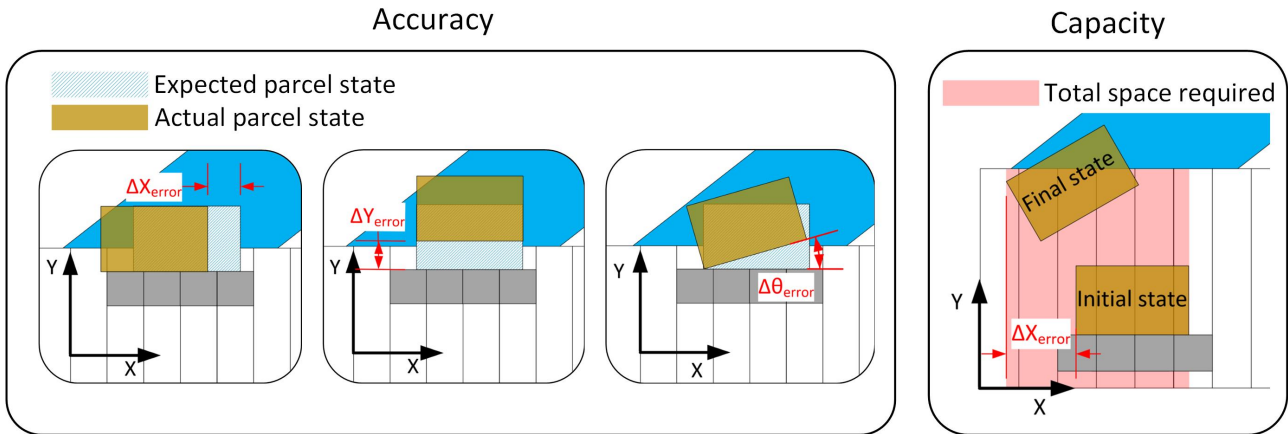


Figure 2. KPIs

2. Parcel behaviour analysis

The behaviour of parcels is influenced by a range of different aspects, three of which can not be influenced. These are the following:

- Parcel characteristics: (*dimensions, weight, overall geometric shape, base shape, packaging material, content, structural rigidity and yield strength*);
- System configuration and settings: (*outfeed angle and transport speed*);
- Initial state of parcel (input state): (*position and orientation*).

These aspects are referred to as uncontrollable input variables. The whole list of uncontrollable variables is summarized in table 4 in the appendix.

The behaviour of parcels is also influenced by the design (shape and material) of the parcel interaction components, which are the sliders and carriers. Moreover, the slider trajectory also influences the behaviour. The design of these components is translated into parameters which represent their most important properties (see Figure 3). Parameters such as friction coefficients are split into orientation and direction-dependent components to gain detailed insights into the influence of certain properties. Moreover, the tangential slider friction coefficient (indicated as μ_{s_tan} in the figure) is a function of the parcel orientation.

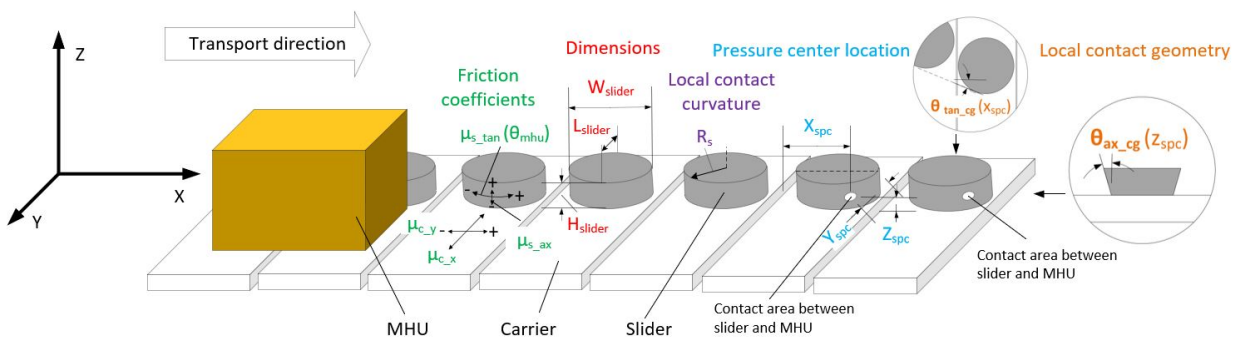


Figure 3. (controllable) design variables

Numerous modes of potentially unwanted parcel behaviour are identified from analysis and observation of the sorting process. The influence of the design parameters and input variables on each mode are analyzed using available formulas and theories. These insights offer the basis for a

realistic critical load scenario test. Such a scenario relates to a parcel with poor characteristics (given the specific problem being tested) in a critical initial position and sorter settings. The parcel behaviour during such a critical scenario is tested on the setup illustrated in Figure 8. A tracking camera records the parcel trajectory throughout the sorting process. The KPIs are extracted from this measurement data.

From this analysis, seven problems prove to impact the KPIs significantly and thus require improvement (Figure 4).

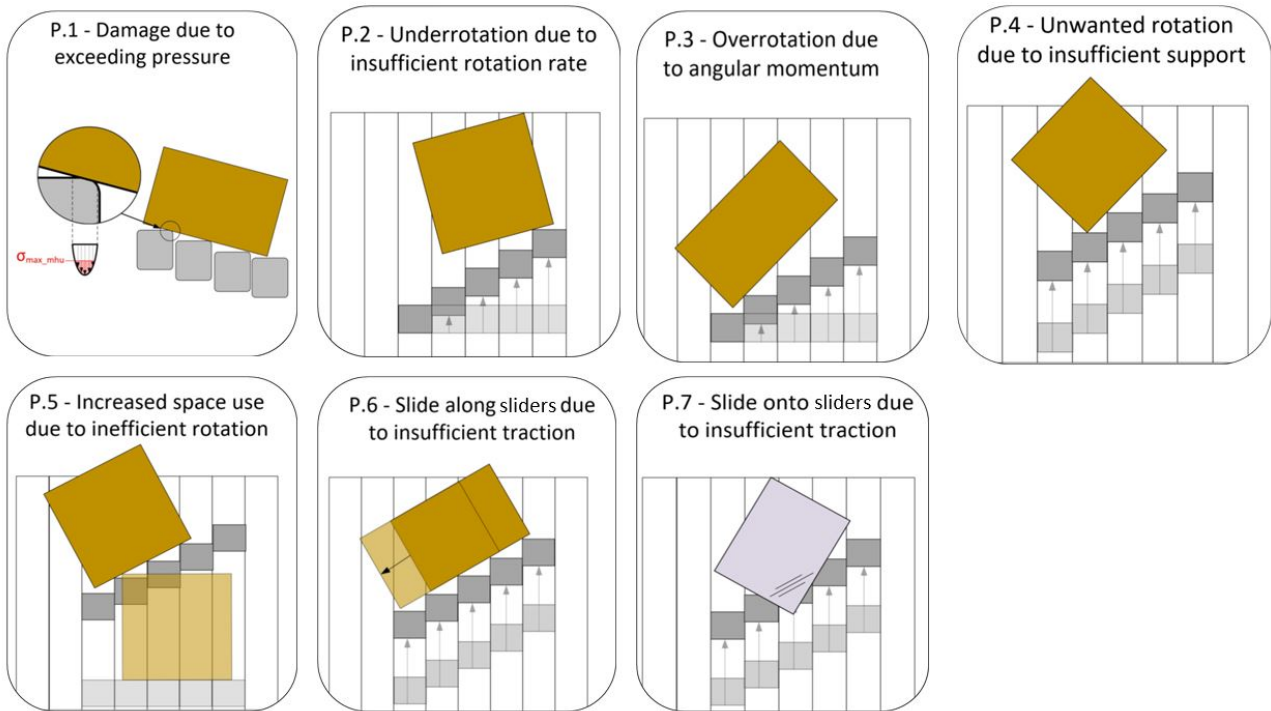


Figure 4. Most significant unwanted parcel behaviour

3. Conceptual solutions

To reduce these problems, both improved slider trajectories and improvements to the design of the sliders and carriers are explored.

In the current sort strategy, there is certain unwanted behaviour related to the rotation of parcels (Problem P.2, P.3 and P.4 in Figure 4). Based on the analysis of these problems, an improved slider trajectory is derived. This new trajectory reduces the angular velocity during the sorting process. This decrease in angular velocity is expected to significantly improve the parcel rotation behaviour.

3.1 Concept design

Since the design parameters have been used for analyzing the parcel behaviour, it is possible to define objectives for each design parameter in order to reduce the problems. These design parameter objectives are summarized in table 2 and 3. This presentation of the design objectives gives a clear overview of any present conflicts.

Both the shape and friction characteristics of the concept design are carefully chosen based on these objectives. Conflicts on the parameter level are resolved by looking at the component level. For example in the table can be seen that there are multiple conflicting objectives for the tangential

slider friction coefficient (μ_{s_tan}). Yet, when looking specifically at direction-dependent components, it can be found that the majority of the conflicts have differing directions (indicated with a "+" or "-" symbol). A single-direction friction material or component would in this case thus resolve these conflicts. Taking into the boundary conditions also provides an opportunity to resolve conflicts. Using this methodology resulted in the concept design shown in Figure 5.

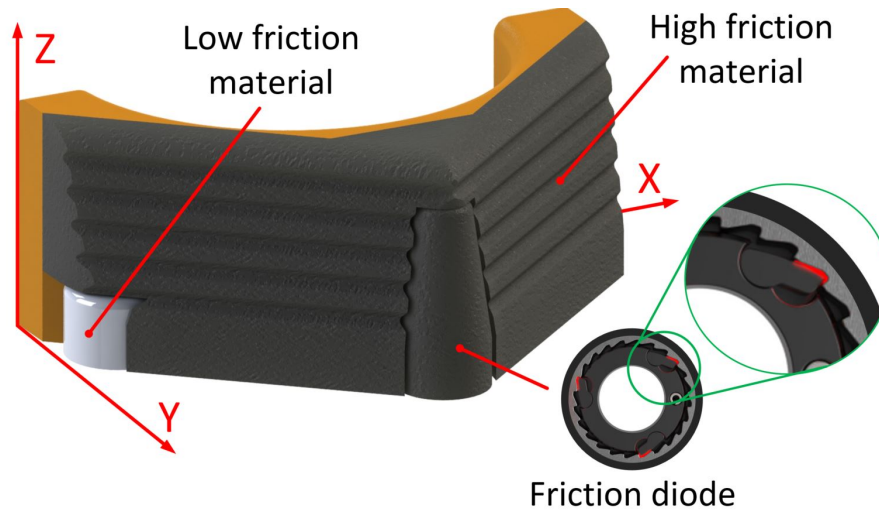


Figure 5. Final concept slider design

The main features of the new design are shown in Figure 6. The slider's shape is carefully chosen to satisfy the pressure center location and contact geometry objectives. Components with specific friction properties are positioned at specific positions on the slider. Due to this, parcels encounter four different friction coefficients depending on their orientation and direction of movement (see Figure 7).

3.2 Experimental results

Experiments are performed to assess the effectiveness of the design and slider trajectory improvements. One of the aspects of the concept design that requires testing and assessment is the friction diode. A prototype is therefore created which can be mounted on the test setup (Figure 9).

The new slider trajectory, which decreases the angular velocity, aims to reduce the overrotation of parcels (problem P.3). Figure 10 shows the performance improvement (%) in terms of the orientation error using the new trajectory. This is calculated using Equation 1. The solution almost completely eliminates the overrotation (after a distance of 500 mm).

The rotation behaviour using the prototype also showed significant improvement. The rotation rate increased (as can be seen in Figure 11 and 12). The distance required to rotate the parcel to its desired orientation is reduced up to 34%. Also, the rotation is done in a more efficient way when looking at the x-displacement (Figure 13), reducing the displacement in this direction by 16 %.

Moreover, problem P.6 is also mitigated as is shown in Figure 14. This Figure shows the x-position of a parcel during the sort action. After some initial shift due to rotation, it can be seen that the prototype functions as expected and prevents further sliding of the parcel along the sliders.

Finally, the whole slider design features rounded edges with a minimum radius (confidential). This curvature is validated (on test setup 15) to be sufficient to prevent damage due to contact pressure.

4. Conclusion

In conclusion, a methodology of KPIs-based testing with a tracking camera enabled analyzing the effect of unwanted parcel behaviour on the system performance for a broad range of parcel types. The most significant problems related to parcel behaviour have been identified (Figure 4). An improved slider trajectory has been proposed and tested for effectiveness. Moreover, a concept design based on design parameter objectives is presented. The new design improves parcel behaviour significantly. Finally, the carrier design can be used as a final measure for improving the remaining problematic parcel behaviour. This can be done based on the design objectives presented in Table 2 and 3.

References

- [1] Maarten de Jager. “Increasing the flexibility of a push divert sorter by designing an individual actuated slider-carrier system with local intelligence: A feasibility study”. In: (2018).
- [2] Kevin M Lynch and Frank C Park. *Modern robotics*. Cambridge University Press, 2017.
- [3] Matthew T Mason. “Mechanics and planning of manipulator pushing operations”. In: *The International Journal of Robotics Research* 5.3 (1986), pp. 53–71.
- [4] Tomasz Piątkowski. “Active fence with flexible link”. In: *Journal of Theoretical and Applied Mechanics* 48.1 (2010), pp. 87–109.
- [5] Tomasz Piątkowski. *Analiza i modelowanie procesu sortowania strumienia małogabarytowych ładunków jednostkowych*. Wydawnictwa Uczelniane Uniwersytetu Technologiczno-Przyrodniczego, 2010.
- [6] Tomasz Piątkowski. “Model and analysis of the process of unit-load stream sorting by a manipulator with torsional disks”. In: *Journal of Theoretical and Applied Mechanics* 47.4 (2009), pp. 871–896.
- [7] Tomasz Piątkowski. *Modelling and analysis of dynamic properties of tilt tray manipulator*. New trends in mechanisms, Academica-Greifswald, Germany, 2008.
- [8] Statista. *Global parcel shipping volume between 2013 and 2026 (in billion parcels)*. 2021. URL: <https://www.statista.com/statistics/1139910/parcel-shipping-volume-worldwide/>.

Appendix 1. Conceptual design

Tables 2 and 3 show design parameter objectives to reduce the seven problems which were found. Moreover, also constraints and objectives on other important aspects are given, these are: control, wear, noise and energy use.

Table 2. Combined design parameter objective table (part 1)

	Reference	H_{slider}	L_{slider}	W_{slider}	μ_{s_tan}	μ_{s_ax}	x_{spc}	γ_{spc}	z_{spc}
Performance related	F.1				Min + $-30 \leq \theta_{mhu} \leq 30$				
	F.2	Max				Max +			
	F.3				Min - $30 \leq \theta_{mhu} \leq 60$		Min		
	F.4				Min + $-30 \leq \theta_{mhu} \leq 30$		Max		Min
	F.5	Sequential sort			Min - $30 \leq \theta_{mhu} \leq 60$		Min		
		Parallel sort			Max $0 \leq x_{spc} \leq W_{slider}$ $-90 \leq \theta_{mhu} \leq 90$ $0 \leq \theta_{mhu} \leq 30$		Center (for all θ_{mhu})		
	F.6 F.7		>30 mm						
Control related Wear related Noise related Energy use related		Min (m_{slider})			$\theta_{mhu} = 60 \pm 5$ $\theta_{mhu} = 30 \pm 5$		Minimize variation over all θ_{mhu}	Min	Min
Boundary condition							$0 \leq x_{spc} \leq W_{slider}$	$0 \leq \gamma_{spc} \leq \frac{1}{2}L_{slider}$	$0 \leq z_{spc} \leq \frac{1}{2}H_{slider}$

Table 3. Combined design parameter objective table (part 2)

	Reference	θ_{tan_cg}	θ_{ax_cg}	μ_{c_x}	μ_{c_y}	R_s
Performance related	F.1	Max		>		
	F.2				Min	
	F.3			Max		
	F.4	Max		<		
	F.5	Sequential sort		>		
		Parallel sort				
	F.6 F.7				>	
Control related						
Wear related						
Noise related						
Energy use related				Min	Min	
Boundary condition		$-90 \leq \theta_{tan_cg} \leq 90$	$-90 \leq \theta_{ax_cg} \leq 90$			

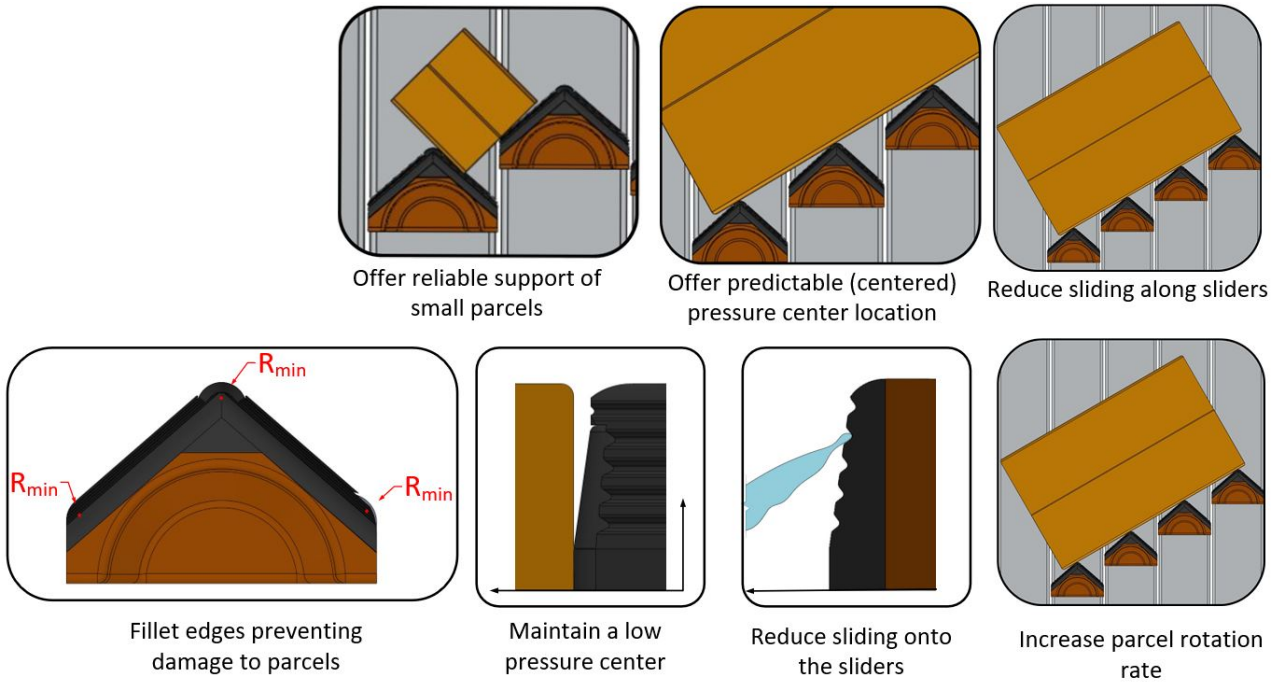


Figure 6. Main features of new slider design

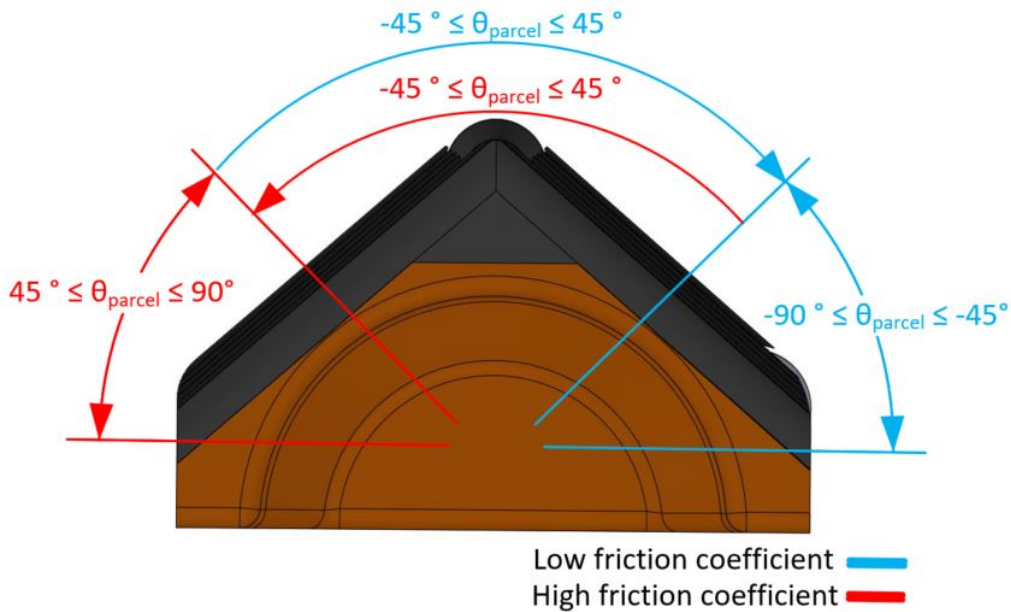


Figure 7. Friction coefficients slider

Appendix 2. Experiments

The test setup used for the parcel behaviour experiments is shown in Figure8. The slider trajectories can be generated on a dedicated computer. The motion of the parcel is measured by tracking reflective markers attached to the parcel with a tracking camera positioned above the setup. The KPIs are derived from a data file extracted from the camera.

The friction diode prototype shown in Figure9 consist of metal component with a diameter of 30 mm which has a ratchet and pawl mechanism inside, enabling rotation in only one direction. A

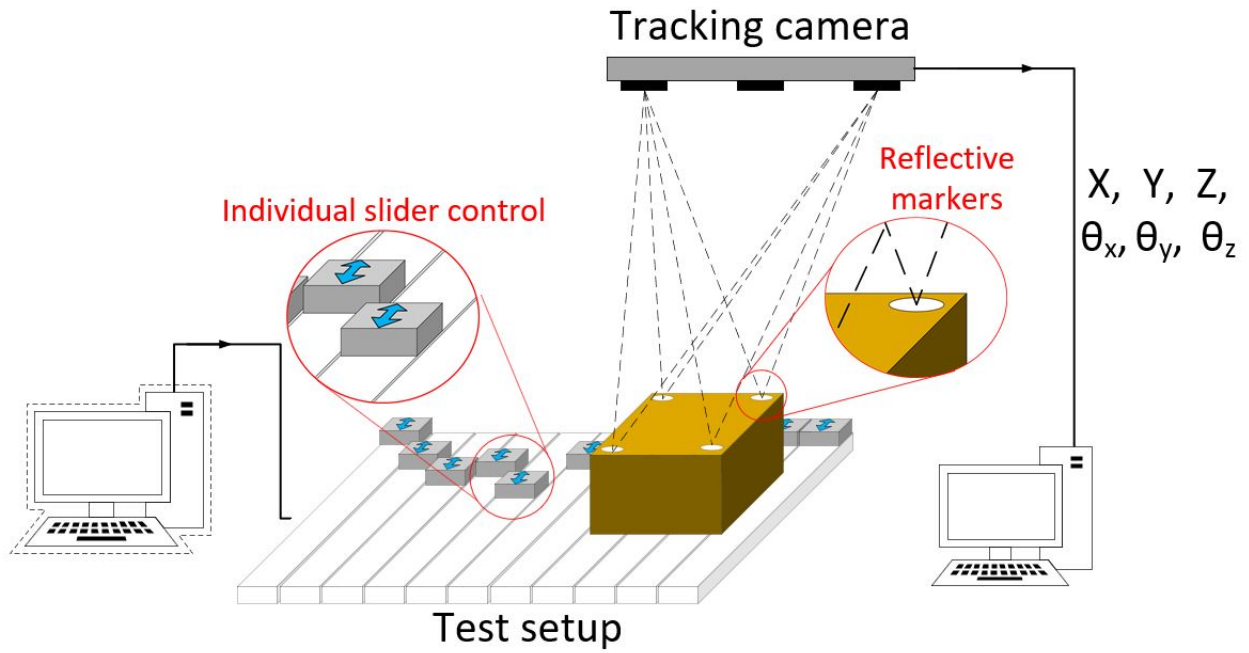


Figure 8. Test setup for simulating sort behaviour

rubber tape around the ring provides a high friction coefficient. This component thus effectively has a high friction coefficient in one direction and a low friction coefficient in the other direction.



Figure 9. Friction diode prototype

Appendix 3. Measurement result graphs

The measurements below show the performance improvement (%) of the solutions in terms of the orientation error. The position of an outfeed (in the y-direction) depends on the initial position of a parcel, therefore the motion of the parcel is plotted over the entire range of initial y-positions. The first possible outfeed position is highlighted with the vertical line. The overrotation is reduced significantly as can be seen in the graph.

$$\frac{|\Delta\theta_{error_old}| - |\Delta\theta_{error_new}|}{|\Delta\theta_{error_old}|} * 100\% \quad (1)$$

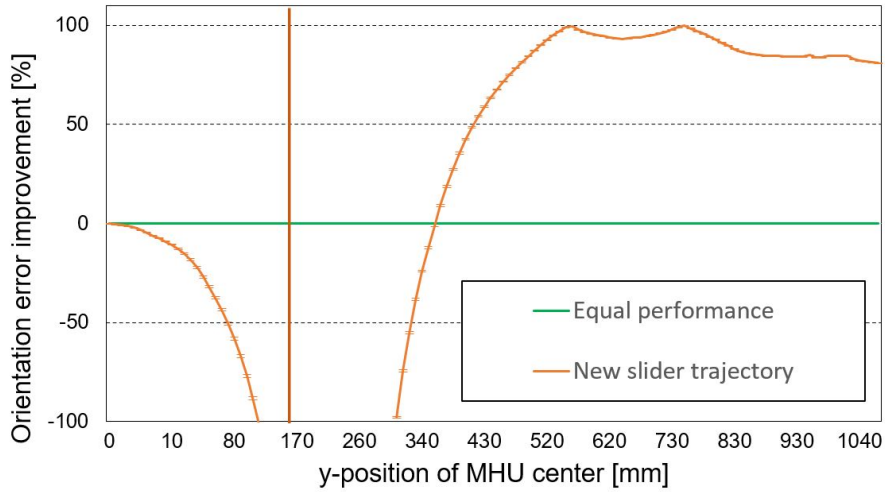


Figure 10. Reduce overrotation with the new slider trajectory - test results

Graph 11 and 12 show the orientation of a parcel throughout the sort process for both the current slider design and the prototype design. The rate of rotation is significantly improved with the prototype. Due to this the prototype requires 34% less distance in the y-direction to reach its desired orientation.

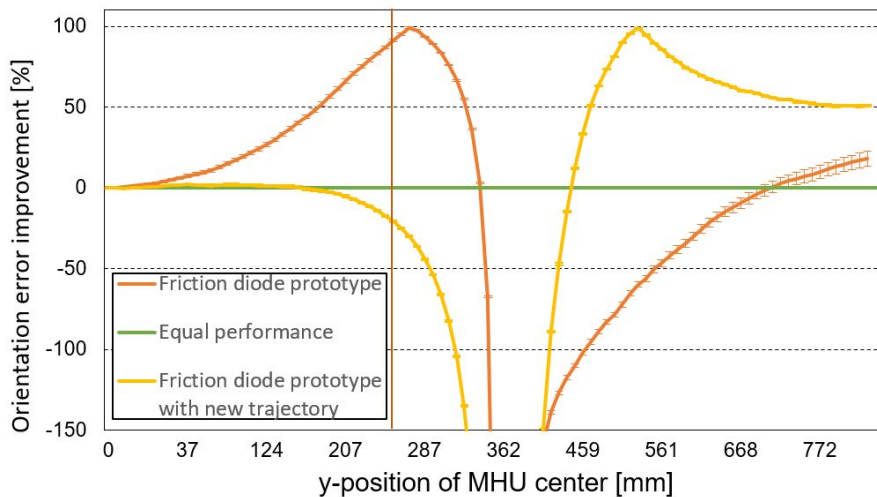


Figure 11. Increased rotation rate using prototype design - test results

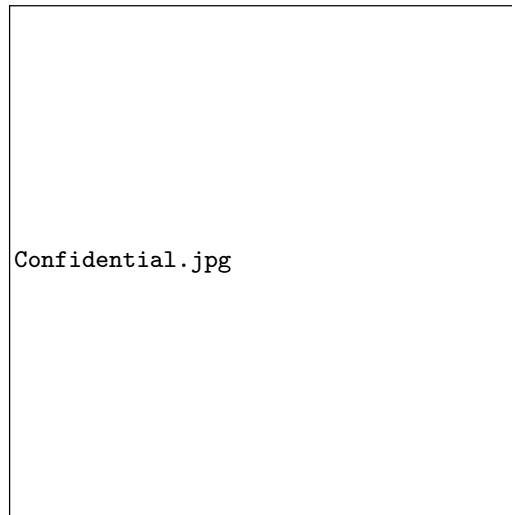


Figure 12. Increased rotation rate using prototype design (-30 degrees initial orientation) - test results

Graph 13 and shows the displacement of a parcel in both directions for the current design and the prototype. The amount of space required in the x-direction is decreased by 14 % when using the prototype.

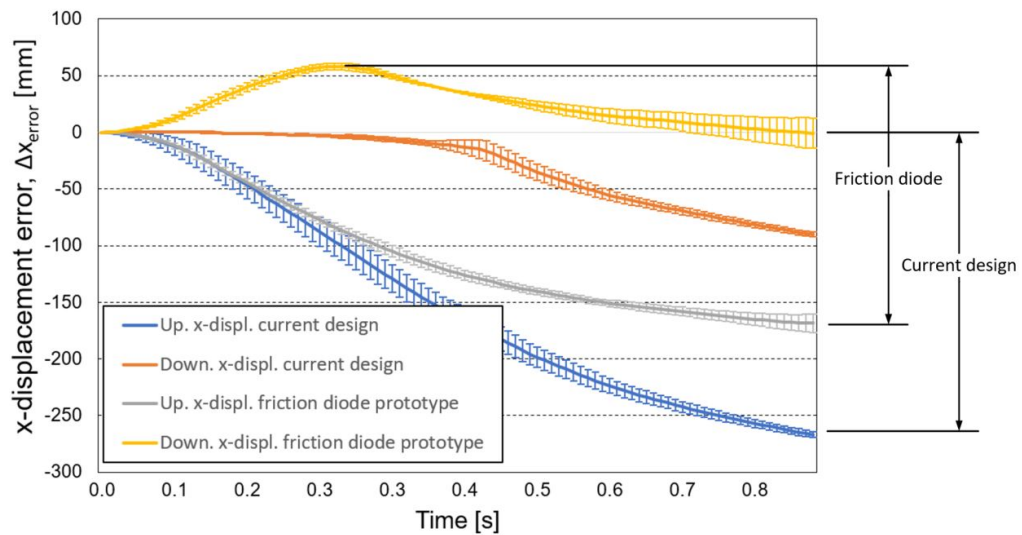


Figure 13. Improved rotation center using prototype design - test results

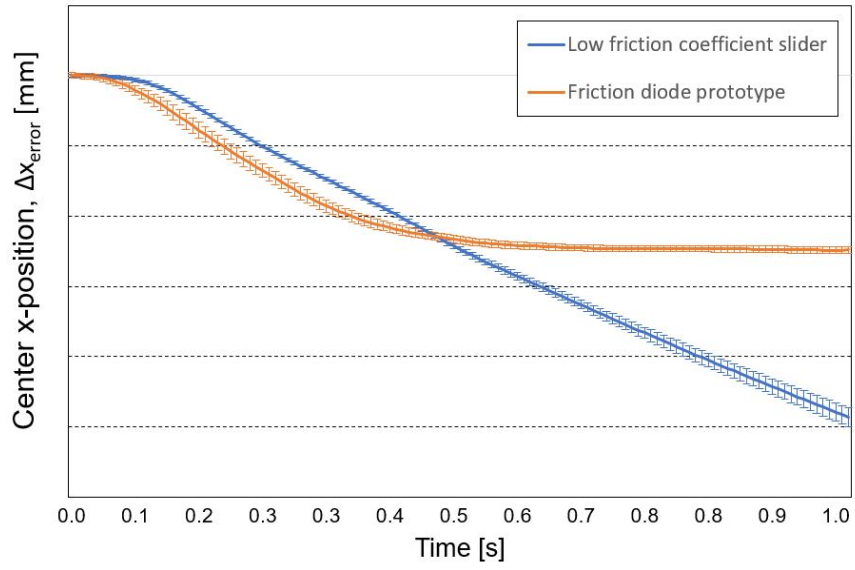


Figure 14. Reduce slide along sliders using prototype design - test results

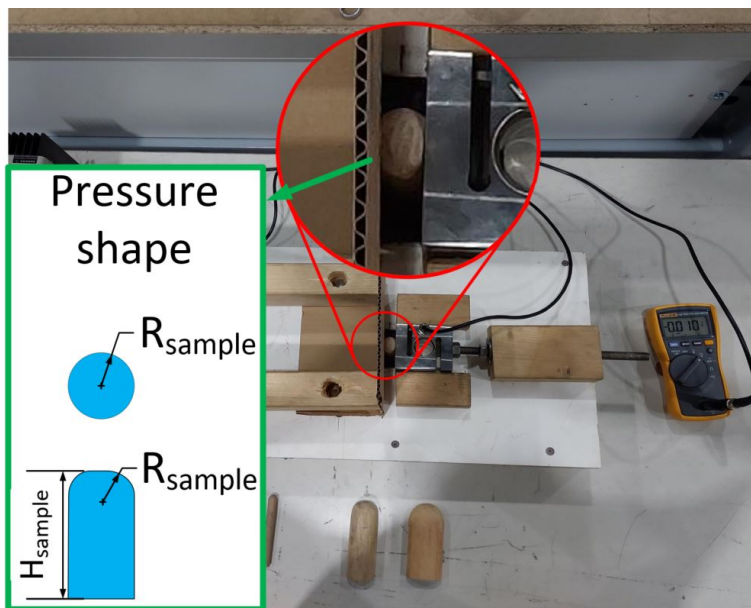


Figure 15. Test setup pressure test

Appendix 4. Input variables

Table 4. (Uncontrollable) input variables

	Input variables	Description	Range
Parcel characteristics	L_{Parcel}	Parcel length	$50 \leq L_{Parcel} \leq 2438 \text{ mm}$
	W_{Parcel}	Parcel width	$50 \leq W_{Parcel} \leq 1067 \text{ mm}$
	H_{Parcel}	Parcel height	$1 \leq H_{Parcel} \leq 914 \text{ mm}$
	m_{Parcel}	Mass of Parcel	$0.02 \leq m_{Parcel} \leq 70 \text{ mm}$
	I_{x_Parcel}	Moment of inertia of Parcel around x-axis	No range defined
	I_{y_Parcel}	Moment of inertia of Parcel around y-axis	No range defined
	I_{z_Parcel}	Moment of inertia of Parcel around z-axis	No range defined
	x_{com}	COM position in x-direction	$\frac{1}{3}L \leq x_{com} \leq \frac{2}{3}L$
	y_{com}	COM position in y-direction	$\frac{1}{3}W \leq y_{com} \leq \frac{2}{3}W$
	z_{com}	COM position in z-direction	$0 \leq z_{com} \leq \frac{2}{3}H$
	Structural rigidity		Rigid, semi-rigid, limp or soft
	Strength		Strong, average or weak
	Content stability		Fixed, semi-fixed, semi-loose or loose
	Pressure profile between slider and Parcel		Centered or spread out Concentrated or distributed
Parcel input state	$y_{Parcel_initial}$	Initial parcel position in y-direction (when fed to the sorter)	$200 \leq y_{Parcel_initial} \leq (W_{sorter} - 200) \text{ mm}$
	$x_{Parcel_initial}$	Initial parcel position in x-direction (when fed to the sorter) with respect to the carriers	$0 \leq x_{Parcel_initial} \leq 127 \text{ mm}$
	$\theta_{Parcel_initial}$	Initial orientation (around z-axis)	$-30 \leq \theta_{Parcel_initial} \leq 30$
Sorter settings	$v_{transport}$	Transport speed of sorter (in x-direction)	$1 \text{ m/s} \leq v_{transport} \leq 3.5 \text{ m/s}$
	v_{γ}	Divert speed	1,27 m/s
	$a_{\{slider\}}$	slider acceleration	$-1 \text{ m/s}^2 \leq a_{slider} \leq 10 \text{ m/s}^2$
	$\alpha_{outfeed}$	Outfeed angle	$20 \leq \alpha_{outfeed} \leq 30$ (wish: up to $\alpha_{outfeed} = 45$)
	W_{sorter}	Sorter width	1000 mm, 1300 mm and 1400 mm
		slider/carrier pitch ¹⁾	
	Sort direction		Single sided and dual sided
	Sort strategy		Parallel and sequential
1) The slider/carrier pitch is fixed since the new carriers should be retrofitable on older generation sorters.			